Terms and Conditions of Use of Digitised Theses from Trinity College Library Dublin

Copyright statement

All material supplied by Trinity College Library is protected by copyright (under the Copyright and Related Rights Act, 2000 as amended) and other relevant Intellectual Property Rights. By accessing and using a Digitised Thesis from Trinity College Library you acknowledge that all Intellectual Property Rights in any Works supplied are the sole and exclusive property of the copyright and/or other IPR holder. Specific copyright holders may not be explicitly identified. Use of materials from other sources within a thesis should not be construed as a claim over them.

A non-exclusive, non-transferable licence is hereby granted to those using or reproducing, in whole or in part, the material for valid purposes, providing the copyright owners are acknowledged using the normal conventions. Where specific permission to use material is required, this is identified and such permission must be sought from the copyright holder or agency cited.

Liability statement

By using a Digitised Thesis, I accept that Trinity College Dublin bears no legal responsibility for the accuracy, legality or comprehensiveness of materials contained within the thesis, and that Trinity College Dublin accepts no liability for indirect, consequential, or incidental, damages or losses arising from use of the thesis for whatever reason. Information located in a thesis may be subject to specific use constraints, details of which may not be explicitly described. It is the responsibility of potential and actual users to be aware of such constraints and to abide by them. By making use of material from a digitised thesis, you accept these copyright and disclaimer provisions. Where it is brought to the attention of Trinity College Library that there may be a breach of copyright or other restraint, it is the policy to withdraw or take down access to a thesis while the issue is being resolved.

Access Agreement

By using a Digitised Thesis from Trinity College Library you are bound by the following Terms & Conditions. Please read them carefully.

I have read and I understand the following statement: All material supplied via a Digitised Thesis from Trinity College Library is protected by copyright and other intellectual property rights, and duplication or sale of all or part of any of a thesis is not permitted, except that material may be duplicated by you for your research use or for educational purposes in electronic or print form providing the copyright owners are acknowledged using the normal conventions. You must obtain permission for any other use. Electronic or print copies may not be offered, whether for sale or otherwise to anyone. This copy has been supplied on the understanding that it is copyright material and that no quotation from the thesis may be published without proper acknowledgement.

Analysis of the elastic and inelastic behaviour of healthy and diseased arterial tissue

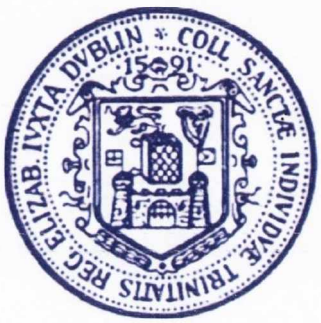

A thesis submitted to the University of Dublin in partial fulfilment of the requirements for the degree of

Doctor in Philosophy

Eoghan Maher, BA, BAI

Trinity College Dublin

2012

Supervisor

Dr. Daniel J. Kelly

Declaration

I declare that this thesis has not been submitted as an exercise for a degree at this or any other university and it is entirely my own work.

I agree to deposit this thesis in the University's open access institutional repository or allow the library to do so on my behalf, subject to Irish Copyright Legislation and Trinity College Library conditions of use and acknowledgement.

Summary

Mechanical factors play a key role in determining the success of clinical procedures such as balloon angioplasty and stenting that aim to increase lumen size in atherosclerotic lesions. Finite element modelling is commonly used to model such surgical interventions but the accuracy of these models is limited by the accuracy of the material model used for both the artery and plaque. It is evident that a thorough understanding of the mechanical behaviour of both healthy and diseased arterial tissue is desirable to aid in the treatment of atherosclerosis. In particular, little data is available relating to the inelastic mechanical properties of either arterial tissue or atherosclerotic plaques. The objective of this thesis is to further characterise the mechanical properties of healthy and diseased arterial tissue with a particular focus on stress softening and permanent set following non-physiological levels of loading.

Human carotid atherosclerotic plaque specimens, classified using ultrasound imaging, were mechanically loaded in uniaxial tension and compression. It was found that calcified plaques tended to be the stiffest while echolucent plaques were the least stiff. It was also noted that high variability was seen between samples taken from the same plaque and within each classification highlighting the inhomogeneous nature of atherosclerotic plaques. In a further study cyclic compression tests were performed on plaque samples to quantify their inelastic behaviour. It was observed that an approximately linear relationship existed between the inelastic strains on unloading and the peak strains applied. The clinical classification had no significant effect on the inelastic strains. The test data was characterized using a constitutive model that accounts for permanent deformation and stress softening to describe the plaque behaviour on unloading.

The anisotropic response of healthy arterial tissue to vessel overstretch was next determined. In order to determine the site specific response, arterial tissue from the aorta, carotid, femoral and coronary arteries were tested in cyclic compression, while circumferential and longitudinal tensile experiments were carries out on aortic and carotid artery samples. The

biochemical composition of each tissue was also determined. Larger inelastic strains were observed in arteries that had a higher ratio of collagen to elastin content. In the aorta and carotid arteries it was observed that inelastic strains were greatest in the radial direction and smallest in the circumferential. It was suggested that inelastic deformations were largely a result of overstretching of the smooth muscle component of the artery wall and that the collagen fibres and the elastin fiber network in the media allow greater elastic recoil. No significant differences in stress softening were found between artery types or loading directions at high magnitudes of applied strain.

An anisotropic inelastic constitutive model was proposed to describe the inelastic behaviour of arterial tissue that included elastic and inelastic damage for both the fibrous and matrix components. It was found that the model was able to provide a good quality fit for the experimental data for aorta and carotid arteries. The model fits suggested that inelastic damage largely occurred within the matrix component of the tissue. A finite element analysis of a simplified balloon angioplasty was undertaken to explore the effects of plaque mechanical properties on the predicted magnitudes of lumen gain. The model results suggest that the use of the inelastic model had significant effects on the predicted magnitudes of lumen gain and that greater damage occurred in calcified plaques.

In conclusion, the results of this thesis provide further insight into plaque mechanical properties and furthermore, it is one of the first to quantify inelastic deformations in both plaque and healthy arterial tissue. The proposed anisotropic inelastic model of arterial tissue and the associated mechanical test data can, in the future, be used in the optimisation of medical devices using computational methods such as finite element modelling.

Acknowledgements

Firstly I would like to thank my supervisor Dr. Daniel Kelly for all his support over the last 4 years. From the beginning, his guidance and encouragement have been invaluable to achieving all that I have and I am grateful for all that he has done. This project could not have been accomplished without our partners in other institutions Arthur and Tríona in DCU and Niamh and Sherif in UCHG.

For technical support when I was beginning in the world of mechanical testing and computational research my thanks go to Peter O'Reilly, Mick Reilly and Alex Lennon. Thanks also to Joan, Sheena and Nicole for being a great help in keeping me organised.

My experience during the course of the project would have been a lot less interesting if it wasn't for the other people in the department; the tea breaks were always enjoyable. Thanks to Steve, Tat, Thomas, Alanna, Oana, Hanifeh, Darren, Conor, Tariq, Eamon, Michael, Colin, Andy, Gráinne and enough other people to fill an appendix (not included).

Last but by no means least I want to thank my family for all their support and especially for their patience with me over the last few months. I would not be in the position I am now if not for them.

Publications and presentations arising from this study

Papers

Maher, E., Creane, A., Sultan, S., Hynes, N., Kelly, D. J., Lally, C. 2011. ***Inelasticity of Human Carotid Atherosclerotic Plaque.*** Annals of Biomedical Engineering, *in press*.

Maher, E., Creane, A., Sultan, S., Hynes, N., Kelly, D. J., Lally, C. 2009. ***Tensile and compressive properties of fresh human carotid atherosclerotic plaques***. J Biomech, 42**,** 2760-7.

Presentations

Maher, E., Creane, A., Sultan, S., Hynes, N., Lally, C., Kelly, D.J., ***Interaction of plaque and artery determine lumen gain in balloon angioplasty,*** In Proceedings of the 17th Annual Conference of the Bioengineering Section of the Royal Academy of Medicine in Ireland; January 2011

Maher, E., Creane, A., Sultan, S., Hynes, N., Lally, C., Kelly, D.J., ***A Constitutive Model to Describe Plasticity in Fresh Human Carotid Atherosclerotic Plaque.*** In Proceedings of the 17th Congress of the European Society of Biomechanics; July 2010.

Maher, E., Creane, A., Sultan, S., Hynes, N., Lally, C., Kelly, D.J., ***A Constitutive Model to Describe Plasticity in Human Atherosclerotic Plaque.*** In Proceedings of the 16th Annual Conference of the Bioengineering Section of the Royal Academy of Medicine in Ireland; January 2010

Maher, E., Creane, A., Sultan, S., Hynes, N., Lally, C., Kelly, D.J., ***Mechanical Characterization of Fresh Human Carotid Atherosclerotic Plaque.*** Proceedings of the ASME 2009 Summer Bioengineering Conference; June 2009

Maher, E., Creane, A., Sultan, S., Hynes, N., Lally, C., Kelly, D.J., ***Uniaxial Mechanical Properties Of Fresh Human Carotid Atherosclerotic Plaque.*** 12th Annual Sir Bernard Crossland Symposium; Queen's University; April 2009

Maher, E., Creane, A., Sultan, S., Hynes, N., Lally, C., Kelly, D.J., ***Tensile and Compressive Properties of Fresh Carotid Atherosclerotic Plaques.*** In Proceedings of the 16th Annual Conference of the Bioengineering Section of the Royal Academy of Medicine in Ireland; January 2009

Maher, E., Lally, C., Kelly, D.J., ***Change in the Risk of Plaque Rupture with plaque development.*** In Proceedings of the 16th Annual Conference of the Bioengineering Section of the Royal Academy of Medicine in Ireland; January 2008

Table of contents

List of figures

List of tables

Nomenclature

Basic kinematics and stress

$\mathbf{X}$, $\mathbf{x}$	Position of a particle in the undeformed and deformed configuration
Ω_0, Ω	Undeformed reference and deformed spatial configurations
$\boldsymbol{U}$, $\boldsymbol{u}$	*Displacement field vector in the reference and spatial configuration*
t	*Time*
$\mathbf{F}_{ij}$	Deformation gradient tensor
$\mathbf{C}_{ij}$	Right Cauchy-Green strain tensor
$\mathbf{E}_{ij}$	Green-Lagrange strain tensor
$\mathbf{I}_{ij}$	2nd order identity matrix
$I_i(C)$	Invariants of the right Cauchy-Green strain tensor
λ_i	Principle stretches
J	Jacobian determinant (volume ratio)
$\mathbf{T}$, $\mathbf{t}$	Traction tensor in the reference and spatial configurations
$\boldsymbol{\sigma}_{ij}$	Cauchy stress tensor
$\mathbf{P}_{ij}$	1st Piola-Kirchhoff stress tensor
$\mathbf{S}_{ij}$	2nd Piola-Kirchhoff stress tensor

D_{int}	Internal dissipation

Hyperelasticity

ψ	Internal strain-energy density function
$\mathbb{C}_{ijkl}$	Elasticity tensor in the material description
$\mathbb{c}_{ijkl}$	Elasticity tensor in the spatial description
$\mathbb{C}^{\tau J}$	Jaumann tangent modulus
$\mathbb{c}^{abaqus}$	Scaled Jaumann tangent modulus for use in Abaqus user materials
p	Hydrostatic pressure term for incompressible model
$\bar{\mathbf{F}}_{\mathbf{ij}}, \bar{\mathbf{C}}_{\mathbf{ij}}$	Modified deformation gradient and right Cauchy-Green strain tensors
$\bar{I}_i$	Modified strain invariants
ψ_{vol}, ψ_{iso}	Volumetric and isochoric components of energy functions
$\mathbf{S}_{\mathbf{vol}}$, $\mathbf{S}_{\mathbf{iso}}$	Volumetric and isochoric components of 2nd Piola-Kirchhoff stress
$\mathbb{P}$	Projection tensor
$\mathbb{I}$	4th order identity tensor
$\mathbb{C}_{vol}, \mathbb{C}_{iso}$	Volumetric and isochoric components of elasticity tensor in material description

Anisotropic hyperelasticity

$\mathbf{m}_0$, $\mathbf{n}_0$	Unit vectors in the fibre directions

M, N	Structural tensors of m_0 and n_0 respectively
$\bar{I}_4, \bar{I}_6$	Modified strain invariants for anisotropic material, equivalent to square of stretch in the fibre directions
$\mathbf{S_{isch}}$	Isochoric 2nd Piola-Kirchhoff stress component for anisotropic material
ψ_{isch}	Isochoric part of strain-energy
ψ_m, ψ_4, ψ_6	Strain-energy of isotropic component and two fibre components respectively
$\mathbb{C}_{isch}$	Isochoric elasticity tensor in material description for anisotropic material
$\bar{\mathbb{C}}_{m,4,6}$	Isochoric elasticity tensor of the matrix and fibres respectively
β	Fibre angle measured from the circumferential direction

Inelastic constitutive model

Isotropic inelastic model

D	Damage variable
$\mathbf{F}^*$	Deformation gradient at maximum deformation in the load history
J^*	Jacobian determinant at maximum deformation in the load history
$\mathbf{C}^*$	Right Cauchy-Green strain tensor at maximum deformation in the load history
$\boldsymbol{\sigma}_{IL}, \mathbf{S}_{IL}, \mathbf{P}_{IL}$	Initial loading stress tensors
$\boldsymbol{\sigma}_{IN}, \mathbf{S}_{IN}, \mathbf{P}_{IN}$	Inelastic stress tensors
N	Function of C^*

ψ_{IL} Strain-energy during initial loading phase

α Maximum value of ψ_{IL} in the load history

ϕ Yield criterion for damage to progress (damage surface)

$\mathbb{C}_{IL}$ Elasticity tensor in the material description during the initial loading phase

Anisotropic elastic damage

ψ_{ED} Elastically damaged strain-energy function

$\psi_{m,4,6}$ Isochoric 'undamaged' strain-energy functions

$\mathbf{S_{ED}}$ Elastically damaged isochoric stress tensor

$D_{m,4,6}$ Damage variable for the matrix and two fiber directions respectively

$(1 - D_i)$ Reduction factors for the matrix and two fiber directions respectively

$\bar{\mathbf{S}}_{\mathbf{m,4,6}}$ Isochoric 'undamaged' stress for the matrix and two fiber directions respectively

$\phi_{m,4,6}$ Yield function (damage surface) for the matrix and two fiber directions respectively

Ξ_i^t Equivalent strain

Ξ_i^m Maximum equivalent strain in the load history

$N_{m,4,6}$ Normals to damage surfaces

$\mathbb{C}_{m,4,6}$ Elastically damaged elasticity tensors for the matrix and two fiber directions

$\bar{\mathbb{C}}_{m,4,6}$ Isochoric 'undamaged' elasticity tensors

Inelastic damage

$\mathbf{S_{IN}}$	Inelastic stress tensor
$\mathbf{S_{IN}^{i}}$	Inelastic stress tensors related to material components where $i = m, 4, 6$
I_i^*	Maximum value of the strain invariants in the load history, $i = 1, 4, 6$
$\varphi_{m,4,6}$	Yield criteria for evolution of inelastic stresses
ψ_{IN}^{i}	Dissipated internal strain-energy due to damage of components, $i = m, 4, 6$
$\mathbb{C}_{INi}$	Inelastic elasticity tensor modifiers for each material component, $i = m, 4, 6$

Error measures

E	Relative error
χ	Root mean square error
χ_{pd}	Root mean square error of permanent deformation prediction
χ_s	Root mean square error of the stress prediction
n	Number of experimental data points
q	Number of strain-energy function constants

Chapter 1 Introduction

1.1 Background

Atherosclerosis is an inflammatory cardiovascular disease that affects medium and large sized arteries. It occurs in the artery wall causing intimal thickening, i.e. thickening of the inner layer of the artery, and the development of stenotic lesions, also known as plaques (Libby, 1995). These stenotic lesions can result in a loss of patency (i.e. reduction in lumen cross-sectional area) or blockage in the artery, restricting blood flow through the vessel. Cardiovascular diseases like atherosclerosis are one of the major causes of mortality in the western world (Lloyd-Jones et al., 2009). As a result, research into the pathology and treatment of atherosclerosis and other cardiovascular diseases is vital. There are a number of known indicators or risk factors for the incidence of atherosclerosis in a patient including age, diabetes, gender, blood cholesterol level, smoking, physical activity, etc. (Berenson et al., 1998; Martini, 2006). While much of the risk factors above indicate a primarily biochemical influence on plaque development, the prevalence of atherosclerotic lesion development at regions with complex geometry (Malek et al., 1999) also indicates that biomechanical factors also play a role.

One location with a complex geometry in the arterial tree where atherosclerosis occurs is at the carotid bifurcation. The leading cause of stroke is carotid artery disease and the disease is responsible for 20-30% of the new or recurrent strokes that occur each year in the US (Baroncini et al., 2006). As there has only been limited success in the treatment of a stroke once it has occurred (Schwamm et al., 2005), it is better to focus on the prevention of stroke incidence. Acute stroke often results from the sudden rupture of asymptotic plaques, known as vulnerable plaques, in regions of expansive remodelling where no restriction of blood flow occurs (Glagov et al., 1988; Naghavi et al., 2003). The large number of strokes occurring in these patients who are often asymptomatic shows the need for better understanding of the atherosclerotic lesions, including their mechanics, in order to determine better indicators of the disease.

Percutaneous interventions such as angioplasty and stenting are surgical procedures that aim to revascularise a stenosed artery. Balloon angioplasty is a procedure involving the insertion of a catheter mounted nylon or PVC balloon into the cardiovascular system, usually through the femoral artery. The balloon is guided to the target lesion and a pressure is applied to the balloon internally in order for it to expand. The first reported balloon angioplasty was performed clinically in the late 1970's (Gruntzig et al., 1979). However it became apparent that the procedure led to high incidences of restenosis (re-narrowing of the lesion) which led to the first reported cases of stenting, the inflation of a balloon catheter mounted stainless steel mesh to restore artery patency (Sigwart et al., 1987). Stents are commonly made from coiled wire, multiple rings linked together or laser cut from tubes. The function of a stent is to maintain post intervention lumen size by limiting the elastic recoil of the artery. Stenting has been observed to reduce the rate of restenosis that occurs within 6 months of the procedure from 30-40% for balloon angioplasty to 15-30% for bare metal stents (Bashore, 2008; Erbel et al., 1998). Stents are mostly made from metallic materials, the most common being stainless steel.

Stenting of peripheral arteries has proved problematic in comparison to coronary stenting and is not performed as regularly. There are a number of possible reasons to account for this discrepancy in the success rate of similar procedures. The mechanical environment is more complex in peripheral arteries such as the superficial femoral artery (Cheng et al., 2006) and carotid artery (Robertson et al., 2008; Vos et al., 2003) due to movement of limbs. This complex loading environment is an important consideration and as a result shape-memory alloys such as Nitinol have been introduced for stenting of peripheral arteries. Another important factor is the variation of the in the structure and composition of arteries throughout the arterial tree (Cox, 1978; Martini, 2006) which results in variation in mechanical behaviour of arteries (Holzapfel et al., 2005; Schulze-Bauer et al., 2003). This highlights the need for an understanding of the specific target artery's mechanical behaviour in order to effectively design suitable medical devices. Studies comparing properties of different arteries may also provide insight to the structure-function relationship in arterial tissue.

Endarterectomy is a surgical procedure where the artery wall is cut open and plaque is removed, restoring a larger lumen diameter. There is much debate over whether stenting or endarterectomy is the best choice of treatment for carotid lesions. One of the main attractions of stenting over endarterectomy is that stenting is seen to be less invasive than endarterectomy (Fayad, 2007). Early randomized trials comparing the two procedures showed much higher success rates with endarterectomy, however improvements in carotid stenting procedural safety and clinical outcomes has led to stenting being proposed as a viable option (Liu et al., 2009). Other randomized studies have indicated that the surgical outcome is similar between carotid endarterectomy and stenting for high risk surgical patients (Gurm et al., 2008) while a single centre study has shown similar for asymptomatic patients (Tang et al., 2008). It is widely accepted however that the possible benefits of stenting won't be known until more randomized studies are performed, however stenting is a viable option for certain patient subsets (Fayad, 2007; Tang et al., 2008). Recent guidelines from the American Heart Association and American Stroke Association have recommended that carotid stenting is indicated as an alternative in average risk patients (Furie et al., 2011). Knowledge of the mechanical behaviour of carotid arteries and carotid plaques is important to the continued improvements in the developing field of endovascular treatment of carotid stenosis.

1.2 Finite Element Modelling

Finite element (FE) modelling is a commonly used tool for evaluating medical devices whose small size has led to difficulties in using more traditional methods for assessing deformations and strains. Modelling is often used to analyse the performance of stent designs during expansion; for example predicting the peak stresses and strains and measuring stent foreshortening and elastic recoil. It allows the evaluation of the effect that altering a design has on its performance with relative ease (Chua et al., 2004a). It is important to understand how a stent would perform in an *in vivo* environment and finite element modelling can allow insights to the behaviour of a stent during expansion in these conditions prior to costly animal studies and clinical trials. To this end stent-artery and stent-plaque-artery interactions have been investigated using a finite element approach. Using this method the effects that stent expansion has on the target vessel can be analysed. The

effect of stent expansion on stresses in the plaque and arterial wall are commonly investigated (Early et al., 2009), as the peak stresses experienced by the artery can be used as an indication of arterial injury due to stent expansion and hence the likelihood of restenosis (Schwartz and Holmes, 1994). Analyses have been performed to investigate other effects such as tissue prolapsed between the stent and artery (Prendergast et al., 2003), which would influence the post-stenting mechanical environment, and lumen gain[1] (Early and Kelly, 2010) which can be used to assess the success of a stent in terms of target vessel revascularisation.

For a FE analysis to be used to properly assess the interaction between a diseased artery and a specific stent design, the stent, artery wall and plaque need to be modelled accurately. While stents are commonly made from materials like stainless steel which are well defined, artery and plaque material properties have not been as well characterised. Artery and plaque material properties are most commonly defined by hyperelastic constitutive models and do not consider inelastic behaviour of the tissue. This inelasticity will play a key role in determining lumen gain following procedures such as angioplasty and stenting.

1.3 Characterisation of Tissue Mechanical Behaviour

Due to the difficulty in obtaining fresh human arterial tissue for mechanical testing, animal tissue is often used to investigate artery mechanical properties. The most commonly used animals for this type of mechanical testing are pigs due to the similarities of human and porcine vascular systems. The use of porcine tissue as a basis for the mechanical characterisation of arterial properties can be further validated by the regular usage of pigs in pre-clinical trials for vascular devices. It is thus also desirable to be able to predict the behaviour of a stent in a porcine artery. In order to correctly interpret the implications of animal trials it is important to understand the differences between various arteries in both species. Comparison of the mechanical properties of arteries from different locations of the arterial tree may provide information on the relationship between arterial structure

[1] *Lumen gain is defined as increase in the cross-sectional area of the arterial lumen following surgical intervention which if sufficient will allow for normal blood flow to occur.*

and mechanical properties which will allow for a more thorough evaluation of pre-clinical and clinical results.

The loading behaviour of arteries throughout the arterial tree have been investigated through mechanical testing of human and porcine tissue (Holzapfel et al., 2005; Lally et al., 2004; Schulze-Bauer et al., 2003; Schulze-Bauer et al., 2002). The constitutive stress-strain behaviour of arterial tissue is usually described using a hyperelastic material model. In a hyperelastic material the constitutive response is usually given in terms of a strain-energy density function. Artery properties have been presented in the form of an isotropic model (Delfino et al., 1997; Lally et al., 2004); recently however, it is more common to use anisotropic hyperelastic models. These anisotropic models are typically Fung-type exponential functions (Fung and Liu, 1995; Schulze-Bauer et al., 2002) or based on strain invariants (Holzapfel et al., 2005). The strain invariant based anisotropic model use invariants, typically the 4^{th} and 6^{th} strain invariants I_4 and I_6, which introduce preferred directions into the material and these invariants, I_4 and I_6, are equivalent to the square of the stretch in the preferred *'fibre'* directions. However the inelastic properties of the tissue on unloading are not as well characterised. Models have been developed to describe viscoelastic behaviour of arteries such as hysteresis, based on pseudo-elasticity (Fung et al., 1979) or other methods. Viscoelastic models that include creep and relaxation behaviour are commonly based on the use of internal variables (Holzapfel and Gasser, 2001; Simo, 1987). Other models include softening effects that occur due to damage in the tissue. These models are generally use continuum damage mechanics and introduce a stress softening effect (or Mullins effect) that is dependent on the maximum deformations the material has undergone (Simo, 1987). This approach has been used to model the softening and failure behaviour of fibrous soft tissues (Natali et al., 2005; Peña et al., 2008) and have been applied to arterial tissue with similar success (Alastrué et al., 2007; Balzani et al., 2006; Calvo et al., 2007).

Inelastic residual strains in soft tissue have not been as well defined in the literature. Residual strains have been observed in arterial tissue loaded beyond the physiological domain (Holzapfel et al., 2000) and the same authors have proposed a constitutive model based on multi-

surface plasticity (Gasser and Holzapfel, 2002) to simulate this behaviour. However neither of the above papers quantifies the residual strains that occur in the tissue. Other researchers have applied inelastic models to describe inelastic strains in mouse skin (Ehret and Itskov, 2009) and brain tissue (Franceschini et al., 2006). Franceschini *et al* applied the theory of pseudo-elasticity to describe softening and permanent set[2] in brain tissue based on constitutive models for particle-filled rubbers (Dorfmann and Ogden, 2004; Ogden and Roxburgh, 1999). Further studies are needed to adequately quantify and model inelastic strains in arterial tissue.

Compared to arterial tissue relatively few studies have been performed to quantify the mechanical properties of atherosclerotic plaques. While the difficulty in obtaining human arterial tissue for mechanical characterisation can be somewhat overcome by the use of animal data, atherosclerosis needs to be induced in animals over a period of weeks using a cholesterol-lipid diet (Hayashi and Imai, 1997). Tests on human atherosclerotic plaques have been performed on tissue from abdominal aorta (Lee et al., 1991; Lee et al., 1992) and aorto-iliac (Salunke et al.; Topoleski and Salunke, 2000; Topoleski et al., 1997). Holzapfel *et al.* (2004) have also investigated the anisotropic properties of iliac atherosclerotic arteries. Only the studies by Topoleski *et al.* report specifically on the inelastic behaviour of aortic plaques. As the mechanical properties of healthy arterial tissue vary throughout the arterial tree it is likely the same is true for atherosclerotic plaques. To the author's knowledge, prior to the commencement of this research no studies had been performed to characterise the mechanical behaviour of carotid atherosclerotic plaques. This lack of test data has led to simplifications of the modelling of plaque material properties, where it is modelled as linear elastic (Chua et al., 2004b), rigid (Gasser and Holzapfel, 2007a) or as a isotropic hyperelastic (Early et al., 2009; Lally et al., 2005) tissue.

2 Permanent set describes an irreversible deformation that remains in a material after it has been subjected to load.

1.4 Aims of the Study

The objective of this thesis is to further characterise the mechanical properties of healthy and diseased arterial tissue in order to improve the capabilities of finite element modelling to evaluate stent performance in an atherosclerotic artery. This thesis will pay particular attention to carotid tissue due to the increasing use of endovascular treatment for carotid lesions. Comprehensively addressing this objective requires a number of studies:

1. The first objective is to determine the *elastic* mechanical properties of carotid atherosclerotic plaques through uniaxial tensile and compressive testing. These mechanical properties will be characterised using an isotropic hyperelastic constitutive model which will allow the currently used finite element models to be adapted to model carotid procedures with relative ease.
2. Next the inelastic mechanical behaviour, specifically stress softening and inelastic strains, of carotid plaques is to be investigated. An isotropic inelastic model will be presented to characterise the inelastic mechanical behaviour, with stress softening modelled through a typical continuum damage mechanics framework and the inelastic strains adapted from a basis in pseudo-elasticity.
3. The third objective is to quantify the anisotropic inelastic properties of healthy porcine tissue at a number of locations in the arterial tree. This inelastic healthy arterial data is to be compared to biochemical composition in an attempt to provide insight into the relationship the structure and function of arteries.
4. An anisotropic inelastic model is then proposed to describe the observed arterial behaviour. In this model the softening is defined by continuum damage mechanics applied separately to the fibres and base matrix of a structurally based model. The inelastic strains will be defined through an additive split in the stress tensor.
5. Finally, it is intended to illustrate the use of the constitutive model by using the finite element methods to simulate balloon angioplasty in simplified carotid artery geometry. This finite element model will make use of the anisotropic inelastic model presented for both artery and plaque mechanical properties. A systematic investigation will be

undertaken into the influence of plaque properties on the stresses that occur in the plaque and artery on expansion, the post-angioplasty lumen gain and the stresses in both tissues post-angioplasty.

Ultimately it is hoped that the mechanical test data will improve the understanding of healthy and diseased cardiovascular behaviour due to overstretching during treatment of atherosclerosis. It is hoped that the test data and model provided can be used as a tool to improve the predictive capabilities of finite element models of angioplasty and stenting and hence in the optimisation of device design. If used in combination with patient specific geometries of the carotid bifurcation, it could possibly be used in the future as the basis for a tool to aid in determining the suitability of stenting as a treatment option for a specific carotid lesion.

Chapter 2 Literature Review

2.1 Introduction

In this chapter an overview of the mechanics of healthy and diseased arterial tissue is provided. To model the mechanics of arterial tissue numerically a fundamental knowledge of the composition and structure of arteries is needed. Therefore, this section begins with a discussion of the main components of the arterial wall, their function and mechanical properties. The cardiovascular disease atherosclerosis is discussed, focussing on its development, treatment and the mechanical properties of atherosclerotic plaques. Finally, the methods used to appropriately model healthy and diseased arterial tissue are described, in particular the fundamentals of large deformation non-linear solid mechanics and the implementation of elastic and inelastic behaviour as relevant to arterial tissue.

2.2 Arterial structure and function

While the precise anatomy of arteries varies depending on location, the basic composition of the arterial wall is similar at all sites in the arterial tree. Arteries consist of three layers: the intima (tunica intima), media (tunica media) and adventitia (tunica externa), see Fig 2.1. The intima is the innermost layer of the arterial wall and contains the endothelium, a thin basal membrane and internal elastic lamina. The endothelium is a monolayer of endothelial cells lining the inner surface of the artery. The cells are mechanosensitve and are important in the regulation of arterial function. The basal membrane and internal elastic lamina are made up of elastic fibres. The intima is thin in young healthy arteries and is generally mechanically insignificant. However in humans, the intima thickens with increasing age and becomes more significant (Holzapfel et al., 2005). This intimal thickening can be caused by atherosclerosis but can also be seen in healthy arteries (Velican and Velican, 1985). The media is the middle layer of the artery wall. It is commonly the thickest layer

and consists of smooth muscle cells, elastin, collagen fibres and ground matrix. The media is divided up into a number of discrete fibre reinforced concentric layers separated by fenestrated elastin laminae. Collectively, the elastic lamina, collagen fibres and smooth muscle have a near circumferential helical orientation. The elastic lamina and collagen fibres have a wavy structure in the longitudinal and circumferential direction when unloaded and when loading increases they straighten in the direction of loading, increasing the stiffness of the artery wall as they are recruited, see Fig 2.2. This mechanism limits the expansion of the artery as a result of applied internal pressures. The outermost layer of the artery wall is the adventitia. The adventitia is comprised of elastin and collagen fibres and ground substance. The adventitia connects the artery to the surrounding tissue. The collagen fibres form a helical structure embedded in the ground matrix. At physiological pressures the adventitia has low stiffness which greatly increases at high pressures.

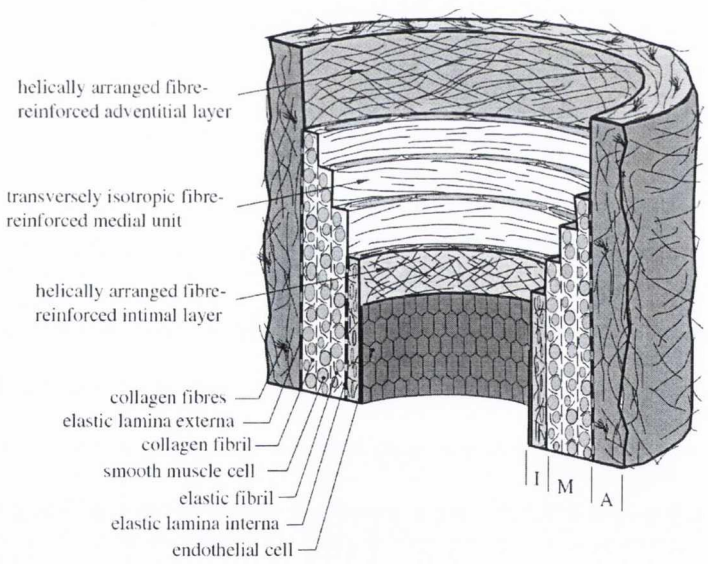

Figure 2.1: The structure of a healthy artery showing intimal, medial and adventitial layers and their components (Gasser et al., 2006)

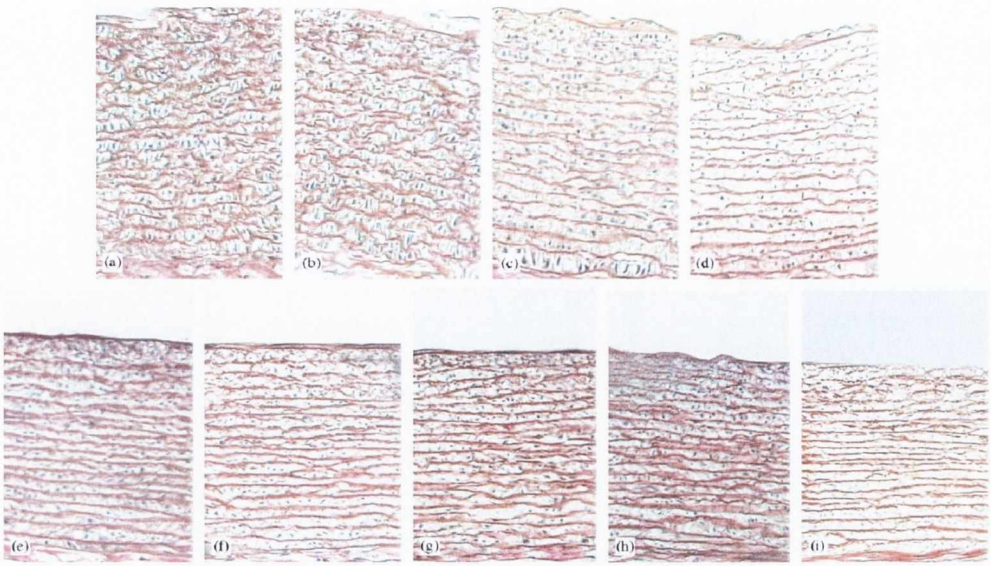

Figure 2.2: The wavy structure of elastic laminae and fibres straightens during loading. The elastic laminae and and fibres are stained orange and smooth muscle cell nuclei black. Loading increases gradually from (a) to (i) (Sokolis et al., 2006)

As mentioned the precise arterial structure varies depending on location. This is a result of the need for different functions in the body at various sites of the arterial tree. Arteries can be divided into two broad categories: elastic arteries and muscular arteries, see Fig. 2.3. Elastic arteries are generally characterised by large diameters and a high proportion of elastin in the media. Muscular arteries generally have a smaller diameter and a relatively thicker media which contains more smooth muscle than elastin or collagen fibres. Elastic arteries are generally located near the heart (e.g. aorta, common carotid) and the large elastin content allows for dissipation of the large pressure differences that occur during the cardiac cycle. Their larger cross-section allows a larger blood flow rate to feed into the smaller muscular arteries nearer the periphery without a significant drop in pressure. The smooth muscle cells in muscular arteries actively contract and expand in order to maintain pressure and blood flow rates.

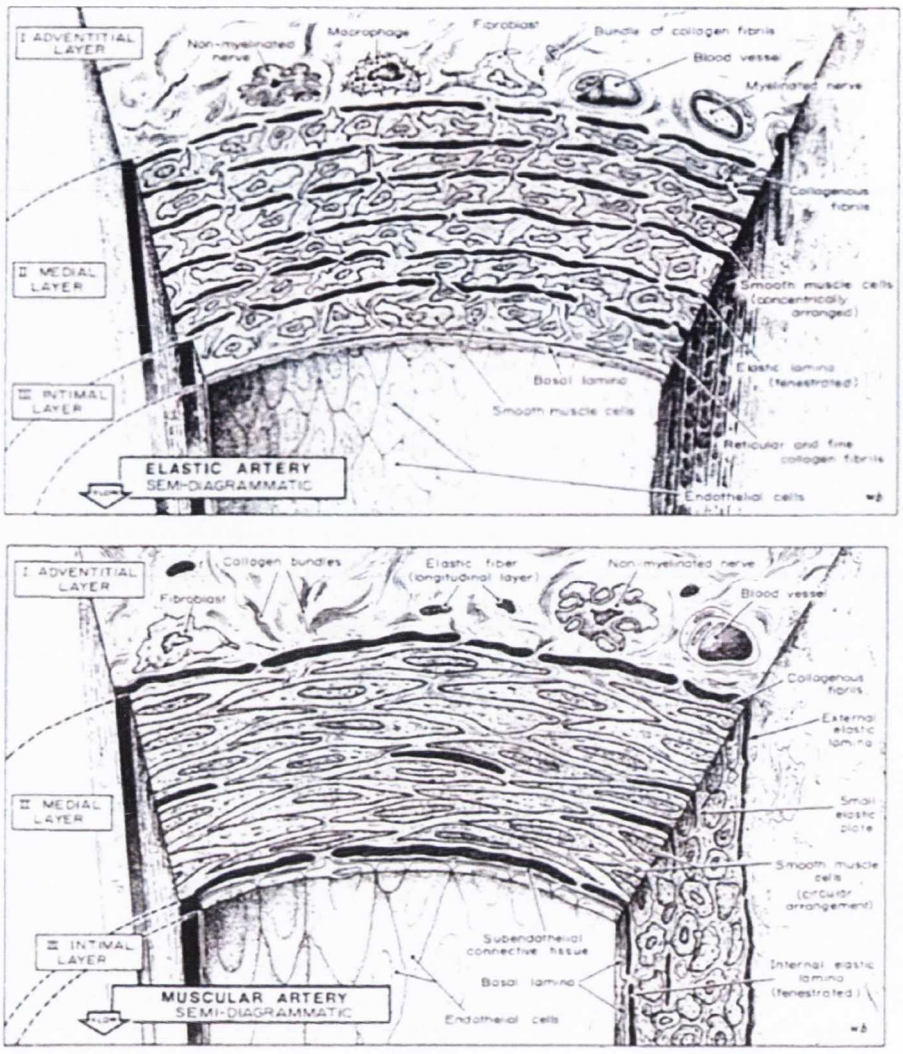

Figure 2.3: Cross-section of elastic (top) and muscular (bottom) arteries (Berne et al., 1979)

2.3 Pathology of Atherosclerosis

Atherosclerosis is a disease that occurs in the artery wall causing intimal thickening and often loss of patency in the artery. In most cases arterial lesion development occurs over a period of more than 40 years, with the early stages observed called fatty streaks occurring from the age of 11-12 (Insull, 2009). Libby (1995) summarised the development of atherosclerotic lesions as follows. Low-density lipoprotein (LDL) accumulates in the arterial wall. These LDLs are modified by enzymes and oxidised which provoke an inflammatory response: endothelial cells secrete adhesion

molecules and together with chemokines which are also secreted draw monocytes and T-cells into the arterial wall. The monocytes turn into macrophages in the intima and ingest the modified LDLs. The macrophages become filled with fat droplets and are now called foam cells. The foam cells and T-cells accumulate to become what is known as 'fatty streaks', the earliest stage of an atherosclerotic plaque. The plaque progresses as inflammatory molecules promote its growth and smooth muscle cells migrate from the media to the intima to form a fibrous plaque cap over the lipid core. With disease progression further inflammatory substances secreted by foam cells may weaken the plaque cap resulting in rupture and thrombus formation. Insull (2009) describes the development of atherosclerosis as a continuum of histological changes in the arterial wall in a similar way. It is also thought that injury to the vessel wall, whether mechanically or chemically induced, may result in or contribute to the initiation of atherosclerosis which would than progress as described above. Insull further describes atherosclerosis development in terms of a number of classes based on gross appearance. Five major classes were described: nonatherosclerotic intimal lesions; progressive atherosclerotic lesions; thin-cap fibroatheroma; calcified nodules; and fibrocalcific plaque. It was also discussed that some of these plaque classes, such as thin cap atheromas, may result in acute events due to thrombus formation, while others, like fibrocalcific plaques, may result in terminal cases due to advanced stenosis without thrombus, see Fig. 2.4.

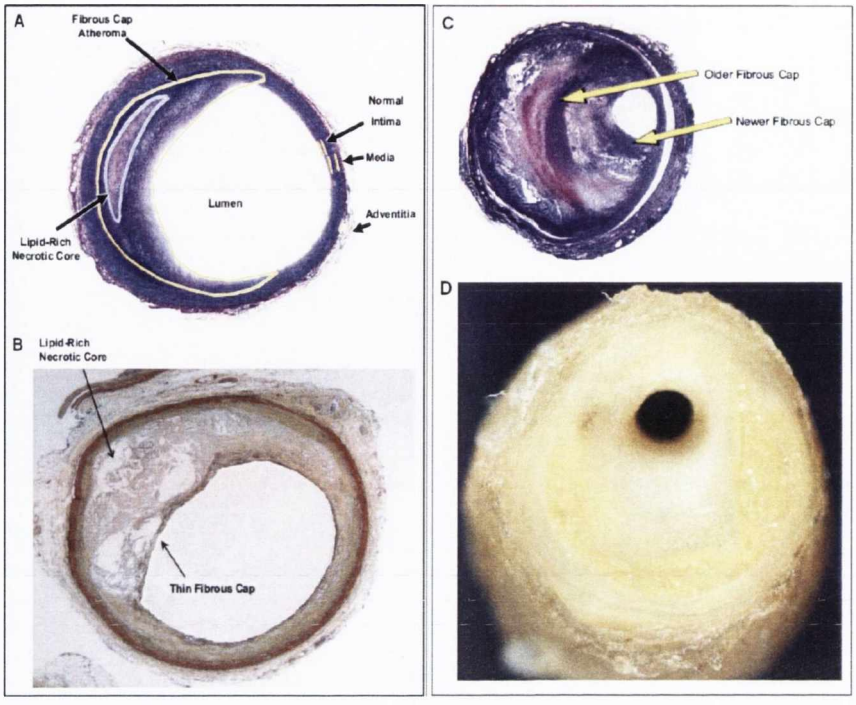

Figure 2.4: Histologic examples of 4 atherosclerotic plaque types. (A)Coronary fibrous cap atheroma in a 24-year-old man. (B)Thin fibrous cap atheroma. (C)Healed plaque rupture. (D) Stenosis of the anterior descending coronary artery in a 40-year-old man (Insull, 2009)

Stary et al (1995; 1994) give a more detailed analysis of similar classes of plaque. This class system is used by the America Heart Association and describes six main classes which incorporate the classes above. Classes I-III describe early to intermediate plaque development while classes IV-VI describe advanced lesions. Little change in the description of types I-III has occurred over time and they are not of significant clinical importance. The more advanced lesions are probably best described using a more updated classification (Stary, 2000) better able to describe the development of these advanced stages summarised in Fig. 2.5. Figure 2.5 illustrates the existence of more than one sequence of plaque evolution through the advanced plaque classifications. Type I and II lesions are characterised by an increase in the number of macrophages filled with foam cells with layers of these macrophages found in type II. Type II lesions can be divided by location into plaques formed at highly susceptible sites such as at the carotid bifurcation and sites that are less susceptible to plaque growth. The plaques at susceptible sites are more likely

to progress to type II lesions. The development of isolated small pools of extracelluar lipid describes this progression to type III lesions.

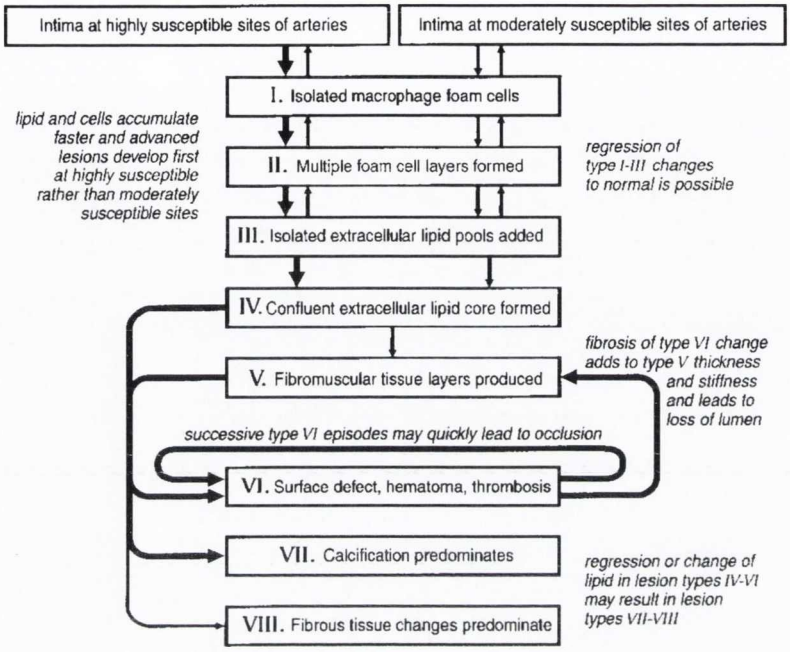

Figure 2.5: Sequence of evolution of atherosclerotic lesions (Stary, 2000)

Stage IV legions occur as the lipid pools accumulate to form a large lipid core which may become necrotic in some plaques as seen in Fig. 2.4. Increases in fibrous tissue formation characterise development into type V and VIII lesions, an increase in calcified tissue type VII and a disruption or damage of the lesion leading to thrombus formation type VI. As the plaque progresses the size of the plaque increases, especially between stages III and IV. However this increase in plaque size may not lead to a reduction in lumen size due to expansive remodelling of the vessel. Despite the lumen diameter not decreasing these lesions are still dangerous due to structural weaknesses (Naghavi et al., 2003). Plaque types IV, V, VII and VIII are all prone to disruption and are called vulnerable plaques. Naghavi et al (2003) discuss likely causes of clinical symptoms of vulnerable plaque formation from these advanced types, see Fig. 2.6.

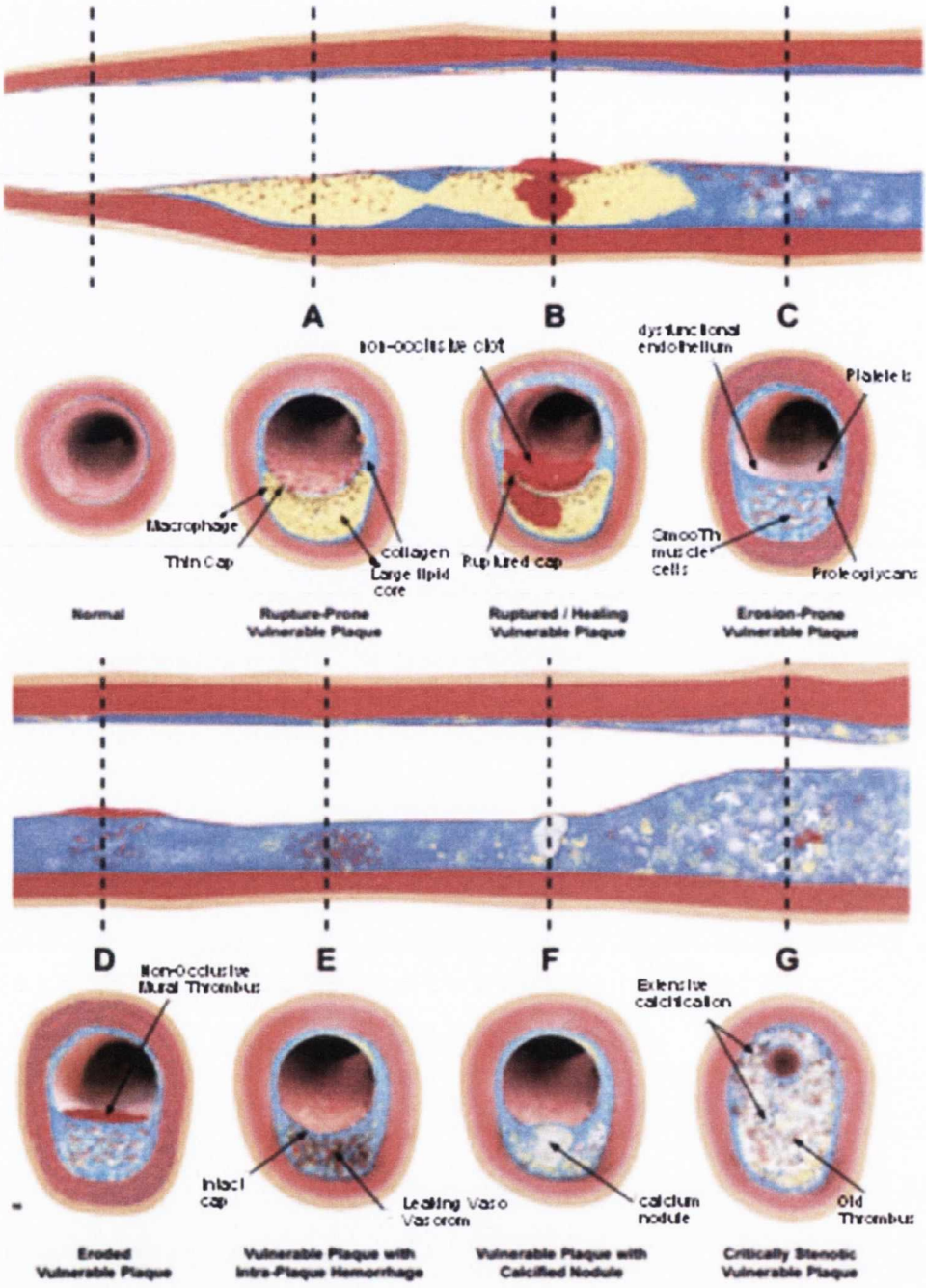

Figure 2.6: Types of vulnerable plaque as underlying causes for clinical symptoms, adapted from Naghavi et al (2003)

2.4 Soft tissue mechanical properties

2.4.1 Stress-state in the arterial wall

In order to design the experimental testing protocol that most appropriately determines the mechanical behaviour of both healthy and diseased arterial tissue it is important to understand the stress-state induced in the tissue as a result of arterial geometry. Arteries like many soft tissues are pressurised soft tubes (Humphrey and Delange, 2004). In some soft tissues such as veins or aneurysms it is appropriate to assume that the thickness of the wall is significantly less than the inner radius of the vessel and analysing the tissue as a thin-walled pressurised cylinder. In arteries however, the thickness of the vessel wall relative to its internal radius generally means considering the artery as a thick-walled cylinder. To add to the complexity of the problem, the structure of the artery wall leads to a highly nonlinear, anisotropic response. Furthermore the zero stress-state of the artery does not correspond to the unloaded state of an intact artery. In their i*n vivo* state, arteries are pre-stressed, which can be observed by the shortening of an arterial segment axially when excised from a body and the opening of the segment when cut along its length, see Fig 2.7. Pre-stressing of a thick walled cylinder acts to smooth the stress gradients within the arterial wall.

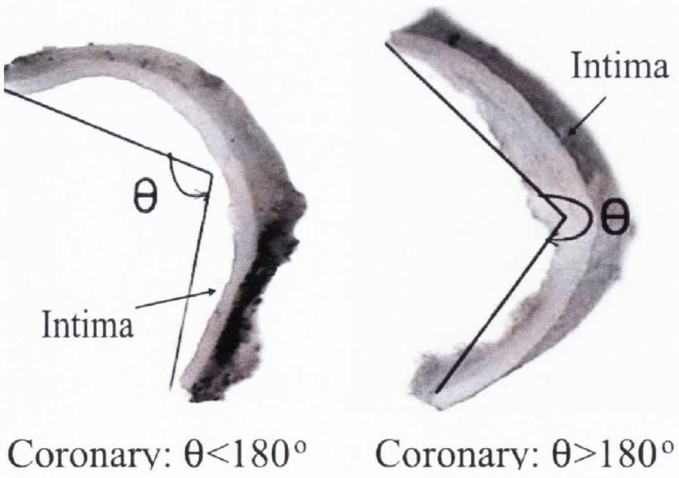

Figure 2.7: Photos of coronary rings cut radially to reveal sectors with opening angles < 180° (left) and > 180° (right). (Guo et al., 2005)

Solving the thick-walled cylinder problem in which large deformations and non-linear material behaviour must be incorporated is challenging. Nonetheless, much important information

on the stress-state in arteries can be illustrated by considering the simplest thick-walled cylinder problem: that of a cylinder pressurised to small strains that exhibits linear elastic, homogeneous and isotropic (LEHI) behaviour, see Fig. 2.8. Figure 2.8 shows the stress-state in the circumferential, σ_t, and radial, σ_r, directions in a thick-walled cylinder.

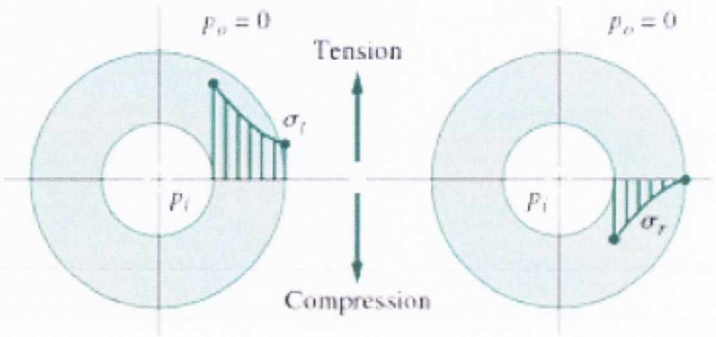

Figure 2.8: Tangential and radial stress distributions across the wall thickness of an internally pressurised thick-walled cylinder (Collins et al., 2009)

The stress equations of equilibrium for this problem can be expressed generally as:

$$\frac{\partial \sigma_r}{\partial r} + \frac{1}{r}\frac{\partial \tau_{r\theta}}{\partial \theta} + \frac{\partial \tau_{rz}}{\partial z} + \frac{\sigma_r - \sigma_\theta}{r} = 0$$

$$\frac{\partial \tau_{\theta r}}{\partial r} + \frac{1}{r}\frac{\partial \sigma_\theta}{\partial \theta} + \frac{\partial \tau_{\theta z}}{\partial z} + 2\frac{\tau_{\theta r}}{r} = 0 \qquad \text{(Eqn. 2.1)}$$

$$\frac{\partial \tau_{zr}}{\partial r} + \frac{1}{r}\frac{\partial \tau_{z\theta}}{\partial \theta} + \frac{\partial \sigma_z}{\partial z} + \frac{\tau_{zr}}{r} = 0$$

Where *r, θ and z* refer to the radial, circumferential and longitudinal directions respectively, σ the normal stress and τ the shear stress. For this simplified problem it is further assumed that the artery is completely axisymmetric, i.e. $\partial/\partial\theta = 0$, and that there are no variations in stress axially, i.e. $\partial/\partial z = 0$ (Humphrey and Delange, 2004). Due to uniform radial expansion and symmetry we also have the relationships $\tau_{rz} = \tau_{\theta z} = \tau_{r\theta} = 0$. The equilibrium equations thus simplify to:

$$\frac{\partial \sigma_r}{\partial r} + \frac{\sigma_r - \sigma_\theta}{r} = 0 \qquad \text{(Eqn. 2.2)}$$

Combining this equilibrium equation with the standard equations for the three principal strains for LEHI behaviour and integrating for the stress gives the following relationships.

$$\sigma_r = \frac{P_i {r_i}^2 - P_o {r_o}^2}{{r_o}^2 - {r_i}^2} - \frac{(P_i - P_o){r_i}^2 {r_o}^2}{r^2({r_o}^2 - {r_i}^2)}$$

$$\sigma_\theta = \frac{P_i {r_i}^2 - P_o {r_o}^2}{{r_o}^2 - {r_i}^2} + \frac{(P_i - P_o){r_i}^2 {r_o}^2}{r^2({r_o}^2 - {r_i}^2)} \qquad \text{(Eqn. 2.3)}$$

where σ_r and σ_θ are the radial and circumferential stress respectively, P_i and P_o are the internal and external pressure applied to the cylinder, r_i and r_o are the internal and external radii of the cylinder and r is the radius at which the stress is being calculated. The full derivation can be found in Humphrey and Delange (2004), Section 3.6. If we assume that the external pressure is zero, as is the case in the majority of structural analyses of arteries, Eqn. 2.3 reduces to

$$\sigma_r = \frac{P_i {r_i}^2}{{r_o}^2 - {r_i}^2}\left(1 - \frac{{r_o}^2}{r}\right) \qquad \sigma_\theta = \frac{P_i {r_i}^2}{{r_o}^2 - {r_i}^2}\left(1 + \frac{{r_o}^2}{r}\right) \qquad \text{(Eqn. 2.4)}$$

It is thus clear that for an internally pressurised thick walled cylinder (e.g. an artery) the circumferential stress will be greater in magnitude than the radial stress. Furthermore the stress-state in the longitudinal direction needed to maintain vessel length during expansion (i.e. assuming vessel tethering) can be derived as (Humphrey and Delange, 2004),

$$\sigma_z = \frac{P_i {r_i}^2}{{r_o}^2 - {r_i}^2} = \frac{P_i {r_i}^2}{2at + t^2} \qquad \text{(Eqn. 2.5)}$$

for an incompressible material. t is the thickness of the cylinder. It can be seen that the longitudinal stress has a greater magnitude than the radial stress but less than the circumferential stress in this idealised case. This explains why studies of healthy arterial tissue commonly focus on circumferential and longitudinal tensile behaviour. However it should be noted that the differences in the stresses is dependent on the external and the radius at which the stress is being calculated (i.e. r_o/r) and that the significant thickening of an artery due to the development of atherosclerosis can result in the differences in magnitudes of the circumferential and radial stresses at the inner

surface to be much less significant, see Fig. 2.9. As a result radial compressive studies of atherosclerotic plaques are much more common as described later in this chapter. The effect that the residual stresses in the artery wall have is to reduce the magnitude of the circumferential and longitudinal stresses and to homogenise the stresses across its thickness, see Fig. 2.10. As the radial stress at the inner cylinder wall is determined by the boundary condition $\sigma_r = -P_i$ the ratio of the magnitudes of the circumferential and residual stresses at the inner surface due to an applied internal pressure will be reduced when considering residual strains. For a more detailed analysis of large strain deformations of thick-walled cylinder including residual stresses see Humphrey (2002).

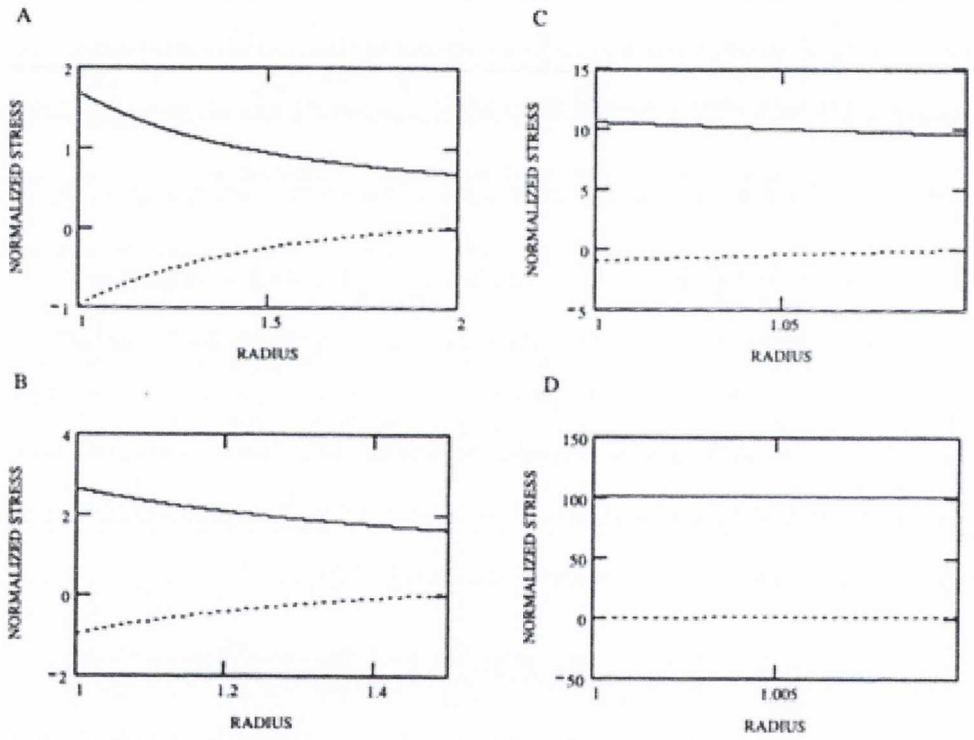

Figure 2.9: Computed transmural stress distributions in a thick-walled cylinder. Stresses are normalised by the internal pressure P_i, giving σ_θ/P_i (solid curves) and σ_r/P_i (dashed curves)Results are considered for different sets of inner and outer radii: for A, $r_i = 1$ and $r_o = 2$; in B $r_i = 1$ and $r_o = 1.5$; in C $r_i = 1$ and $r_o = 1.1$; in D $r_i = 1$ and $r_o = 1.01$.

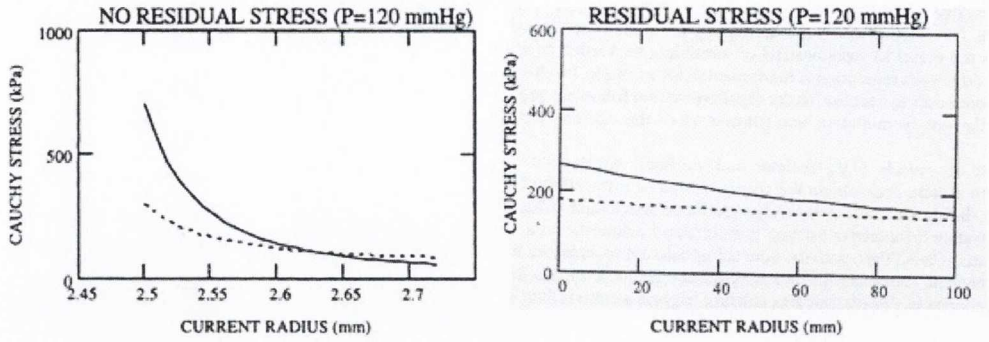

Figure 2.10: Predicted transmural distribution of circumferential (solid line) and axial (dashed line) stresses in an internally pressurised thick walled cylinder where it is assuming no residual stress and residual stress is present respectively.

2.4.2 Arterial mechanics

Arterial tissue has a highly nonlinear response to loading which is most often attributed to the mechanical properties of elastin and collagen, where the artery is considered to be composed of wavy collagen fibres embedded in an elastin matrix. At low strains the less stiff elastin bears the load. As strain is increased the collagen fibres straighten and are *recruited*, see Fig. 2.2. The collagen fibres are significantly stiffer than the elastin (Burton, 1954; Milnor, 1982) and as they begin to bear load the artery stiffens considerably. Experiments by Roach et al illustrate this behaviour well (Roach and Burton, 1957). These experiments investigated the individual contribution of collagen and elastin by selectively digestion of artery samples in order to isolate the elastin and collagen. A comparison between elastin, collagen and an untreated artery is shown in Fig. 2.11. Arteries are also generally considered to be an incompressible tissue based on measuring volume changes due to loading (Carew et al., 1968; Girerd et al., 1992). Radial compression tests have shown that arterial tissue is only slightly compressible at physiological load levels in compression (Chuong and Fung, 1984) and thus an incompressible (or nearly incompressible) assumption is generally appropriate.

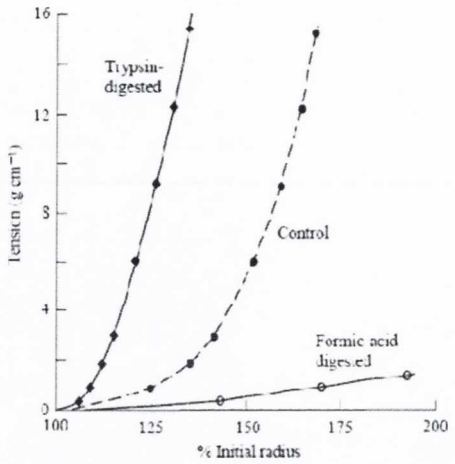

Figure 2.11: Comparison of mechanical response of elastin (formic acid treated artery), collagen (artery treated with trypsin) and untreated artery wall (control). (Roach and Burton, 1957)

A number of studies have investigated the mechanical properties of arterial tissue. A large number of these have been performed on animal arteries (Bund et al., 1996; Lally et al., 2004; Vito and Demiray, 1982; Zhou and Fung, 1997). Many of the earlier studies were performed on arteries harvested from canines (Gow et al., 1974; Zhou and Fung, 1997) or rats (Cox, 1977; Zanchi et al., 1998). More recently however it has been more common for these studies to use porcine arteries (Dixon et al., 2003; Lally et al., 2004; Stemper et al., 2007a) as porcine arteries are more anatomically similar to human arteries than those of other animals (Swindle and Moody, 1992). The reason for testing animal tissue is the relative difficulty in obtaining fresh human tissue samples (Lally et al., 2004). Despite these anatomical similarities comparative studies have shown that porcine and human arteries behave differently both in loading (van Andel et al., 2003) and in failure (Stemper et al., 2007a). This shows the importance of testing human tissue whenever possible. There have been comparatively fewer studies exploring the mechanical properties of human arterial tissue (Carmines et al., 1991; Holzapfel et al., 2005; Ozolanta et al., 1998; Schulze-Bauer et al., 2003).

A number of testing methodologies have been used to characterise arterial behaviour. Three common methodologies are inflation extension tests (Fung and Liu, 1995; Schulze-Bauer et al., 2003), uniaxial tests (Holzapfel et al., 2005; Stemper et al., 2007a) and biaxial tests (Lally et al.,

2004). Uniaxial tests are tests where a strip or dog-bone shaped sample is loaded in one direction; biaxial tests are where a square artery wall segment is loaded in two directions; and inflation extension tests are where intact artery segments are inflated, usually with a pressurised gas or liquid, while an axial force is applied to the arteries. As the artery is loaded circumferentially and axially in an inflation extension test it is considered a type of biaxial test. A reason for performing biaxial testing is that early studies indicated that arteries were anisotropic (Cox, 1975) and more recent mechanical testing has confirmed the anisotropic nature of arterial tissue (Schulze-Bauer et al., 2003; Zhou and Fung, 1997). Histological studies have shown that collagen fibres have orientations within the artery layers that would greatly contribute to the observed anisotropy, see Fig. 2.12 (Holzapfel, 2006). An advantage of uniaxial testing is a smaller sample size is necessary than with biaxial testing. To account for the anisotropy of the tissue with uniaxial tests researchers have performed tensile tests in both circumferential and axial directions for the one artery (Holzapfel et al., 2005; Holzapfel et al., 2002).

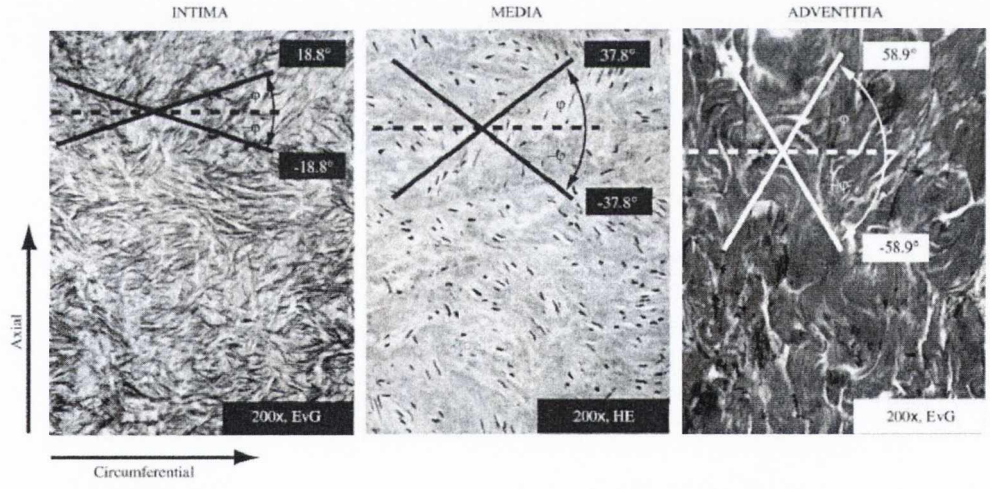

Figure 2.12: Contrast enhanced histological images of intimal, medial and adventitial strips with a circumferential orientation. Mean fibre directions for each layer are indicated by lines and angles on each image. (Holzapfel, 2006).

Arteries consist of three distinct concentric layers: the intima, media and adventitia. The differences between each layer can be seen with histology, see Fig. 2.12 (Holzapfel, 2006; Holzapfel et al., 2005). While testing the intact artery's mechanical behaviour can be considered

appropriate as the artery will behaviour in vivo should be similar to the testing data, a layer specific experimental approach can give a better understanding of artery mechanical function at a tissue level (Holzapfel et al., 2005). A few studies have performed layer specific testing on arteries. Some of these have separated the arteries into two layers for testing, an intima and media layer and an adventitia layer (Fung and Liu, 1995; Pandit et al., 2005).

One of the more comprehensive studies mechanically tested all three of the layers separately, see Fig. 2.13 (Holzapfel et al., 2005). The results of these studies indicate that in aged humans the intima is the stiffest of the three arterial layers and hence the most mechanically significant layer in both loading directions, see Fig. 2.13. Holzapfel et al (2005) further showed that the intima and media had similar ultimate tensile strengths but that the ultimate tensile strength of the adventitia was significantly higher. It was also seen that while the media was stiffer in the circumferential direction, the intima and adventitia were generally stiffer in the longitudinal direction, highlighting the composite nature of arterial tissue.

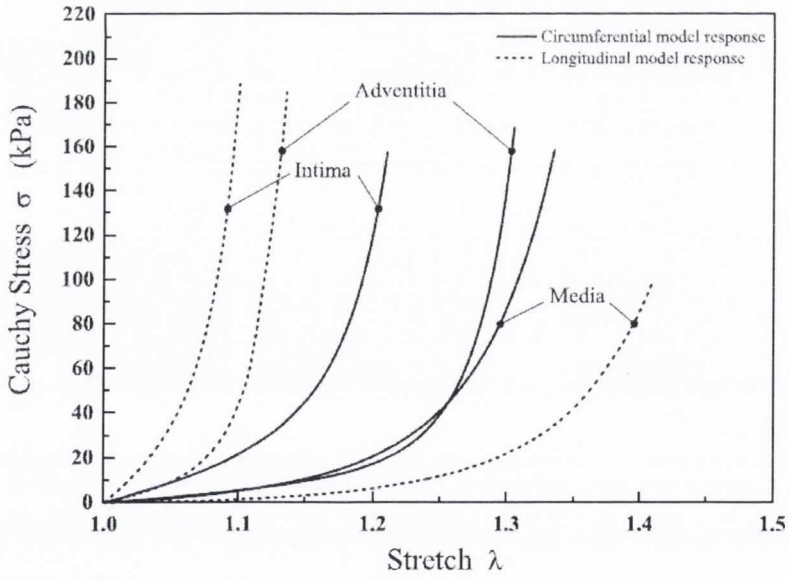

Figure 2.13: Mean arterial layer behaviour due to uniaxial loading in circumferential and longitudinal directions (Holzapfel et al., 2005)

Arteries are not a truly elastic material. In a truly elastic material the loading and unloading behaviour of the material are the same. In arterial tissue there is a difference between the loading and unloading response. Fung et al (1979) coined the term pseudoelasticity to describe this difference in behaviour. In the physiological pressure range arteries exhibit a phenomenon known as preconditioning when cyclically loaded and unloaded, where the arterial response softens for a number of cycles before reaching an equilibrium state, see Fig. 2.14. A difference in the loading and unloading curves is still present in the equilibrium state and this behaviour is known as hysteresis. Arteries display other viscoelastic responses such as creep at physiological levels. Beyond the elastic range of the material however (point I in Figure 2.15) arteries experience a significant softening effect during the first loading cycle and exhibit residual inelastic (non-vanishing) strains on unloading. These behaviours are thought to be the result of elastoplastic and/or damage mechanisms (Holzapfel et al., 2000).

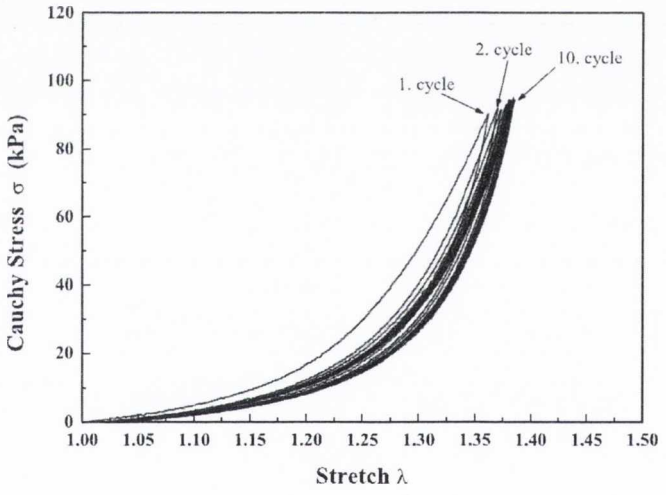

Figure 2.14: Preconditioning behaviour of healthy human coronary intimal tissue (Holzapfel et al., 2005)

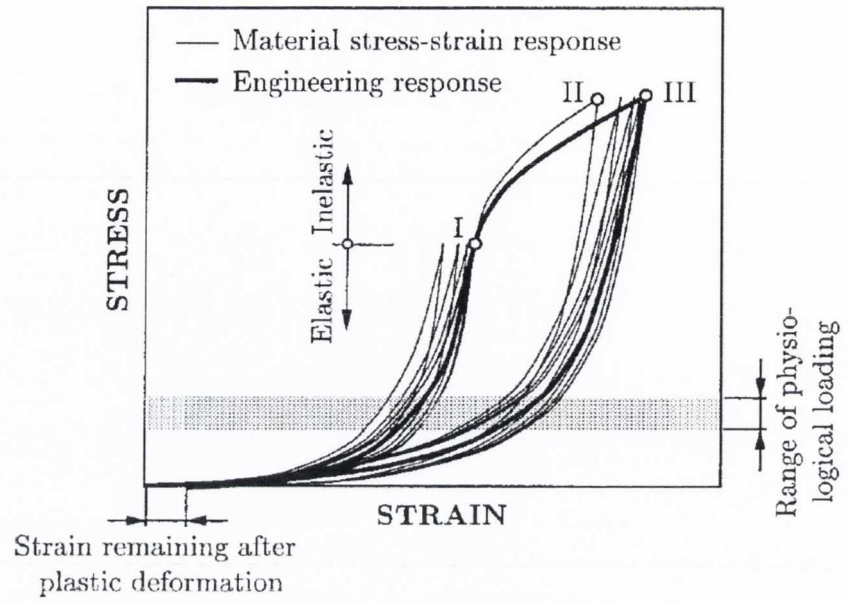

Figure 2.15: Typical stress-strain behaviour of arterial tissue tested in cyclic uniaxial tension. Point I represents the limit of (visco) elastic response. Loading beyond this point (to point II) induces significant softening and inelastic strains. Repeated cycles result in further softening (preconditioning response) until point III is reached. (Holzapfel et al., 2000)

2.4.3 Atherosclerotic plaque mechanics

Little experimental data has been presented on the mechanical properties of atherosclerotic plaques. The absence of sufficient test data impedes our complete understanding of plaque behaviour and inhibits our ability to adequately use finite element modelling to predict lesion response to stenting or angioplasty. Of the few studies of the mechanical properties of atherosclerotic plaques the majority have been radial compressive tests of aortic tissue. To compound the lack of mechanical test data a consistent plaque classification methodology has not been used. Lee et al classified plaques by histological examination as hypocellular, cellular or calcified (Lee et al., 1991) and in another study as fibrous, non-fibrous and calcified using intravascular ultrasound classifications (Lee et al., 1992). Loree et al (Loree et al., 1994) used the same histological classification as above while histology has been used to classify plaques as fibrous, calcified or atheromatous plaque(Salunke et al., 2001; Topoleski and Salunke, 2000; Topoleski et al., 1997). Finally hrMRI has been used to divide complex plaque morphologies into components including diseased

(fibrous) and non-diseased (no appreciable disease) media and intima (Holzapfel et al., 2004). Only some studies performed testing at 37 °C (Holzapfel et al., 2004; Salunke et al., 2001; Topoleski et al., 1997).

Lee et al (1991) dynamically tested the fibrous cap of abdominal aortic plaques in radial compression as well as analysing the plaque cap creep behaviour and related their findings to the histological cap classification. It was found that hypocellular caps were 1-2 times stiffer than cellular and calcified were 4-5 times as stiff. The plaque stiffness was also found to be frequency dependant. It was observed that the creep strains were highest in cellular samples and lowest in calcified samples. In a further study Lee et al (1992) performed radial compression relaxation tests on abdominal aortic plaque caps. These results were compared to classifications from intravascular ultrasound imaging and it was found that non-fibrous plaque caps had the lowest static stiffness and longest relaxation time, calcified caps had the highest stiffness and lowest relaxation times and fibrous caps had values in between the other classifications. It was again seen that the lowest creep strains were found in calcified plaques while the highest were observed in non-fibrous ones. The data on dynamic stiffness and creep indicate that atherosclerotic plaques are not elastic materials and display viscoelastic behaviour. In contrast to the study above, Loree et al (1994) found no significant difference between the static circumferential tangential moduli of hypocellular, cellular and calcified plaques and further concluded after comparison to the previously mentioned study (Lee et al., 1992) that cellular and hypocellular plaques were anisotropic in the physiological loading range. The study by Loree et al was one of only two studies to test the tensile properties of atherosclerotic plaques.

Topoleski et al (1997) investigated cyclic compressive behaviour in aortoiliac plaques. Three types of plaque behaviour were identified based on the concepts of repeatability and recoverability and related to results from histology, see Fig. 2.16. Two cyclic loading phases of 15 cycles were applied with an unloaded rest period in between. Repeatability was defined as the stabilisation of the stress-strain response during cyclic loading (as with preconditioning discussed earlier for healthy arteries) and if the behaviour during the second phase of loading matched the

first phase the sample was recoverable. Type 1 behaviour was characterised by repeatability and recoverability and was found only in plaques containing calcified tissue. Type 2 behaviour was repeatable but only partially recoverable and was found in samples containing fibrous tissue and modified media. Type 3 behaviour was found in samples where recovery was absent and was observed for atheromatous plaques. This is the only paper to date to discuss unrecoverable inelastic behaviour of plaques loaded beyond the physiological domain. Salunke et al (2001) studied the compressive stress relaxation behaviour of aortoiliac plaques when subjected to successive stress relaxation tests and compared the results to histology and to similar tests on healthy vessels. They found that during the initial loading cycle to 25% compressive stretch that calcified and fibrous plaques behaved similarly and that both were stiffer than atheromatous plaques. It was further found that the calcified and fibrous plaques relaxation responses were similar for successive tests although they didn't reach the same peak stress on loading.

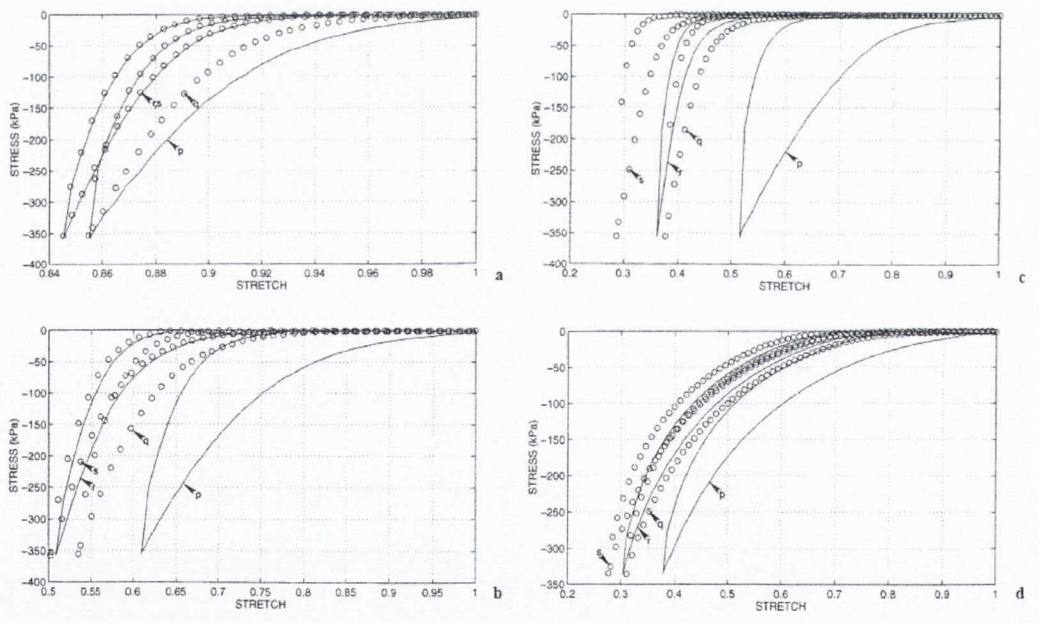

Figure 2.16: (a) Type 1 behaviour of calcified plaques. (b) Type 2 behaviour of fibrous plaques. (c) Type 3 behaviour of atheromatous plaques. (d) Type 3 behaviour of healthy arterial tissue. The 1st and 15th cycle of phase I and phase II loading are shown: p indicating 1st cycle in phase I, q first cycle of phase II, r 15th cycle of phase I and s the 15th cycle of phase II. (Topoleski et al., 1997)

Holzapfel et al (2004) performed probably the most in depth study of the mechanical properties of atherosclerotic plaque to date. The anisotropic behaviour of the constituent components of diseased iliac arteries was investigated. Each artery specimen was separated into its different artery and plaque component layers, as determined by high resolution MRI, and tested in biaxial tension. Only the lipid pool was excluded from mechanical testing, however it was noted that it is usual to assume the lipid pool behaves as a nearly incompressible fluid in finite element analyses. The authors saw marked heterogeneity in lesions histologically and using high resolution MRI. The tissues were found to behave in a non-linear and anisotropic way, with little hysteresis occurring. In general it was seen that the diseased layers were found to be stiffer than healthy arterial tissue, see Fig. 2.17. The study also reported ultimate failure stresses and stretches and found significant differences between layers. The lowest fracture stresses were seen in the fibrous cap. All the studies mentioned above have been performed on cadaveric material.

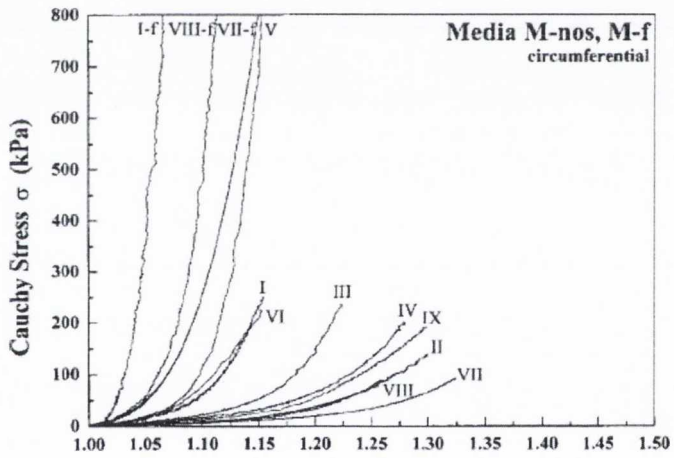

Figure 2.17: Uniaxial tensile stress-stretch response of human medial tissue in the circumferential direction. Labels I-IX refers to healthy media samples taken from different plaque specimens respectively. I-f, VII-f and VIII-f refer to fibrotic (diseased) media s samples taken from the respective specimens (Holzapfel et al., 2004).

2.5 Constitutive modelling of arterial tissue

As arteries exhibit highly non-linear behaviour as described in the previous section, their constitutive behaviour is commonly described by a hyperelastic constitutive model. This section gives a brief description of the constitutive relationship of a hyperelastic material. For a more detailed discussion of hyperelastic material behaviour and the full derivations of the equations in this section refer to Holzapfel (2000) or Humphrey (2002). Constitutive modelling of arterial tissue and other soft tissues previously described in the literature is also discussed.

2.5.1 Basic kinematics

If we consider a particle with position **X** in the undeformed configuration Ω_0 that is deformed and has position **x** in the deformed configuration Ω (Fig. 2.18) we can define the displacement field vector, **U** as:

$$\mathbf{U}(\mathbf{X}, t) = \mathbf{x}(\mathbf{X}, t) - \mathbf{X} \quad \text{(Eqn. 2.6)}$$

U is a function of the referential position **X** and time t which characterise the material (Langrangian) description of the displacement field. If the displacement vector was in terms of the current position x and t we would have the displacement field in the spatial (Eulerian) description.

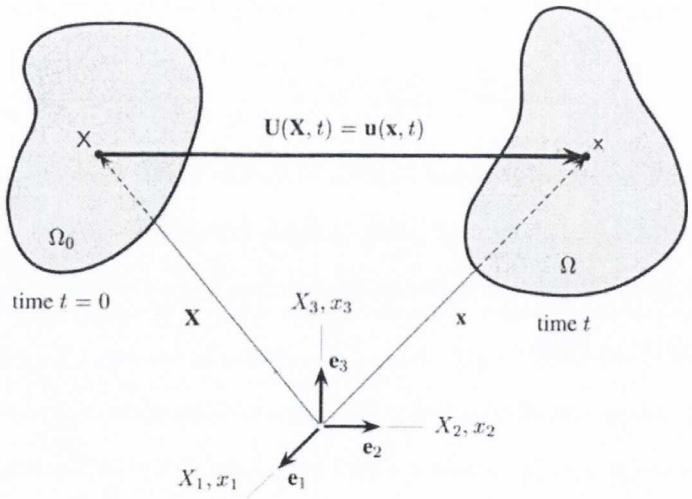

Figure 2.18: Displacement field of a particle (Holzapfel, 2000)

For a continuum body the deformation gradient tensor, **F**, is used to fully describe the deformation of the body. **F** describes the change in an infinitesimal line element, connecting a point in the body to a neighbouring point ($d\mathbf{X}$ in the reference configuration and $d\mathbf{x}$ in the deformed). The deformation gradient tensor is defined as the gradient of the transformation $\mathbf{x}(\mathbf{X}, t)$ with respect to the material coordinates **X** at a given time. Another way of stating this is that if a material vector in the initial undeformed configuration $d\mathbf{X}$ becomes the vector $d\mathbf{x}$ when under loading in the deformed configuration, the deformation gradient tensor is given by Eqn. 2.7. A characterisation of any quantity of a material (e.g. motion, stress, etc.) with respect to the undeformed coordinates (undeformed configuration) is referred to as being in the material or Lagrangian description. The spatial or Eulerian description is a characterisation of a quantity with respect to the deformed configuration.

$$F_{ij} = \frac{\partial x_i}{\partial X_j} \qquad \text{(Eqn. 2.7)}$$

where dx_i and dX_j are the components of the material vector in the deformed and undeformed configurations. The deformation gradient tensor can also be related to the gradient of the displacement field.

$$\mathbf{F} = \mathbf{I} + Grad[\mathbf{u}] \qquad where \qquad Grad[\mathbf{u}] = \frac{\partial \mathbf{u}(\mathbf{X},t)}{\partial \mathbf{X}} \qquad \text{(Eqn. 2.8)}$$

The deformation gradient tensor is not objective. Objectivity is defined here as an indifference (or invariance) to changes in the frame of reference, that for example may occur through translation or rigid body rotation. Objective measures of deformation can be calculated from the deformation gradient tensor such as the right Cauchy-Green deformation tensor, **C**, Eqn. 2.9, or the Green-Lagrange strain tensor, **E**, Eqn. 2.10.

$$\mathbf{C} = \mathbf{F}^T\mathbf{F} \qquad \text{(Eqn. 2.9)}$$

$$\mathbf{E} = \frac{1}{2}(\mathbf{C} - \mathbf{I}) \qquad \text{(Eqn. 2.10)}$$

where **I** is the identity matrix, where $I_{ij} = 1$ when $i = j$ and $I_{ij} = 0$ otherwise. The principal strain invariants can be given as a function of the right Cauchy-Green strain tensor or the principal stretches.

$$I_1 = tr(\mathbf{C}) = \lambda_1^2 + \lambda_2^2 + \lambda_3^2 \qquad \text{(Eqn. 2.11)}$$

$$I_2 = \frac{1}{2}\left[tr(\mathbf{C})^2 - tr(\mathbf{C}^2)\right] = \lambda_1^2\lambda_2^2 + \lambda_1^2\lambda_3^2 + \lambda_2^2\lambda_3^2 \qquad \text{(Eqn. 2.12)}$$

$$I_3 = \det(\mathbf{C}) = \lambda_1^2\lambda_2^2\lambda_3^2 = J^2 \qquad \text{(Eqn. 2.13)}$$

where I_i and λ_i, $i = 1, 2, 3,$ are the principal strain invariants and principal stretches respectively. J is the determinant of **F**, commonly referred to simply as the Jacobian determinant or the volume ratio. It represents the change in volume of the material ($J = 1$ for an incompressible material) and is given by:

$$J = \det(\mathbf{F}) = \lambda_1\lambda_2\lambda_3 \qquad \text{(Eqn. 2.14)}$$

2.5.2 Stress

In an externally loaded body an internal loading state will be generated that can be described by a vector known as the traction vector which is the force measured per unit surface area and is a function of the normal to the cross-section orientation and the position at a given time. Cauchy's stress theorem states that there exist unique second-order tensors $\boldsymbol{\sigma}$ and **P** such that:

$$\mathbf{t}(\mathbf{x}, t, \mathbf{n}) = \boldsymbol{\sigma}(\mathbf{x}, t)\mathbf{n} \qquad \mathbf{T}(\mathbf{X}, t, \mathbf{N}) = \mathbf{P}(\mathbf{X}, t)\mathbf{N} \qquad \text{(Eqn. 2.15)}$$

where **t** and **T** are the Cauchy traction tensor (force per unit surface area in the current configuration) and the first Piola-Kirchhoff traction tensor (force per unit surface area in the reference configuration). **n** and **N** are the normals to the orientation of the cross-section in the current and reference configurations. $\boldsymbol{\sigma}$ is the Cauchy stress tensor and represents the real stresses inside the body associated to the actual deformed configuration. **P** is the first Piola-Kirchhoff stress tensor which is a generally unsymmetric tensor describing stress in the reference configuration. **P** is also commonly known as the nominal stress tensor. As **P** is not objective another stress measure is commonly used in nonlinear solid mechanics. The 2nd Piola-Kirchhoff stress can be defined as:

$$\mathbf{S} = \mathbf{F}^{-1}\mathbf{P} = J\mathbf{F}^{-1}\boldsymbol{\sigma}\mathbf{F}^{-T} \qquad \text{(Eqn. 2.16)}$$

2.5.3 Isotropic hyperelastic material

For a hyperelastic material there exists a Helmholtz free energy function, ψ, which can be expressed as a function of the deformation of the material; usually the right Cauchy-Green strain tensor, **C**, its invariants $I_1(\mathbf{C})$, $I_2(\mathbf{C})$, $I_3(\mathbf{C})$ (Eqn. 2.11 - 2.13) or the principal stretches λ_1, λ_2, λ_3, see Eqn. 2.17. ψ is a measure of the internal strain-energy potential of the material.

$$\psi(C) = \psi(I_1(\mathbf{C}), I_2(\mathbf{C}), I_3(\mathbf{C})) = \psi(\lambda_1, \lambda_2, \lambda_3) \qquad \text{(Eqn. 2.17)}$$

For an incompressible material the Jacobian is equal to 1 as there is no change in volume of the material. Stresses in the material can be determined by differentiating the strain-energy function with respect to the deformation. In this case the second Piola-Kirchhoff stress, S, is said to be work conjugate to the Green-Lagrange strain and is given by

$$\mathbf{S} = \frac{\partial \psi}{\partial \mathbf{E}} = 2\frac{\partial \psi}{\partial \mathbf{C}} \qquad \text{(Eqn. 2.18)}$$

Work conjugate pairs are variables whose products give us a measure of work done or the change in energy. The second Piola-Kirchhoff stress is a stress measure in the material description. If the

strain-energy function is given in terms of the strain invariants the chain rule can be used to determine **S**.

$$\mathbf{S} = 2\sum_{a=i}^{3} \frac{\partial \psi(I_1, I_2, I_3)}{\partial I_a} \frac{\partial I_a}{\partial \mathbf{C}} \qquad \text{(Eqn. 2.19)}$$

where the derivatives of the invariants with respect to **C** are defined below.

$$\frac{\partial I_1}{\partial \mathbf{C}} = \mathbf{I} \qquad \text{(Eqn. 2.20)}$$

$$\frac{\partial I_2}{\partial \mathbf{C}} = I_1\mathbf{I} - \mathbf{C} \qquad \text{(Eqn. 2.21)}$$

$$\frac{\partial I_3}{\partial \mathbf{C}} = I_3\mathbf{C}^{-1} \qquad \text{(Eqn. 2.22)}$$

Substituting Eqns. 2.20-2.22 into Eqn. 2.19 gives a general form of the second Piola-Kirchhoff stress in terms of the three strain invariants. Once the second Piola-Kirchhoff stress has been defined we can define other stress measures. As it is used in finite element modelling, and commercial finite element packages such as Abaqus, the Cauchy stress is the most important here. The Cauchy (or true) stress is a stress measure with respect to the spatial (or deformed) configuration. It can be found using a scaled push forward transformation called the Piola transformation, which can be found by finding $\boldsymbol{\sigma}$ from Eqn. 2.16, i.e. $\boldsymbol{\sigma} = (1/J)\mathbf{F}\mathbf{S}\mathbf{F}^T$.

The elasticity tensor is a tensor that forms a relationship between the stress and strain tensors. The material representation of the elasticity tensor $\mathbb{C}$ can be defined by differentiating the second Piola-Kirchhoff stress with respect to the right Cauchy-Green strain, Eqn. 2.23. $\mathbb{C}$ is said to possess major and minor symmetries, (Eqn. 2.24).

$$\mathbb{C} = 2\frac{\partial \mathbf{S}(\mathbf{C})}{\partial \mathbf{C}} = 4\frac{\partial^2 \psi(\mathbf{C})}{\partial \mathbf{C}^2} \qquad \text{(Eqn. 2.23)}$$

$$\mathbb{C}_{ABCD} = \mathbb{C}_{CDAB} \qquad \mathbb{C}_{ABCD} = \mathbb{C}_{BACD} = \mathbb{C}_{ABDC} \qquad \text{(Eqn. 2.24)}$$

The spatial representation of the elasticity tensor, $\mathbb{c}$, can be given by performing a push forward operation on $\mathbb{C}$ scaled by J^{-1}. This is termed the Piola transformation of $\mathbb{C}$.

$$\mathbb{c}_{abcd} = J^{-1}\chi * (\mathbb{C}) = J^{-1}F_{aA}F_{bB}F_{cC}F_{dD}\mathbb{C}_{ABCD} \qquad \text{(Eqn. 2.25)}$$

For Abaqus material models the Jaumann tangent modulus, $\mathbb{C}^{\tau J}$, needs to be defined for a solution to converge. For a description on how $\mathbb{C}^{\tau J}$ is derived see Prot et al (2009).

$$\mathbb{C}^{\tau J} = J(\mathbb{c} + \mathbb{C}') \qquad \text{(Eqn. 2.26)}$$

$$with \qquad \mathbb{C}'_{ijkl} = \frac{1}{2}(\delta_{ij}\sigma_{jl} + \delta_{il}\sigma_{jk} + \delta_{jl}\sigma_{ik}) \qquad \text{(Eqn. 2.27)}$$

The finite element package Abaqus, which is used later in this thesis, uses a scaled version of the Jaumann tangent modulus, given below.

$$\mathbb{c}^{abaqus} = J^{-1}\mathbb{C}^{\tau J} \qquad \text{(Eqn. 2.28)}$$

2.5.4 Incompressible hyperelastic material

As stated in the previous section, for an incompressible material there is no volume change and are characterised by the constraint

$$J = 1 \qquad I_3 = 1 \qquad \text{(Eqn. 2.29)}$$

which means that the invariants I_1 and I_2 are the only independent deformation variables. With this constraint comes a change in the expression of the strain-energy function. For a material behaviour defined using strain invariants a suitable strain-energy function is given below

$$\psi = \psi(I_1, I_2) - \frac{1}{2}p(I_3 - 1) \qquad \text{(Eqn. 2.30)}$$

where the scalar $p/2$ serves as an indeterminate Lagrange multiplier. As $I_3 = 1$ the Lagrange multiplier will not affect the internal strain-energy ψ, i.e. there is no energy change due to a change in volume. The scalar p can be referred to as a hydrostatic pressure which results from the incompressibility constraint and will affect the stress in the material. The value of p can be determined from equilibrium equations and boundary conditions. The second Piola-Kirchhoff stress for a hyperelastic material defined by the general strain-energy function in Eqn. 2.30 is given by

$$\mathbf{S} = 2\frac{\partial \psi(I_1, I_2)}{\partial \mathbf{C}} - \frac{\partial[p(I_3 - 1)]}{\partial \mathbf{C}} = -p\mathbf{C}^{-1} + 2\left(\frac{\partial \psi}{\partial I_1} + I_1 \frac{\partial \psi}{\partial I_2}\right)\mathbf{I} - 2\frac{\partial \psi}{\partial I_2}\mathbf{C} \qquad \text{(Eqn. 2.31)}$$

where $\mathbf{I}$ is the identity matrix. The Cauchy stress and the elasticity tensors can be found derived the second Piola-Kirchhoff stress, $\mathbf{S}$, using the method described in Section 2.1.

2.5.5 Compressible hyperelastic material

In a compressible material the deformation can be split into a volumetric part and an isochoric part. The volumetric part concerns volume changing deformation while the isochoric part deals with distortional deformations. The deformation gradient, $\mathbf{F}$, and the right Cauchy-Green strain tensor, $\mathbf{C}$, can be split into these parts by performing multiplicative decompositions of these tensors, Eqn. 2.32.

$$\mathbf{F} = J^{\frac{1}{3}}\bar{\mathbf{F}} \qquad \mathbf{C} = J^{\frac{2}{3}}\bar{\mathbf{C}} \qquad \text{(Eqn. 2.32)}$$

The tensors $\bar{\mathbf{F}}$ and $\bar{\mathbf{C}}$ are related to isochoric deformations while the $J^{1/3}$ and $J^{2/3}$ terms relate to volumetric deformations. We also have the relationship between $\bar{\mathbf{F}}$ and $\bar{\mathbf{C}}$ where $\bar{\mathbf{C}} = \bar{\mathbf{F}}^T\bar{\mathbf{F}}$. As with the deformation the strain-energy function can split into isochoric and volumetric parts. A general strain-energy function is described in a decoupled representation here

$$\psi = \psi_{vol}(J) + \psi_{iso}(\bar{\mathbf{C}}) \qquad \text{(Eqn. 2.33)}$$

The second Piola-Kirchhoff stress is again determined by differentiating the strain-energy function with respect to the deformation. We can see that the second Piola-Kirchhoff stress also consists of volumetric and isochoric parts

$$\mathbf{S} = 2\frac{\partial \psi}{\partial \mathbf{C}} = \mathbf{S}_{vol} + \mathbf{S}_{iso} \quad \text{(Eqn. 2.34)}$$

where the volumetric and isochoric contributions to **S** is given in Eqns. 2.30 and 2.31 respectively

$$\mathbf{S}_{vol} = 2\frac{\partial \psi_{vol}}{\partial \mathbf{C}} = J\frac{\partial \psi_{vol}}{\partial J}\mathbf{C}^{-1} \quad \text{(Eqn. 2.35)}$$

$$\mathbf{S}_{iso} = 2\frac{\partial \psi_{iso}}{\partial \mathbf{C}} = J^{-\frac{2}{3}}\mathbb{P}: 2\frac{\partial \psi_{iso}}{\partial \bar{\mathbf{C}}} \quad \text{(Eqn. 2.36)}$$

where $\mathbb{P}$ is called the projection tensor which is a function of the right Cauchy-Green strain tensor and the fourth order identity tensor, $\mathbb{I}$.

$$\mathbb{P} = \mathbb{I} - {}^{1}/_{3}\,\mathbf{C}^{-1}\otimes\mathbf{C} \qquad \mathbb{I}_{ABCD} = (\delta_{AC}\delta_{BD} + \delta_{AD}\delta_{BC}) \quad \text{(Eqn. 2.37)}$$

where $\delta_{ij} = 1$ if $i = j$ and 0 otherwise and is called the Kronecker delta. The Cauchy stress can be determined by a push forward operation as in the previous sections resulting here in

$$\boldsymbol{\sigma}_{vol} = p\mathbf{I} \qquad \boldsymbol{\sigma}_{iso} = J^{-1}\bar{\mathbf{F}}(\mathbb{P}: 2\frac{\partial \psi_{iso}}{\partial \bar{\mathbf{C}}})\bar{\mathbf{F}}^{T} \qquad \text{(Eqn. 2.38)}$$

The elasticity tensor in the material description is also decoupled into volumetric and isochoric parts, Eqn. 2.39. The full derivation of this tensor is lengthy and can be found in Holzapfel et al (2000).

$$\mathbb{C} = \mathbb{C}_{vol} + \mathbb{C}_{iso} \qquad \text{(Eqn 2.39)}$$

$$\mathbb{C}_{vol} = 2\frac{\partial S_{vol}}{\partial \mathbf{C}} \qquad \mathbb{C}_{iso} = 2\frac{\partial \mathbf{S}_{iso}}{\partial \mathbf{C}} \qquad \text{(Eqn 2.40)}$$

The elasticity tensor in the spatial description can be found by performing the Piola transformation as in previous sections.

2.5.6 Constitutive modelling of vascular tissue

A materials experimental behaviour can be described numerically using a constitutive model. Continuum based constitutive models can be expressed using finite hyperelasticity theory (Holzapfel, 2000). In finite hyperelasticity theory a Helmholtz free energy function is defined for a hyperelastic material to describe that materials constitutive relationship. The Helmholtz free energy function is commonly referred to as a strain-energy density function or strain-energy function (Holzapfel, 2000). It is common practice to describe cardiovascular soft tissue using a hyperelastic model (Humphrey, 2002).

A number of assumptions are commonly made in the modelling of arterial tissue. The first is material homogeneity. This assumption has some validity based on the findings of histological studies, where arteries were seen to be reasonably uniform in the circumferential and longitudinal directions but not in the radial direction (Wolinsky and Glagov, 1964). This means the assumption is reasonably valid for the circumferential and longitudinal directions while for single layer models the material properties are averaged between the three layers. The validity of the homogeneity assumption is thus increased when using a three layer model. Arteries are assumed to be incompressible. Carew et al (1968) found that this assumption can be made for most practical purposes. Arteries can also reasonably be assumed to behave as a cylindrically orthotropic material (Patel and Fry, 1969). This assumption is sometimes simplified to modelling arterial tissue as an isotropic material (Lally et al., 2004).

The strain-energy function is usually expressed as a function of material's principal stretches or strains or its principal strain invariants. Many of the models used to describe vascular tissue are adopted from general theory of hyperelastic materials. One such model is the Mooney-Rivlin model (Mooney, 1940):

$$\psi(I_1, I_2) = \sum_{i,j=0}^{n} c_{ij} (I_1 - 3)^i (I_2 - 3)^j \ , c_{00} = 0 \qquad \text{(Eqn. 2.41)}$$

where ψ is the strain-energy function, I_1, I_2, are the first and second principal strain invariants (Eqns. 2.11 and 2.12) and c_{ij} are the hyperelastic material constants. The Mooney-Rivlin model describes an incompressible, isotropic material and it is often seen in finite element packages expanded to 3, 5 or 9 parameter functions, which results in models that are 1st order, 2nd order and 3rd order polynomials respectively. The first order Mooney-Rivlin model can be reduced to the neo-Hookean model as defined by Treolar (1943):

$$\psi = c_{10}(I_1 - 3) \qquad \text{(Eqn. 2.42)}$$

Another example of an isotropic model is that defined by Ogden as a function of the principal stretches of the material (Ogden, 1984):

$$\psi = \sum_{p=1}^{N} \frac{\mu_p}{\alpha_p} (\lambda_1^{\alpha} + \lambda_2^{\alpha} + \lambda_3^{\alpha} - 3) \qquad \text{(Eqn. 2.43)}$$

where μ_p and α_p are material constants and λ_1, λ_2, λ_3, are the principal stretches.

As stated earlier arteries do not behave like an isotropic material. Models that introduce anisotropic behaviour have been developed. One of the most commonly used forms of anisotropic model is the exponential Fung type model (Fung et al., 1979):

$$\psi = (B/2) exp\left(c_{20} E_{\theta\theta}^2 + 2c_{11} E_{\theta\theta} E_{zz} + c_{02} E_{zz}^2\right) \qquad \text{(Eqn. 2.44)}$$

where B is a stress like material constant c_{20}, c_{11} and c_{02} are dimensionless material constants and $E_{\theta\theta}$ and E_{zz} are the Green strains in the circumferential and longitudinal directions respectively. This Fung type model can be described as a 2D orthotropic model as the strain-energy is defined in terms of the strains in two principal directions. Another orthotropic model defined as a function of Green strains is the polynomial model described by Vaishnav et al (1972).

The orthotropic models discussed above are phenomenological models. In an attempt to more accurately measure arterial behaviour there has been a move to make constitutive models more mechanistic, i.e. related to the actual mechanics of the artery. This is seen in the development of models that incorporate the use of structural tensors to model the effect of collagen fibre orientations (Holzapfel et al., 2000). Holzapfel et al split the strain-energy function into a part related to isotropic deformations and a part for anisotropic deformations.

$$\psi(\bar{\mathbf{C}}, \mathbf{M}, \mathbf{N}) = \psi_{isotropic}(\bar{I}_1) + \psi_{anisotropic}(\bar{I}_4, \bar{I}_6) \qquad \text{(Eqn. 2.45)}$$

This represents a model with two families of fibres where **C** is the right Cauchy-Green strain tensor, **M** and **N** are structural tensors given by the tensor products $\mathbf{m_0}\otimes\mathbf{m_0}$ and $\mathbf{n_0}\otimes\mathbf{n_0}$ respectively. $\mathbf{m_0}$ and $\mathbf{n_0}$ are unit vectors that represent the orientation of collagen fibres in the tissue.

$$[\mathbf{m_0}] = \begin{bmatrix} 0 \\ cos\beta \\ sin\beta \end{bmatrix} \qquad [\mathbf{n_0}] = \begin{bmatrix} 0 \\ cos\beta \\ -sin\beta \end{bmatrix} \qquad \text{(Eqn. 2.46)}$$

where β is the angle between the collagen fibres and the circumferential direction. $\bar{I}_4$ and $\bar{I}_6$ are invariants of $\bar{\mathbf{C}}$, **M** and **N** and are given by:

$$\bar{I}_4 = \bar{\mathbf{C}} : \mathbf{M} \qquad \bar{I}_6 = \bar{\mathbf{C}} : \mathbf{N} \qquad \text{(Eqn. 2.47)}$$

where $\bar{I}_4$ and $\bar{I}_6$ have the physical interpretation of being the squares of the stretches in the fibre directions $\mathbf{m_0}$ and $\mathbf{n_0}$. Other invariants exist for anisotropic fibre models however as the invariants $\bar{I}_4$ and $\bar{I}_6$ have the only clear physical meaning it is usual to express strain-energy functions in terms of these two invariants alone in order to minimize the necessary material constants (Calvo et al., 2007; Holzapfel et al., 2000). The function $\psi_{isotropic}(\bar{I}_1)$ is the isotropic contribution to the strain-energy, due mainly to elastin bearing load in the artery, and it is given here in a neo-Hookean form strain-energy function:

$$\psi_{isotropic}(\bar{I}_1) = {}^{c}/_{2}\,(\bar{I}_1 - 3) \qquad \text{(Eqn. 2.48)}$$

where $c>0$ is a stress like material constant. The anisotropic contribution to the strain-energy is given by the function $\psi_{anisotropic}(\bar{I}_4, \bar{I}_6)$ where the anisotropy is due to the invariants $\bar{I}_4$ and $\bar{I}_6$.

$$\psi_{anisotropic}(\bar{I}_4, \bar{I}_6) = \sum_{i=4,6} \frac{k_1}{2k_2}(exp[k_2(\bar{I}_i - 1)^2 - 1]) \qquad \text{(Eqn. 2.49)}$$

Where k_1 is a stress like material constant and k_2 is a dimensionless constant, k_1, $k_2>0$.

2.5.7 Modelling of inelastic behaviour of arteries

There have been relatively few models of arterial tissue that incorporate damage behaviour. The aspects of damage that have been modelled to the author's knowledge are stress softening and permanent deformation. Calvo et al (2007) developed a anisotropic damage model for fibred biological soft tissues based on previous work in the field of rubber mechanics (Simo, 1987).

$$\psi(\mathbf{C}, \mathbf{M}, \mathbf{N}, D_m, D_f) = \psi_{vol}(J) + (1 - D_m)\bar{\psi}_0^m(\bar{\mathbf{C}}) + (1 - D_f)\bar{\psi}_0^f(\bar{\mathbf{C}}, \mathbf{M}, \mathbf{N}) \qquad \text{(Eqn. 2.50)}$$

where ψ is the strain-energy function that is decoupled into a volumetric part $\psi_{vol}(J)$ and isochoric parts $\bar{\psi}_0^m(\bar{\mathbf{C}})$ and $\bar{\psi}_0^f(\bar{\mathbf{C}}, \mathbf{M}, \mathbf{N})$. More detail on the decoupling of a strain-energy function is given in Section 2.5.5. $\bar{\psi}_0^m(\bar{\mathbf{C}})$ describes the effective isochoric strain-energy of the undamaged matrix and $\bar{\psi}_0^f(\bar{\mathbf{C}}, \mathbf{M}, \mathbf{N})$ describes the effective isochoric strain-energy of the fibres. **M** and **N** are structural tensors, similar to $\mathbf{A_1}$ and $\mathbf{A_2}$ in the model by Holzapfel et al (2000). Damage is incorporated into the model with the reduction factors *(1 - D_m)* and *(1 - D_f)*. D_m and D_f are known as damage variables for the fibre and matrix respectively, with $D_m \in [0,1]$ and $D_f \in [0,1]$. D_m and D_f are functions of the maximum value of strain-energy reached in the loading history. This means that damage is applied to the matrix and fibres separately in this model and as a result loading can induce anisotropy. The formulation of damage modelling similar to that used by Calvo *et al* is discussed in more detail in Chapter 6 of this thesis. Alastrué et al. (Alastrué et al., 2007) apply a similar model but include a stochastic, statistical element to describe fibre distribution and length, see Fig. 2.19.

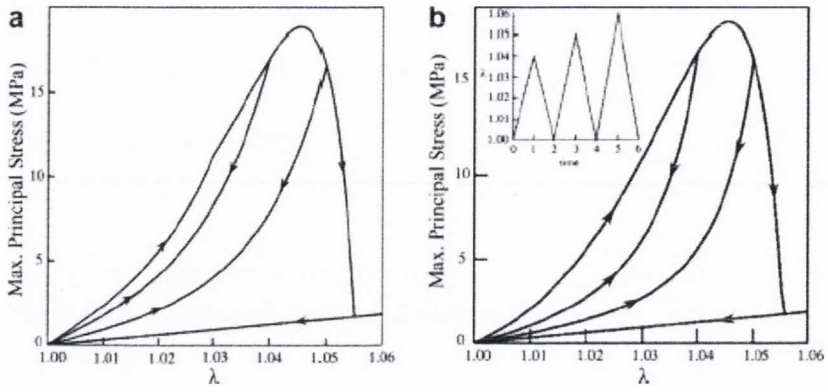

Figure 2.19: Damage model response to cyclic loading for (a) continuum model and (b) stochastic model for the same loading profile (inset). Both models exhibit stress softening and failure. (Alastrué et al., 2007)

The constitutive models in this section have been modified in some cases to incorporate other aspects of arterial mechanical behaviour. Fung et al (1979; 1993) introduced the concept of pseudoelasticity in order to incorporate behaviours such as hysteresis. In pseudoelasticity a unique strain-energy density function can be applied to loading and unloading of the material, which is done here by characterising a unique set of material constants for loading and unloading. Holzapfel et al (Holzapfel et al., 2002) introduced viscoelastic effects to their arterial wall model. Others have developed collagen fibre remodelling algorithms for arteries (Driessen et al., 2003; Hariton et al., 2007).

Few models exist that incorporate the inelastic deformation that occurs in tissue on unloading from non-physiological pressures (e.g. during clinical procedures such as angioplasty). The majority of arterial constitutive models that incorporate inelastic strains only do so for failure of the material. For example the damage model presented by Calvo et al (2007) incorporated criteria for which the reduction factors equal zero which corresponds to failure of the material component. At failure inelastic strains would be induced. Wulandana et al (2005) apply a multi-mechanism approach to describe arterial softening where damage is introduced by the deactivation (failure) of the tissue components when they reach certain level of stretch. While Li et al (2009) apply a similar approach to damage as in the Calvo study. Gasser and Holzapfel (2002) have

developed a model that incorporates permanent deformation using the theory of multi-surface slip plasticity to model slip of collagen fibres in an isotropic matrix. The algorithm and yield criterion used are detailed in the referenced study. However the model was not fit to mechanical test data for arterial tissue. Constitutive models for other soft tissues (Franceschini et al., 2006) have used pseudoelastic approaches to model inelastic deformations and softening similar to what has been used for particle filled rubbers.

2.6 Conclusion

The papers reviewed in this section highlight the key challenges associated with the modelling of healthy and diseased arterial tissue. The loading behaviour of healthy arterial tissue has been quite extensively investigated particularly in the physiological loading regime. Arterial tissue has been characterised as an (nearly) incompressible, highly nonlinear, anisotropic and viscoelastic tissue which behaves as a composite due to the differing structure of the arterial layers. However, while the mechanical behaviour of healthy arteries on unloading and subsequent reloading has been qualitatively described in the literature there is a scarcity of actual mechanical test data in order to describe this behaviour quantitatively.

Relatively few studies have presented data on the mechanical properties of atherosclerotic plaques, for which the loading and unloading behaviour has not been extensively quantified. From these tests it is clear that as with arterial tissue, atherosclerotic plaques are characterised by anisotropic, nonlinear and viscoelastic behaviour. Non-recoverability of mechanical properties also indicates a similar response to overstretch as seen in arterial tissue. Atherosclerotic plaque mechanical properties vary due to their morphology which can be described in a number of different ways depending on the characterisation method used. Healthy arterial mechanical properties vary with site and location; it is likely the same is true for atherosclerotic plaques. The studies to date have predominantly focussed on atherosclerotic plaques from the aorta and as a result constitutive modelling of atherosclerotic lesions in finite element modelling is hampered

when applied to other arterial sites. This thesis aims to characterise the mechanical behaviour of fresh human atherosclerotic plaque tissue removed from the carotid artery during endarterectomy.

A number of constitutive models have been applied to the characterisation of elastic and viscoelastic arterial tissue behaviour, most commonly based on the components of the Green-Lagrange strains or invariants of the right Cauchy-Green strain. Significantly fewer models have been used to characterise the inelastic damaged behaviour of soft tissues due to overstretch, particularly the inelastic effects before failure of the tissue or tissue components. Of the typical inelastic effects observed during unloading, models that incorporate stress softening are the more common, while constitutive models that incorporate inelastic residual deformations on unloading rarely have been compared to arterial mechanical test data. A central objective of this thesis will be to develop constitutive models of healthy and diseased arterial tissue that consider both stress softening and inelastic residual deformations that occur during non-physiological loading of the tissue.

Chapter 3 Tensile and compressive properties of fresh human carotid atherosclerotic plaques

Maher E.[1], Creane A.[2], Sherif Sultan[3, 4], Niamh Hynes[3, 4], Lally C.[1, 2], Kelly D. J.[1]

[1] Trinity Centre for Bioengineering, School of Engineering, Trinity College Dublin, Dublin 2, Ireland.

[2]School of Mechanical and Manufacturing Engineering, Dublin City University, Glasnevin, Dublin 9, Ireland

[3]Western Vascular Institute, Department of Vascular & Endovascular Surgery, University College Hospital Galway, Ireland.

[4]Department of Vascular & Endovascular Surgery, Galway Clinic, Doughiska, Dublin Road, Galway, Ireland.

For thesis purposes the article version presented in this chapter is modified from the original published in the Journal of Biomechanics 2009.

The large majority of the work discussed in this chapter was undertaken by the author of this thesis. The contributions of the other authors to this work are as follows: Dr. Kelly and Dr. Lally had a supervisory role on this study. Mr. Sultan and Ms. Hynes are the lead surgeons who performed the endarterectomy surgeries and liaised with hospital staff to supply imaging, etc. Dr. Creane assisted

the author of this thesis during mechanical testing, principally acting as a pair of 'clean hands' while the biological tissue was being dissected and tested.

3.1 Introduction

Myocardial infarction and stroke are acute pathological events that occur during the chronic process of atherosclerosis (Newby, 2005). Rupture or erosion of the atherosclerotic plaque, and the subsequent thrombosis that results in occlusion or embolisation, are the two main mechanisms involved in such conditions (Davies, 2000). While biomechanical forces have been implicated in plaque fatigue and rupture (Cheng et al., 1993; Ku and McCord, 1993; Loree et al., 1992; Richardson et al., 1989), such stimuli are also thought to play a major role in the modelling and remodelling of such plaques (Glagov et al., 1997). Atherosclerotic plaques contain T cells and lipid-laden macrophages (foam cells), which are derived from blood monocytes (Libby, 1995). T cells produce factors which suppress the production of collagen by the smooth muscle cells (SMCs) and stimulate macrophages to produce matrix metalloproteinases (MMPs) which digest the existing collagen and other extracellular matrix components (Nicolaides et al., 2002). The SMCs within the vessel wall, which play a key role in maintaining the structural integrity of the plaque cap (Geng et al., 1997; Seshiah et al., 2002), are influenced by the level of mechanical stretch they experience (Sotoudeh et al., 2002). This may explain why regions of high strain in artherosclerotic plaques correlate with low levels of SMCs (Schaar et al., 2003). These and other studies confirm that vascular tissue mechanics and biology are intrinsically related in the pathogenesis of atherosclerosis.

A complete understanding of the mechanics of diseased arteries is also critical to optimising the outcomes of interventional procedures such as angioplasty and stenting. This has enabled computational tools such as finite element models to be used in the optimisation of stent design. Early models focussed on the expansion characteristics of balloon expandable (Chua et al., 2003; Dumoulin and Cochelin, 2000; Etave et al., 2001; Migliavacca et al., 2002; Petrini et al., 2004; Tan et al., 2001) and self-expanding stent designs (Whitcher, 1997). The necessity to

understand both lumen gain and vessel injury post-stenting has led to greater interest in modelling stent- plaque-artery interactions (Auricchio et al., 2001; Bedoya et al., 2006; Chua et al., 2004b; Early et al., 2009; Lally et al., 2005; Migliavacca et al., 2004; Rogers et al., 1999). Further studies using anisotropic constitutive equations for the artery wall (Holzapfel et al., 2002) have been performed for both stenting (Kiousis et al., 2007) and for angioplasty (Gasser and Holzapfel, 2007b). As well as aiding the optimisation of stenting procedures, an increased understanding of the mechanical properties of atherosclerotic tissue might be useful in the planning and optimisation of surgical procedures. For example, prior knowledge of the properties of a carotid plaque could inform the decision on whether to stent or perform an endarterectomy, a surgical procedure to remove atherosclerotic plaque material from an artery by separating the plaque from the arterial wall.

Our understanding of the role of vascular mechanics in all aspects of atherosclerosis, from its development to its treatment, is impeded by insufficient experimental data for diseased human tissue. The majority of experimental investigations of atherosclerotic plaques are performed on cadaveric tissue. Lee et al (1991) dynamically tested the fibrous cap of abdominal aortic plaques in radial compression and related their findings to the cap composition as determined by histology. It was found that hypocellular caps were 1-2 times stiffer than cellular and calcified were 4-5 times as stiff. In a further study Lee et al (1992) performed radial compression relaxation tests on abdominal aortic plaque caps. These results were compared to classifications from intravascular ultrasound imaging and it was found that non-fibrous plaque caps had the lowest static stiffness and longest relaxation time, calcified caps had the highest stiffness and lowest relaxation times and fibrous caps had values in between the other classifications. In contrast, Loree et al (1994) found no significant difference between the static circumferential tangential moduli of hypocellular, cellular and calcified plaques. Topoleski et al (1997) investigated cyclic compressive behaviour in aortoiliac plaques. Three types of plaque behaviour were identified and related to results from histology. Salunke et al (2001) studied the compressive stress relaxation behaviour of aortoiliac plaques when subjected to successive stress relaxation tests and compared the results to histology and to similar tests on healthy vessels. They found that during the loading cycle up to 25% compressive stretch

that calcified and fibrous plaques behaved similarly and that both were stiffer than atheromatous plaques. The anisotropic behaviour of diseased iliac arteries was investigated by Holzapfel et al. (2004). Each artery specimen was separated into its different artery and plaque component layers, as determined by high resolution MRI. All the studies mentioned above have been performed on cadaveric material. Given the delay before autopsy, and the fact that there can be changes to soft tissue properties during short term storage (Stemper et al., 2007b), there is a need to obtain data for fresh human tissue.

The objective of this study is to determine the mechanical properties of fresh (tested in less than 2 hours) carotid plaques following removal during endarterectomy. For this purpose uniaxial circumferential tension and radial compression tests were performed on plaque samples. This study also investigates in-patient variability and inter-patient variability between specimens and the relationship between plaque properties and their clinical classification and the location of the sample in the carotid bifurcation.

3.2 Materials and methods

Tensile and compressive tests were performed on samples taken from plaques of the carotid bifurcation. Plaque specimens were removed from 14 patients (9 men and 5 women, 67 ± 8.84yrs, mean ± SD) during routine carotid endarterectomies. All surgeries and tests were performed in the Galway Clinic, Ireland. The study includes 44 compressive and 16 tensile samples obtained from 14 carotid plaques. Table 3.1 includes all patient and lesion details. Plaque classifications were determined independently by a clinician using routine Duplex ultrasound with grey scale imaging (Nicolaides et al., 2002; Tegos et al., 2001). Ethical approval for testing of the human tissue was obtained. From the Galway clinical ethics board.

Table 3.1: Patient/specimen details

Specimen	Gender	Age, yr	Clinical Classification	No. of Compression Samples	No. of Tensile Samples
1	M	67	Mixed	2 T; 0 C; 2 I; 0 E	0 T
2	M	70	Mixed	5 T; 2 C; 2 I; 1 E	0 T
3	F	72	Mixed	3 T; 0 C; 3 I; 0 E	2 T; 2 C; 0 I
4	F	71	Mixed	4 T; 1 C; 2 I; 1 E	1 T; 1 C; 0 I
5	M	51	Mixed(Lightly calcified) proximal vessel, mostly echolucent at focal plaque	5 T; 3 C; 1 I; 1 E	1 T; 1 C; 0 I
6	M	71	Calcified proximally, mixed distally	4 T; 2 C; 1 I; 1 E	2 T; 0 C; 2 I
7	M	83	Calcified Proximally, mixed distally	7 T; 4 C; 2 I; 1 E	0
8	M	73	Calcified Proximally, mixed distally	3 T; 1 C; 1 I; 1 E	1 T; 1C; 0 I
9	F	78	Calcified	8 T; 3 C; 3 I; 2 E	0 T
10	M	65	Mixed	0 T	1 T; 0 C; 1 I
11	M	61	Calcified	1 T; 0 C; 1 I; 0 E	1 T; 1C; 0 I
12	F	63	Mostly calcified, echolucent at origin	0 T	3 T; 3 C; 0 I
13	M	58	Mostly echolucent	2 T; 0 C; 2 I; 0 E	2 T; 2 C; 0 I
14	F	55	Calcified Proximally, mixed distally	0 T	2 T;2 C; 0 I
	Age, mean±SD yr	67±8.84	Total no. of Samples	44 T; 15 C; 20 I; 8 E	16 T; 13 C; 3 I

M, male; F, female; T, total no. of samples for specimen; C, sample from common segment of specimen; I, sample from internal segment of specimen; E, sample from external segment of specimen. Plaque classifications were determined by an independent clinician, who was blinded to the mechanical testing results, based on routine ultrasound with grey scale median imaging.

3.2.1 Sample Preparation

Plaque specimens were prepared for testing immediately following removal in surgery. Specimens were dissected at the bifurcation, separating them into common, internal and external carotid segments, see figure 3.1. Each segment was opened by cutting along the axial direction. Circumferential tensile and radial compressive samples were removed from each of the flat rectangular segments using stainless steel punches. Dog-bone shaped tensile samples were used which had a gauge length and width of 4 mm and 1 mm respectively (Fig. 3.1(b), (c)). Regions were deemed suitable for tensile testing if a sample with relatively consistent composition could be obtained within the gauge length of the dog-bone sample. Due to the small diameter of the external carotid, no tensile samples were obtained from these plaque segments. 4 mm diameter compressive samples were also removed from the specimen. Testing samples were allowed to equilibrate in 0.9 % saline solution for approximately 30 minutes before measurements of the sample dimensions were recorded.

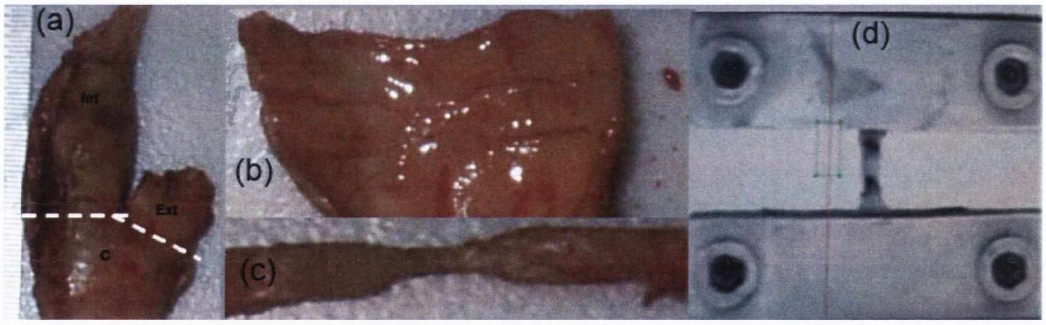

Figure 3.1: (a) Intact carotid plaque specimen. Dotted white lines show where specimen was separated into common (C), internal (Int) and External (Ext) carotid segments. Dog-bone shaped tensile specimen (b) before and (c) after sample is fully excised from common carotid segment. (d) Image from video-extensometer of tensile specimen clamped in tensile grips.

3.2.2 Testing Conditions

Testing was performed using a computer controlled, high precision testing device adapted for testing biological specimens (Bose ElectroForce 3100, Bose Corporation, Gillingham, UK). The testing rig has an electromagnetic driven motor, with a stroke resolution of 0.0015 mm, a maximum

stroke length of 5mm and a minimum load resolution of 6 mN with the 22 N load cell. Screw-based compressive platens and tensile grips were used during testing, and the ability to interchange these allowed the same device to be used for both compressive and tensile testing. All samples were stored in 0.9 % saline solution until testing. All samples were tested within two hours of harvesting.

Unconfined compression tests were performed on the 4 mm diameter compressive samples. A sample was placed on the lower platen and the upper platen was moved to apply a small compressive pre-load of 0.01 N to the sample at a crosshead speed of 0.001 mm/s. This ensured a consistent contact between the platen and the top of the sample and minimal strain in the plaque, <5% in all cases. The sample height was then taken as the distance between the platens at this pre-load. Before testing, preconditioning was achieved by performing 10 loading and unloading cycles to 10% strain at a constant crosshead rate of 1% strain/s. After preconditioning the sample was compressed at the same rate (1%/s) until 60% strain was reached.

For tensile testing, a fast drying permanent marker was used to draw two parallel horizontal lines across the gauge of the samples before testing. The tabs of a dog-bone sample were then clamped in the tensile grips. The tensile grips were lined with sandpaper in order to minimize sample slip within the grips. A tensile pre-load of 0.01 N was applied to the sample at a rate of 0.001mm/s in order to ensure that the true gauge length was measured. The pre-load caused only minimal strain in all samples (< 5%). During the tensile tests strain measurements were taken using a computer based video extensometer, see Fig. 3.1 (d). The extensometer automatically recognised marks and edges, and the gauge length after pre-load and deformation between the gauge marks during testing was recorded by the computer. Before testing the sample thickness was also measured using the video extensometer. Similar preconditioning as with the compressive samples was applied to the tensile sample after which the sample was stretched at a constant rate of 1% strain/s until the maximum stretch allowed by the stroke length of the testing device was reached or until failure occurred in the sample.

3.2.3 Data Fitting and Analysis

A 2nd order isotropic hyperelastic model (Eqn. 3.1) was used to fit to the obtained experimental data in this study. A general 2nd order polynomial hyperelastic strain-energy function can be defined in terms of the strain invariants as follows (Abaqus Inc):

$$\psi = c_{10}(I_1 - 3) + c_{01}(I_2 - 3) + c_{20}(I_1 - 3)^2 + c_{11}(I_1 - 3)(I_2 - 3) + c_{02}(I_2 - 3)^2 \qquad \text{(Eqn. 3.1)}$$

where ψ is the strain-energy function, c_{ij}, $i + j = 1, 2$ the material constants and I_1 and I_2 are the principle strain invariants. The strain invariants can be expressed in terms of the principal stretches as $I_1 = \lambda_{12} + \lambda_{22} + \lambda_{32}$, and $I_2 = \lambda_{12}\lambda_{22} + \lambda_{12}\lambda_{32} + \lambda_{22}\lambda_{32}$. For the case of uniaxial testing of an incompressible material the nominal stress is given by:

$$\mathbf{P} = \frac{\partial \psi}{\partial \lambda} = 2(1 - \lambda^{-3})\left(\lambda \frac{\partial \psi}{\partial I_1} + \frac{\partial \psi}{\partial I_2}\right) \qquad \text{(Eqn. 3.2)}$$

where λ is the stretch in the loading direction. Data fitting was performed using the test data curve fitting function of the finite element package Abaqus 6.7-1, which uses a least squares procedure to obtain the constants C_{ij}, $i + j = 1, 2$. This method aims to minimize the difference in nominal stress between the experimental test data and the data calculated from Eqn. 3.2. The relative error, E, between these two values is given by Eqn. 3.3.

$$E = \sum_i \left[1 - \frac{data\ measured(i)}{data\ calculated(i)}\right]^2 \qquad \text{(Eqn. 3.3)}$$

It is important to ensure that the constants obtained using this method lead to a stable function. This is done by ensuring that the curves produced are positive definite. Stability checking is done automatically in Abaqus when performing a curve fit. Where an unstable curve is produced the constants are modified to produce a stable response.

As an independent measure of the appropriateness of the fit the root mean square error measure χ, which is based on the sum of the square error between calculated and measured data, is used (Eqn. 3.4).

$$\chi = \frac{\sqrt{\frac{\sum_i (data\ measured(i) - data\ calculated(i))^2}{n-q}}}{P_{ref}} \qquad \text{(Eqn. 3.4)}$$

where n is the number of data points and q is the number of strain-energy function constants. The value P_{ref} is the sum of all nominal stresses for each data point divided by the number of data points.

The compressive data were analysed using a number of different criteria: (1) in-patient variation; (2) inter-patient variation; (3) plaque classification; (4) sample location. However due to the significantly lower number of tensile samples, tensile data were analysed and presented together. All the stress strain data are graphed as nominal stress against nominal strain. As the stress strain curves of the material approach failure the curves, in some cases, become noisy. As a result of this a 10% drop in the stress as the strain increases was viewed as material failure here, and the data was not analysed or graphed following such a drop.

3.3 Results

When plaques were grouped by clinical classification, a large amount of variability in the compressive behaviour for both the calcified and mixed plaque specimens was observed, see Fig. 3.2. This variability is less evident for the echolucent samples. Comparing the mean curves for each classification suggested that calcified samples were on average over twice as stiff as the echolucent samples and 1.5 - 2 times stiffer than the mixed plaque. Significant in-specimen variation in the compressive behaviour of human atherosclerotic plaque was observed, see Fig. 3.3. For certain specimens, most notably specimens 2, 7 and 9, there is a large amount of variation between

samples. However for other specimens (1, 4, and 5) a much lower degree of variation was observed. When comparing the variation seen to the clinical classification there appears to be no direct link between plaque classification and in-specimen variation; for example specimen 4 is a mixed plaque but has low variation while specimen 2 is also mixed but has a higher variability. Large variations are also observed in the compressive properties of samples taken from the same vessel section (either common, internal and external) of the plaque, see Fig. 3.4. The average curve for each plaque location does suggest some variation, with the common artery being the stiffest and the external the least stiff; however no firm conclusions can yet be made about differences in plaques between the three carotid vessels.

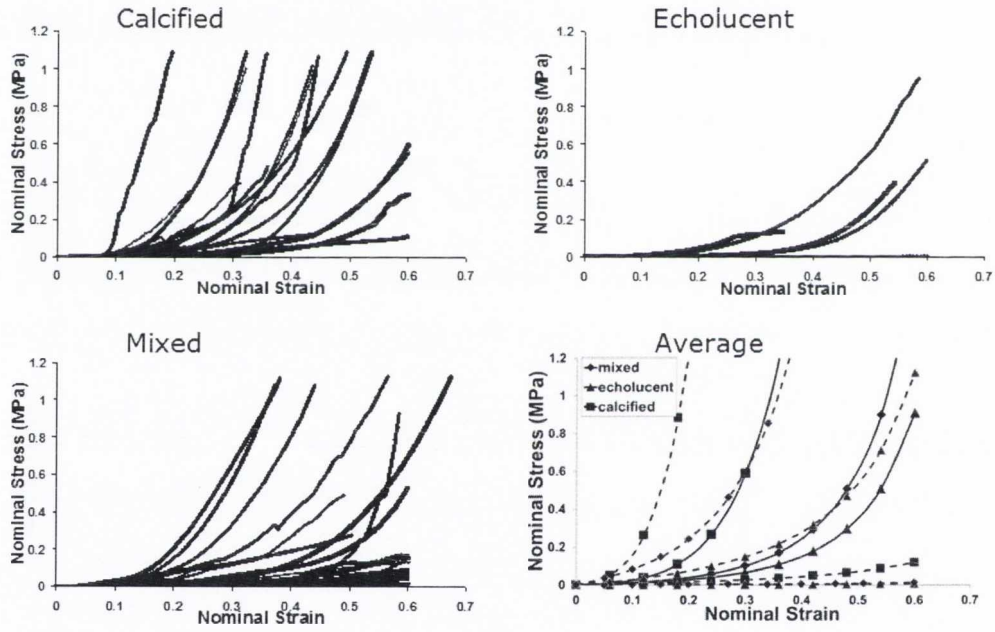

Figure 3.2: Compressive properties of calcified, echolucent and mixed plaques. Average curves for each clinical classification were obtained from the mean set of hyperelastic constants (see Table 3.2). The average curves are represented by solid lines. The dashed lines represent the upper and lower bound values for the stress-strain response in each classification; with the upper and lower bound taken as the stiffest (13(i), 2(iii) and 9(ii)) and least stiff (5(v), 4(iii) and 7(v) respectively) sample for the echolucent, mixed and calcified classifications respectively. These represent

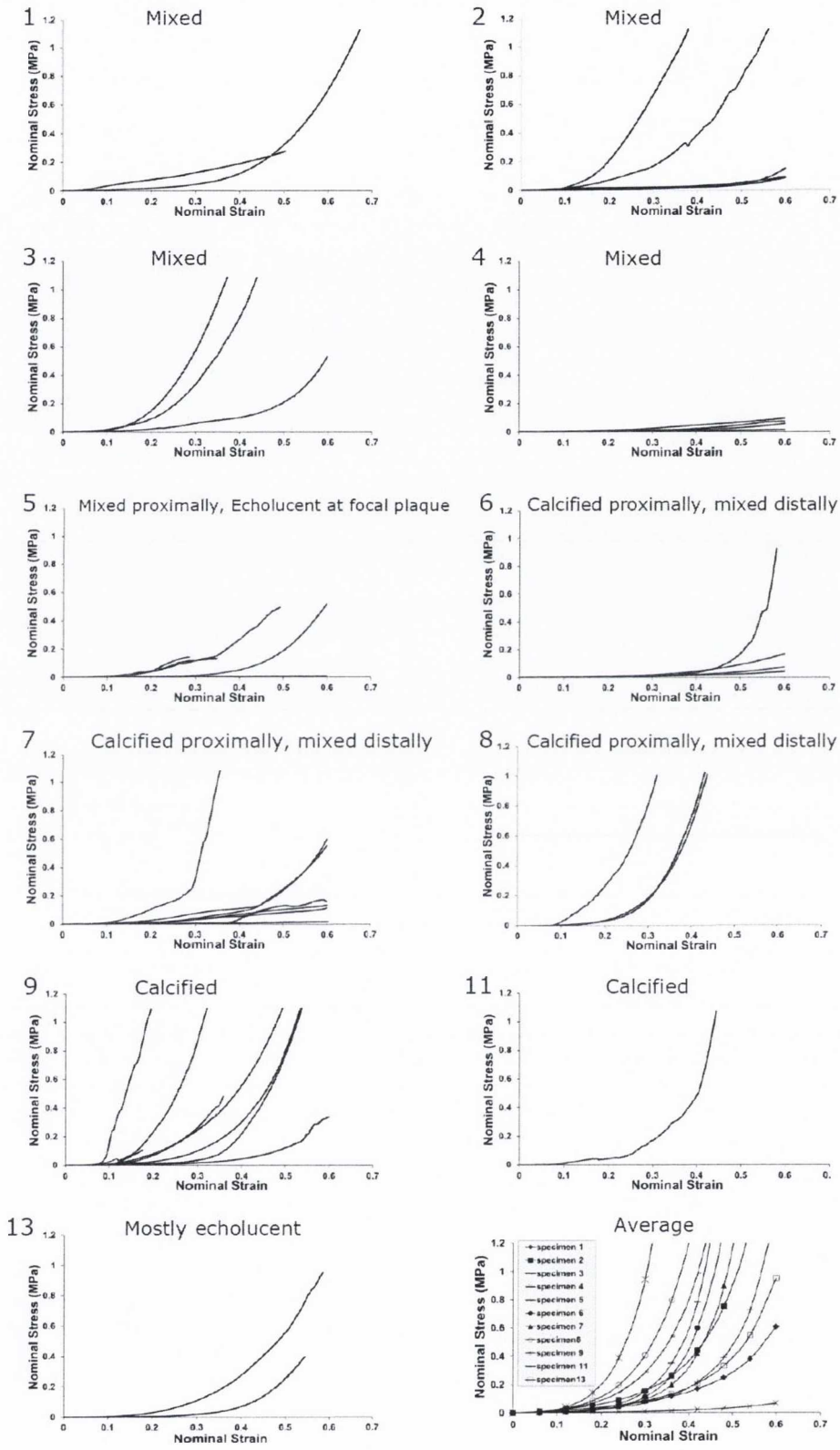

Figure 3.3: Inter-patient variability of compressive samples.

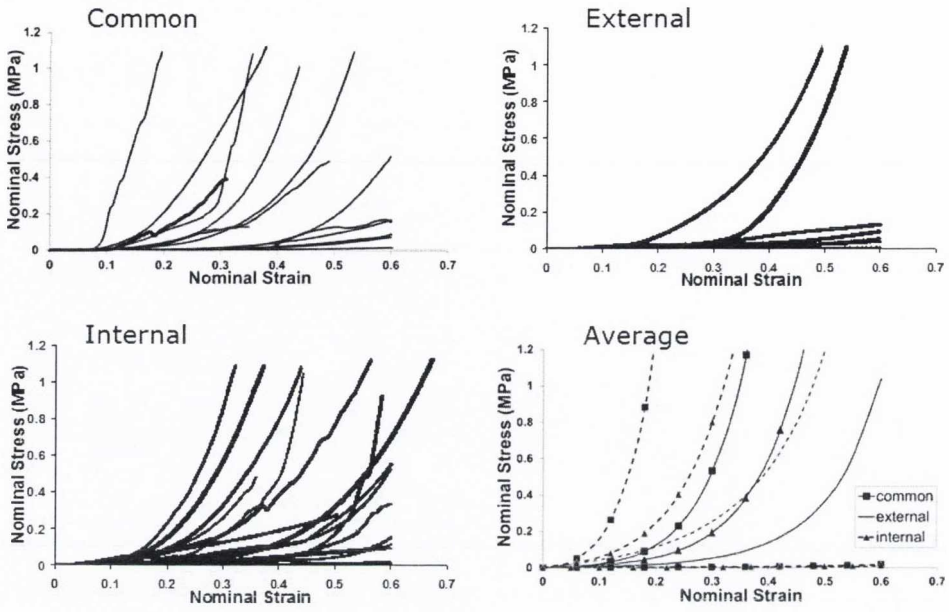

Figure 3.4: Anatomical variation of compressive samples. Average curves for each vessel location were obtained from the mean set of hyper elastic constants (see Table 3.2). Solid lines represent the average curves. The dashed lines represent the upper and lower bound limit for the stress-strain behaviour of each artery location determined by taking the least stiff (7(ii), 4(ii), 5(v)) and stiffest (9(ii), 8(ii), 9(viii)) sample from the common, internal and external segments respectively.

The typical response for a tensile specimen is shown in Fig. 3.5. The strain-time curve was obtained using the data analysed from the video-extensometer. While the force-time curve derived from data from the experimental rig. This data is correlated for each specimen, together with calculating nominal strains from the force and original sample dimensions, to obtain the stress-strain responses shown in Fig. 3.6.

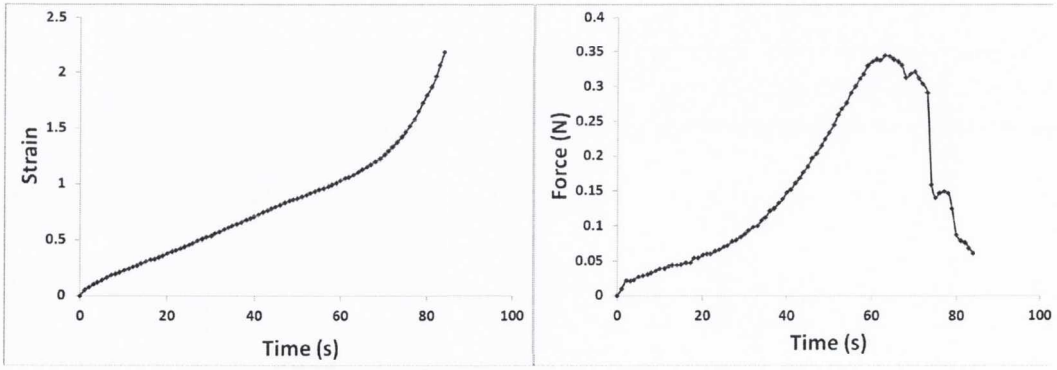

Figure 3.5: Strain-time and force-time curves for tensile sample 4(i)

Significant variability was also observed in the tensile properties of fresh human carotid plaque, see Fig. 3.6. Due to the smaller number of tensile samples, the main conclusion that can be drawn from the tensile data is that there appears to be high variability, both inter-specimen and in-specimen, in the tensile behaviour of these plaques.

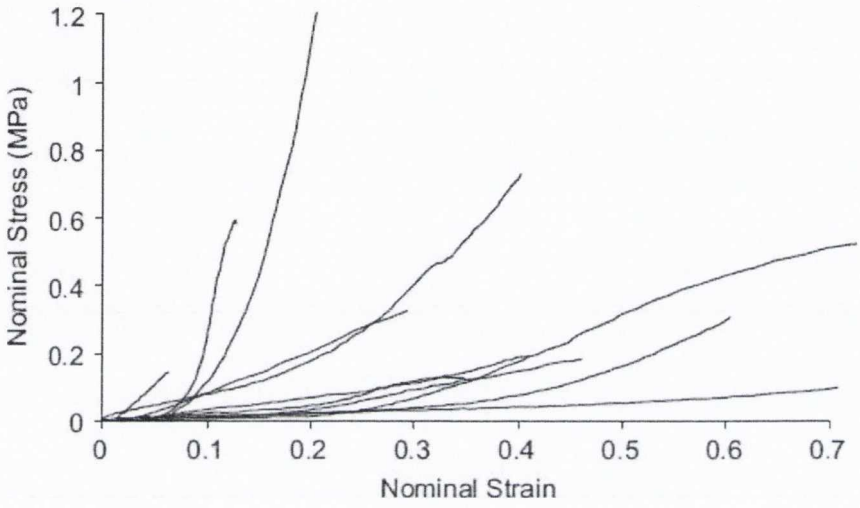

Figure 3.6: Tensile data for each of the carotid plaques tested.

The overall mean material constants obtained from curve fitting the compressive and tensile data to a Mooney-Rivlin model are given in Table 3.2 and 3.3 respectively. The error measure ζ in both Table 3.2 and 3.3 is less than 0.1 in all cases which indicates a good quality of fit. These tables also include information on the mean values for each of the constants obtained from compressive testing for both the samples described by plaque classification and those described by vessel. In the case of tensile data only the overall mean and standard deviation (SD) are reported due to the lower number of samples tested.

Table 3.2: Strain energy constants for compression testing of plaque samples (MPa)

Sample	Classification	Vessel	C10	C01	C20	C11	C02	$\tilde{\xi}$
1 (i)	M	I	0.042	0	0	0	0	0.0994
1 (ii)	M	I	0.0012	0.0208	0.0004	0	0	0.0971
2 (i)	M	Ex	0.0078	0	0	0	0	0.0996
2 (ii)	M	I	0.004	-0.0009	0	0	0.000546	0.0924
2 (iii)	M	C	0.07	0.041	0.126	0.009	0	0.098
2 (iv)	M	C	0.001468	0.0013	0.00012	0	0.00012	0.0296
2 (v)	M	I	0.001	0.053	0	0	0	0.0958
3 (i)	M	I	0.006	0.04	0.2	0	0	0.0693
3 (ii)	M	I	0.002	0.04	0.08	0	0	0.0992
3 (iii)	M	I	0.005	0.0019	0.0062	0.001	0	0.0883
4 (i)	M	C	0.001	0.00271	0	0	0	0.0894
4 (ii)	M	I	0.00868	0	0	0	0	0.0965
4 (iii)	M	I	0.0012	0	0	0	0	0.0873
4 (iv)	M	Ex	0.001	0.0012	0.0002	0	0	0.0964
5 (i)	E	C	0.0001	0.0164	0.0319	0	0	0.0955
5 (ii)	E	C	0.003	0.004	0.001	0.003	0	0.0955
5 (iii)	M	C	0.002	0.015	0.0195	0	0.001	0.086
5 (iv)	M	I	0.001	0.005	0.042	-0.001	0.0086	0.0952
5 (v)	E	Ex	0.00071	0	0	0	0	0.0985
6 (i)	M	C	0.001	0.00556	0	0	0	0.095
6 (ii)	M	C	0.0005	0.00237	0	0	0	0.0776
6 (iii)	M	Ex	0.001	0.00104	0	0	0	0.0869
6 (iv)	M	I	0.0016	0	0	0	0.00465	0.0283
7 (i)	M	C	0.0001	0	0	0	0.0031	0.0998
7 (ii)	M	C	0.0015	0	0	0	0	0.0858
7 (iii)	Ca	C	0.0001	0	0	0	0.1363	0.0996
7 (iv)	Ca	C	0.005	0.002	0.007	0.001	0	0.0974
7 (v)	Ca	I	0.0102	0	0	0	0	0.0924
7 (vi)	Ca	I	0.001	0.012	0.004	0	0	0.0719
7 (vii)	M	Ex	0.0122	0	0	0	0	0.0998
8(i)	Ca	C	0.001	0.0019	0.1	0.004	0	0.071606
8(ii)	Ca	I	0.001	0.06	0.3	0.004	0	0.036145
8(iii)	Ca	Ex	0.001	0.001	0.1	0.01	0	0.005753
9 (i)	Ca	C	0.001	0.0275	0.1478	0	0	0.0973
9 (ii)	Ca	C	-0.0325	0.106	1.275	0.935	0.1	0.0951
9 (iii)	Ca	I	0.002	0.005	0.12	0	.002	0.0563
9 (iv)	Ca	C	-0.005	0.034	0.0177	0	0	0.0908
9 (v)	Ca	I	0.001	0.0012	0.0059	0	0	0.0637
9 (vi)	Ca	I	0.014	0.0172	0.0948	0.181	0.038	0.0966
9 (vii)	Ca	Ex	0.001	0.001	0.025	0.0085	0	0.071606
9 (viii)	Ca	Ex	0.017	0.04	0.03	0	0	0.036145
11 (i)	Ca	I	0.0005	0	0	0	0.0395	0.005753
13 (i)	E	I	0.001	0.038	0	0	0	0.040922
13(ii)	E	I	0.001	0	0.01	0	0.0011	0.090544
Overall	Mean ± SD		.00449±0.01354	.01357±0.02203	.06238±0.197495	.02626±0.1428	.00761±0.02603	.0828±0.0227
Calcified	Mean ± SD		.001144±0.0106	.0193 ± 0.02929	.1392±0.313344	.07147±0.23459	.01974± 0.04111	.0768±0.0261
Mixed	Mean ± SD		.00753±0.01616	.00999±0.01669	.02063±0.04985	.00039±0.00205	.00078±0.00205	.0866±0.0197
Echolucent	Mean ± SD		.00116±0.00109	.01168±0.01618	.00858±0.013698	.0006±0.001342	.00022±0.00049	.0842±0.0244
Common	Mean ± SD		.00314±0.01978	.01623±0.02729	.10768±0.315057	.0595±0.233479	.01503±0.04080	.0873±0.0173
Internal	Mean ± SD		.00527±0.00941	.01466±0.02011	.04317±0.080941	.00925±0.04044	.00472±0.01183	.0801±0.0226
External	Mean ± SD		0.0052±0.00639	0.0055±0.01394	0.0194±0.034876	0.00231±.0043	0±0	.0801±.03236

M - mixed; Ca - calcified; E - echolucent; C - common carotid; I - internal carotid; Ex - external carotid

Table 3.3: Strain energy constants for tension testing of plaque samples (MPa)

Sample	Classification	Vessel	C10	C01	C20	C11	C02	ζ
3 (i)	M	C	0.001	0.05	0.06	0.04	0	0.0674
3 (ii)	M	C	0.001	0.35	1.8	0.4	0.621	0.0967
4 (i)	M	C	0.015	0.0051	0.001	0.0006	0.011	0.0988
5 (i)	E	C	0.01	0.01	0.0159	0.09	0	0.0999
6 (i)	Ca	I	0.001	0.185	0.1	0.05	0.09	0.0969
6 (ii)	Ca	I	0.001	0	0.8	1.82	3.32	0.0995
8 (i)	Ca	C	0.1	0	0.2	0	0.106	0.09918
10 (i)	M	I	0.001	0	9.8	0	0	0.0986
11 (i)	Ca	C	0.001	0.01	0.03	0	0.07	0.0998
12 (i)	Ca	C	0.001	0.1	0.275	-0.005	0.27	0.0503
12 (ii)	Ca	C	0.02	0.005	-0.001	0.02	0.155	0.0989
12 (iii)	E	C	0.004	-0.002	-0.005	0.06	0.14	0.0994
13 (i)	E	C	0.02	0.01	0	0.03	0	0.0457
13 (ii)	E	C	0.048	0.069	0	0.061	0	0.0837
14 (i)	Ca	C	0.1	.025	0	0.59	0	0.0547
14 (ii)	Ca	C	0.05	0	0	0.14	0.4	0.0992
Overall	Mean ± SD		0.0234±0.0339	0.0651±0.1061	0.817±2.441	0.206±0.4606	0.324±0.8177	0.0868±0.0201

M - mixed; Ca - calcified; E - echolucent; C - common carotid; I - internal carotid; Ex - external carotid

3.4 Discussion

Improved understanding of the mechanical properties of diseased human carotid tissue may enhance our understanding of the pathophysiology of atherosclerosis. Rupture and erosion of such plaques are key mechanisms responsible for the development of cerebrovascular events, which are related to the stress levels within the plaque cap. In this study the entire plaque is surgically separated from the artery during endarterectomy. This provided an insight into how the plaque as a whole behaved and also enabled comparison to results from ultrasound imaging with grey scale median values (US/GSM). The imaging technique used here differs from previous studies: Lee et al (1992) used intravascular ultrasound imaging; Holzapfel et al (2004) used hrMRI and histology, while numerous other studies have used only histology. The choice of using US/GSM imaging was made as it is a non-invasive imaging technique that is used routinely in the clinic to determine the optimum treatment. This choice of imaging also enabled imaging to be performed before the surgery, which helped reduce the time between plaque removal and completion of sample testing. The plaque was assumed to behave as an isotropic hyperelastic material. The isotropic material

assumption was made as tests were only carried out in circumferential tension and in radial compression for the specimens due to the constraint of the size of the plaque specimens. While an anisotropic model has been used for other soft tissues such as artery walls (Holzapfel et al., 2002), the high in-specimen inhomogeneity of the plaques may lead to difficulties in modelling a consistent anisotropic behaviour.

The samples tested in this study generally show a non-linear behaviour during both compressive and tensile testing. The non-linear behaviour of plaque tissue has been demonstrated in previous studies (Salunke et al., 2001; Topoleski et al., 1997); the one exception to this non-linear behaviour known to the authors was reported by Holzapfel et al (2004) who reported that calcified tissue behaves almost linearly elastic. This was in contrast to findings in this study as well as others (Loree et al., 1994; Salunke et al., 2001) which generally found non-linear behaviour when testing tissue classified as calcified. While variability between different plaque specimens has been reported before in the literature (Holzapfel et al., 2004), there appears to be no data available on the in-specimen variations seen in the specimens in this study. The in-specimen variation observed in this study suggests that much more localised mechanical testing needs to be performed. Correlation of such data with in vivo imaging of a higher definition than US/GSM currently provides is also necessary.

The inter-patient variability observed in this study provides further support for patient (or lesion) specific stenting (Pericevic et al., 2009). The high variability between the behaviour of different samples would seem to suggest that one stent design may be better suited to a specific lesion than another; and the fact that there seems to be a relationship between the average behaviour of the artery and the classification from the imaging, it may be possible to use US/GSM to better inform the decision regarding the optimum stent design. As anticipated, calcified plaques are on average stiffer than the other plaque types (Figure 3.2). This was also reported by Holzapfel et al. (2004), however Salunke et al (2001) found that there was no significant difference between calcified and fibrous plaques. No definitive conclusion could be drawn from our study regarding the anatomical location of the samples (Figure 3.4). Whilst the average curves seem to indicate that

plaque segments in the common carotid are stiffer than in the internal or external; the large variability means that more testing is required in order for a more definitive conclusion to be reached.

There are a few limitations to the analyses performed in this study. The number of samples, particularly with tensile data, limits the conclusions that may be drawn. The main reason for the limited number of tensile samples is that the samples can be relatively large with respect to the total plaque size and given the in-specimen plaque variability the authors had some difficulty in obtaining samples with a relatively consistent material composition within the gauge. While the largest sample size possible was used for these tensile tests, the 4 x 1 mm gauge length may be insufficient to fully prevent edge effects from the clamps. The tests were also unable to consistently produce failure of the tensile samples, this resulted in not being able to report failure stresses and stretches for this study. The large variability observed in each plaque, plaque classification, and in each branch of the carotid bifurcation limited any statistical analysis of the differences in specimens. This is largely due to the considerable stiffening in some specimens in comparison to others and the fact that specimens exhibit a wide range of failure strains. As a result no statiscal analysis was performed and comparisons are limited to the mean and standard deviations of the constants. However due to the high variability observed it is unlikely that statistically significant differences would be found. Due to the large standard deviations, using the lower bound value for each constant (mean – SD), results in an unstable response as the material constants are negative. The stiffest and least stiff stress-strain responses were used as the upper and lower bounds in Figs. 3.2 and 3.4 as a consequence of this.

However the lack of fresh tissue data as well as the lack of data from human diseased carotid arteries means this data may serve as a basis for constitutive equations used in finite element modelling, with particular relevance to models of carotid lesions. The data can therefore be seen as a basis for predicting outcomes of surgical and interventional procedures using finite element modelling. While the mean curves can be used in finite element analyses, they would only represent plaques with high, medium and low stiffness. Unless the dispersion of data observed in

each clinical classification is modelled it the results may not be representative of the response of the plaque classification modelled, limiting the use of the mean curves in patient specific analyses. With further testing, coupled with correlation to higher definition imaging this limitation may be reduced in the future. Once a plaque has been classified in vivo the mean values of the hyperelastic constants, as well as the upper and lower bound stress-strain responses, could be used to predict a range of tissue responses that could be expected for a given procedure or intervention. Whether the large standard deviations reported in this study actually indicates large patient-to-patient variability in plaque properties that needs to be considered in all computational models, or is merely a consequence of significant variability in the properties of any given plaque and the sampling used in this study, needs to be further investigated using more localised testing. This could possibly be achieved using indentation testing (Barrett et al., 2009). Furthermore higher resolution imaging, which has previously been used to detect the presence of stress rising microcalcifications in plaque fibrous caps (Vengrenyuk et al., 2006), could be used to better characterise the heterogeneous nature of plaque material.

There were also limitations to the testing methodology used as a result of the environment in which tests were performed. As stated all testing of atherosclerotic plaque tissue occurred in the Galway Clinic. Testing occurred in the 'out-patient' room of the surgical theatre in which the carotid endarterectomy were performed. This room formed a link between the theatre and corridor and as a result the size and amount of equipment used needed to small enough not to impede movement into and out of the surgical theatre by hospital staff and to transport to the hospital itself. The equipment used involved a small portable test rig and a video-extensometer to measure strain in tensile testing; both of which were controlled by their respective PC. Due to the size of such equipment and the associated PC's we were limited in what other equipment or rig could be used experimentally. The environment in which testing took place limited the test methodology in two significant ways: the first is that all testing had to be carried out within a set time-frame (approximately 2 hrs); and secondly we were unable to use a second video-extensometer to monitor changes in thickness of specimens in the tensile tests. Ideally samples tested or adjacent specimens would have been used in histology or analysed biochemically to determine tissue content; however,

due to ethical approval it was not possible to analyse samples in college labs and tissue was returned to hospital staff after testing. As a result the experimental data could only be correlated to the results of the Duplex Ultrasound imaging.

In conclusion, this study characterised the radial compressive and circumferential tensile behaviour of fresh carotid atherosclerotic plaques in order to obtain a better understanding of plaque behaviour. The study also aimed to relate these results to imaging which is used clinically to determine if treatment of a lesion is necessary thus giving the results a more applicable clinical significance. It was seen that plaque classifications obtained through US/GSM may be related to the mean behaviour of a lesion. This study represents a step toward better understanding of carotid plaque behaviour; it's relation to its composition and the further use of finite element modelling in stent design. This data would be important in order to obtain an accurate simulation of interventions such as stent expansion or balloon angioplasty that consider lumen gain, vessel stresses and other factors within the carotid artery. Such simulations could be used clinically to help to decide between different treatment options such as stenting and endarterectomy.

Chapter 4 Inelasticity of Human Carotid Atherosclerotic Plaque

Maher E.[1], Creane A.[2], Sherif Sultan[3, 4], Niamh Hynes[3, 4], Lally C.[1, 2], Kelly D. J.[1]

[1] Trinity Centre for Bioengineering, School of Engineering, Trinity College Dublin, Dublin 2, Ireland.

[2]School of Mechanical and Manufacturing Engineering, Dublin City University, Glasnevin, Dublin 9, Ireland

[3]Western Vascular Institute, Department of Vascular & Endovascular Surgery, University College Hospital Galway, Ireland.

[4]Department of Vascular & Endovascular Surgery, Galway Clinic, Doughiska, Dublin Road, Galway, Ireland.

For thesis purposes the article version presented in this chapter is modified from the original published in the Annals of Biomedical Engineering 2011.

The large majority of the work discussed in this chapter was undertaken by the author of this thesis. The contributions of the other authors to this work are as follows: Dr. Kelly and Dr. Lally had a supervisory role on this study. Mr. Sultan and Ms. Hynes are the lead surgeons who performed the endarterectomy surgeries and liaised with hospital staff to supply imaging, etc. Dr. Creane assisted the author of this thesis during mechanical testing, principally acting as a pair of 'clean hands' while the biological tissue was being dissected and tested.

4.1 Introduction

Atherosclerosis is a disease of arteries which commonly results in a reduction of lumen area, caused by a build-up of fatty material in the artery wall, and a corresponding decrease in blood flow through the diseased artery. Common treatments for these stenosed arteries include balloon angioplasty, stenting or a combination of the two. The objective of these procedures is to increase the lumen size through mechanical loading of the stenosed artery. Little is known, however, about the inelastic mechanical behaviour of atherosclerotic plaques and its contribution to lumen gain. A number of authors have investigated the response of atherosclerotic plaques to different loading regimes (Barrett et al., 2009; Ebenstein et al., 2009; Holzapfel et al., 2004; Lee et al., 1991; Lee et al., 1992; Loree et al., 1994; Maher et al., 2009; Topoleski and Salunke, 2000). The characterization of the response to mechanical testing has most commonly been undertaken using hyperelastic material models to describe the effects of monotonic uniaxial loading (Maher et al., 2009). To the author's knowledge, Topoleski and co-workers (2000; 1997) are the only researchers to report specifically on the inelastic behaviour of atherosclerotic plaques. In this study, the response of the plaques to successive cyclic compression loading regimes and successive stress relaxation loading regimes, with unloaded ''rest'' periods in each case, was investigated. The degree of recovery in the mechanical properties during the ''rest'' periods was found to depend on the plaque type, with calcified plaques reported as behaving more elastic than other types. However, further mechanical testing is needed to characterize atherosclerotic plaque response adequately for use in finite element (FE) analyses; in particular the inelastic behaviour needs to be quantified across a wide range of applied strains in order to develop appropriate inelastic material models.

In order to accurately describe a material's mechanical behaviour the development of any constitutive model requires relevant mechanical testing data. Due to the lack of inelastic data discussed above hyperelastic constitutive models are often used in FE analysis of stenting procedures (Chua et al., 2004b; Early et al., 2009; Lally et al., 2005; Liang et al., 2005; Migliavacca et al., 2004; Mortier et al., 2010; Pericevic et al., 2009) in diseased arteries to assess and improve stent performance and design. Others have additionally investigated the artery

behaviour on unloading such as lumen gain post-stenting (Early and Kelly, 2010; Kiousis et al., 2007; Wu et al., 2007). As such models do not consider any inelastic behaviour they are unable to accurately quantify lumen gain post-angioplasty or stenting.

There are few models available in the literature to describe inelastic behaviour of soft tissues such as arteries and plaques. The inelastic effects commonly investigated include softening similar to the Mullins effect (Calvo et al., 2007; Peña et al., 2008; Peña and Doblare, 2009) and unrecoverable deformations (Gasser and Holzapfel, 2002; Tanaka and Yamada, 1990). The softening models are commonly based on continuum damage mechanics (Hokanson and Yazdani, 1997; Miehe, 1995; Simo and Ju, 1987b) or on pseudo-elastic (Dorfmann and Ogden, 2004; Ogden and Roxburgh, 1999) approaches proposed for rubber-like materials. Calvo et al. (2007) proposed an uncoupled anisotropic damage model for fibered biological soft tissues, where damage was defined separately for the matrix and the fibres of the material. Their approach applied continuum damage mechanics to describe irreversible Mullins like softening to the fibres and matrix separately. Peña et al. (2008) proposed a similar model that introduced a further viscoelastic approach that described the hysteresis in fibered soft tissues, while Balzani et al. (2006) applied damage to the fibre direction components only. Volokh and Vorp (2008) extended the typical softening hyperelastic theory to include a constant to describe the maximum possible energy that a material can accumulate before failure occurs. A number of other models have been proposed to model the softening behaviour of soft tissues (Emery et al., 1997; Hokanson and Yazdani, 1997; Li and Robertson, 2009). Gasser and Holzapfel (2002) developed a rate-independent elasto-plastic constitutive model for fibre-reinforced biological tissues. They use the concept of multi-surface plasticity as the basis of their constitutive framework to induce inelastic deformations in the tissue. Gasser and Holzapfel (2007a) used this model to describe the media in a FE analysis of a balloon angioplasty. In this study, the plaque was modelled as a rigid body and the inelastic constants for the media were assumed presumably due to the unavailability of suitable mechanical test data for the inelastic behaviour of vascular soft tissue. Other studies (Li and Robertson, 2009; Wulandana and Robertson, 2005) have used multi-mechanism models where damage is introduced in the elastin and collagen separately, and a residual strain results when the elastin fails. Alternative

approaches to incorporating inelastic deformations involve approaches based on pseudo-elasticity (Dorfmann and Ogden, 2004) and network alterations of chain models (Diani et al., 2006).

The objective of this study is to determine the inelastic radial compressive behaviour of human carotid atherosclerotic plaque. The inelastic mechanical properties of the plaque tissue were investigated using a cyclic radial compressive loading regime. This regime allowed the altered stress–strain behaviour resulting from increasing strain in the load history of the tissue to be observed and the residual inelastic deformations in the tissue to be quantified. In order to concisely describe the observed experimental phenomena, we present a phenomenological constitutive model incorporating inelastic effects. The model has been adapted from a basis in pseudo-elastic theory. Such analysis should be seen as a first step toward the complete characterization of the inelastic behaviour of atherosclerotic plaque. It is believed that this data, when combined with further tensile test data, could be used to improve the predictive ability of FE models and hence aid in the optimization of stent designs in order to achieve maximum lumen gain post-stenting.

4.2 Materials and methods

4.2.1 Constitutive model

An isotropic phenomenological constitutive model was implemented that incorporates the inelastic behaviour of vascular soft tissue, including inelastic deformations and softening effects. The proposed constitutive relationship can be expressed in terms of the Cauchy Stress, $\boldsymbol{\sigma}$,

$$\boldsymbol{\sigma} = (1-D)(\boldsymbol{\sigma}_{IL} - \boldsymbol{\sigma}_{IN}) \qquad \text{(Eqn. 4.1)}$$

$$\textit{where} \quad \boldsymbol{\sigma}_{IL} = 2J^{-1}\mathbf{F}\frac{\partial \psi_{IL}}{\partial \mathbf{C}}\mathbf{F}^{T} \quad \textit{and} \quad \boldsymbol{\sigma}_{IN} = 2J^{*-1}\mathbf{F}^{*}\frac{\partial N}{\partial \mathbf{C}^{*}}\mathbf{F}^{*T} \qquad \text{(Eqn. 4.2)}$$

F, *J*, and **C** are the deformation gradient tensor, the Jacobian determinant, and right Cauchy-Green strain tensor, respectively. **F***, *J**, and **C*** are the values of the deformation gradient tensor, Jacobian determinant, and right Cauchy-Green strain tensor calculated when the deformation in the

load history of the material is at a maximum. $\boldsymbol{\sigma}_{IN}$, the inelastic stress tensor, is not a function of and does not generally change with changes in deformation. $\boldsymbol{\sigma}_{IN}$ is only updated when certain criteria, discussed later, are met that result in the evolution of the function N. The initial value of $\boldsymbol{\sigma}_{IN}$ is the null, or zero, tensor. The inelastic stress tensor acts to reduce the stress in the material and results in an altered zero stress state on unloading. If the material is loaded in any direction, a residual or inelastic strain will result on unloading to the zero-stress state. $\boldsymbol{\sigma}_{IL}$, the initial loading stress tensor, is a stress tensor calculated by differentiating a strain-energy density function, ψ_{IL} with respect to the right Cauchy-Green strain tensor.

ψ_{IL} is the strain-energy density of the theoretical undamaged, or elastic, material and is equal to the strain-energy during initial loading. ψ_{IL} is a function of the right Cauchy-Green strain tensor $\mathbf{C}$ and is expressed in Eqn. 4.3 as an exponential function of the first principal invariant of $\mathbf{C}$, I_1 as proposed by Delfino et al (1997).

$$\psi_{IL}(\mathbf{C}) = \psi_{IL}(I_1(\mathbf{C})) = \frac{a}{b}\left(\exp\left(\frac{b}{2}(I_1 - 3)\right) - 1\right) \qquad \text{(Eqn. 4.3)}$$

where a and b are material constants. It should be noted that any number of commonly used isotropic constitutive models could potentially be used to fit to experimental data here.

N is a function of the right Cauchy-Green strain tensor of the material at its peak deformation in the loading history, $\mathbf{C}^*$ and results in inelastic behaviour on unloading. N is described below as a function of the first principle invariant of $\mathbf{C}^*$,

$$N(\mathbf{C}^*) = c^*(I_1^* - 3) \qquad \text{(Eqn. 4.4)}$$

where c^* is a material constant. N only evolves under certain criteria described below.

The peak deformation state is defined here as the deformation state at which ψ_{IL} is a maximum. This leads to the first criterion, for which the function N can evolve, where

$$\phi = \psi_{IL} - \alpha \leq 0, \qquad and \qquad \alpha(t) = \max_{s \in [0,t]} \psi_{IL}(s) \quad \text{(Eqn. 4.5)}$$

and α is the maximum value of ψ_{IL} during the history time interval [0,t]. The second criterion for the evolution of N is that $\mathbf{C}^*$ is only updated on unloading from the maximum deformation state. This second criterion can be accounted for in a similar method as in the discussion of isotropic damage in hyperelastic materials by Naghdi and Trapp (1975). $\dot{\psi}_{IL} < 0$ describes unloading of the material. Thus, the criteria for evolution of $\mathbf{C}^*$ and hence N and σ_{IN} is given below

$$if \quad \phi = 0 \quad and \quad \dot{\psi}_{IL} < 0, \qquad \therefore \quad \mathbf{C}^* = \mathbf{C} \qquad \text{(Eqn. 4.6)}$$

The initial value of $\mathbf{C}^*$ is the identity tensor as no deformation has occurred. This results in the initial value of N being zero. Thus, during initial loading the material response is described purely by ψ_{IL} as stated previously in this section.

The *(1-D)* term in Eqn. (4.1) introduces a stress softening factor to the model that allows the constitutive response of the model to better fit to the stress–strain behaviour on unloading of the material observed experimentally in this study. D is called the softening parameter and is a function of the maximum and current values of the function ψ_{IL}.

$$D(\alpha(t), \psi_{IL}(\mathbf{C})) = \zeta_\infty \left(1 - e^{\frac{-(\alpha(t) - \psi_{IL}(\mathbf{C}))}{i}} \right) \qquad \text{(Eqn. 4.7)}$$

where $\zeta\infty \in [0,1]$ and i are material constants and $\alpha(t)$ is the maximum value of ψIL in the loading history as described in Eqn. (4.5). As the material is initially loaded $\alpha(t) = \psi_{IL}(\mathbf{C})$ which implies that $D = 0$ and that the stress softening factor has no effect on the stress in the material. The limits of ζ_∞ restrict the softening parameter D such that $D \in [0,1]$. The material elasticity tensor $\mathbb{C}$ (Eqn. 4.8) can be found using the product and chain rules for differentiation and the assumption that the inelastic stress tensor is not dependent on the current deformation of the material.

$$\mathbb{C} = \begin{cases} (1-D)\mathbb{C}_{IL}, & \phi = 0 \; and \; \dot{\psi}_{IL} > 0 \\ (1-\mathrm{D})\mathbb{C}_{IL} - \frac{\partial D}{\partial \psi_{IL}} \boldsymbol{S_{IL}} \otimes \boldsymbol{S_{IL}} + \frac{\partial D}{\partial \psi_{IL}} \boldsymbol{S_{IL}} \otimes \boldsymbol{S_{IN}} & otherwise \end{cases} \quad \text{(Eqn. 4.8)}$$

where $\mathbb{C}_{IL} = 2\frac{\partial \mathbf{S}_{IL}}{\partial \mathbf{C}}$ $\mathbf{S_{IL}} = J\mathbf{F}^{-1}\boldsymbol{\sigma}_{\mathbf{IL}}\mathbf{F}^{-T}$ $\mathbf{S_{IN}} = J\mathbf{F}^{-1}\boldsymbol{\sigma}_{\mathbf{IN}}\mathbf{F}^{-T}$ (Eqn. 4.9)

4.2.2 Mechanical testing

Cyclic compressive tests were performed on samples taken from plaques of the carotid bifurcation. Plaque specimens were removed from eight patients (five men and three women, 66.13 ± 9.13 years, mean ± SD) during routine carotid endarterectomies. All surgeries and tests were performed in the Galway Clinic, Ireland. The study includes 21 compressive samples obtained from eight carotid plaques. Table 4.1 includes all patient and lesion details. Plaque classifications were determined independently by a clinician using routine Duplex ultrasound with gray scale imaging (Nicolaides et al., 2002; Tegos et al., 2001). Ethical approval for testing of the human tissue was obtained prior to commencing this study from the Galway Clinical Ethics board.

Table 4.1: Patient/specimen details

Specimen	Gender	Age, yr	Clinical Classification	No. of Samples
1	Male	83	Calcified proximally, mixed distally	2
2	Female	71	Mixed	2
3	Male	65	Mixed, mostly echolucent	5
4	Male	61	Calcified	3
5	Female	63	Mostly calcified, echolucent at the origin	2
6	Male	73	Calcified proximally, mixed distally	2
7	Male	58	Mixed	3
8	Female	55	Calcified proximally, mixed distally	2
	Age, mean±SD yr	66.13±9.13	Total no. of samples	21

4.2.2.1 Sample preparation

Plaque specimens were prepared for testing immediately following removal in surgery. Specimens were dissected at the bifurcation, separating them into common, internal and external carotid segments as described in Maher et al (2009).Each segment was opened by cutting along the axial direction. 4-mm diameter cylindrical radial compressive samples were removed from each of the flat rectangular segments using stainless steel punches. Testing samples were allowed to equilibrate in 0.9% saline solution for approximately 30 min before measurements of the sample dimensions were recorded.

4.2.2.2 Testing conditions

Testing was performed using a computer controlled, high precision testing device adapted for testing biological specimens (Bose ElectroForce 3100, Bose Corporation, Gillingham, UK). The testing rig has an electromagnetic driven motor, with a stroke resolution of 0.0015 mm, a maximum stroke length of 5 mm, and a minimum load resolution of 6 mN with a 22 N load cell. Samples were tested inside a water bath filled with 0.9% saline solution in order to maintain sample hydration during testing. All samples were tested at room temperature within 2 h of harvesting.

Unconfined cyclic compression tests were performed on cylindrical compressive samples. A sample was placed on the lower platen and the upper platen was moved to apply a small compressive pre-load of 0.01 N to the sample at a crosshead speed of 0.001 mm/s. This ensured a consistent contact between the platen and the top of the sample and minimal strain in the plaque, <5% in all cases. The sample height was then taken as the distance between the platens at this pre-load. Loading was under strain control and several strain levels were applied with five loading–unloading cycles for each loading level. Samples were loaded and unloaded at a rate of 5% strain/s. The loading levels were between 10 and 50% strain in 10% increments and unloading was to the 0% strain level in each case, see Fig. 4.1. This testing methodology is similar to that used to determine stress softening in rubbers (Li et al., 2008; Woo et al., 2008). Preliminary testing was performed on porcine arterial tissue in an attempt to rule out possible visco-elastic or poro-elastic response of the tissue. A resting period of 2 h at 0% strain was added every five cycles before the

peak strain value was increased. No significant difference was found between the levels of inelastic deformation on unloading between arterial samples tested with or without the relaxation period present. This indicates that no significant recovery of the tissue occurred which suggests that the inelastic response was in line with the theoretical concept presented here.

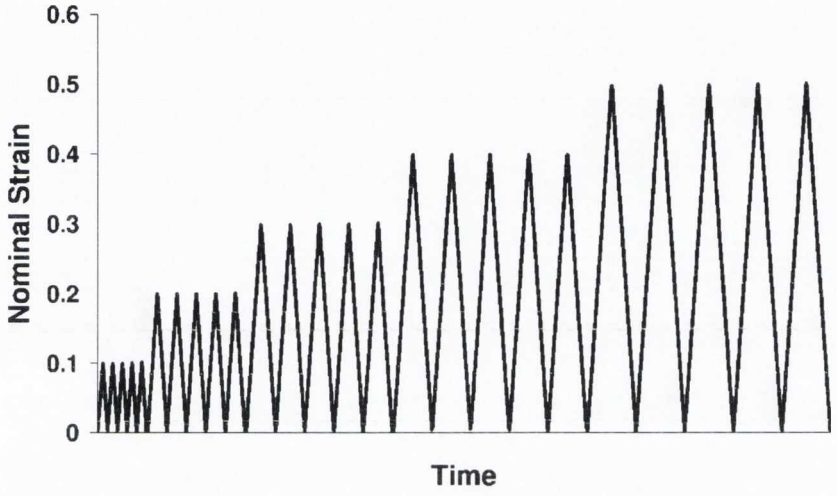

Figure 4.1: Cyclic loading applied to samples.

4.2.2.3 Data fitting and analysis

The data fitting assumes that homogeneous deformation occurred in the tissue during uniaxial loading. A typical stress–strain response of atherosclerotic plaque is seen in Fig. 4.2. The *loading envelope* is defined as a curve composed of the peak stress–strain points of each strain level (see Fig.4.2). These points are the maximum stress–strain points in the first cycle at each new strain level. It has been observed in rubbers that the monotonic loading behaviour of a material is similar to this loading envelope (Li et al., 2008) As the variable nature of atherosclerotic plaque properties (as seen in a previous study (Maher et al., 2009)) rules out testing monotonic and cyclic behaviour separately, the loading envelope is assumed to be indicative of the plaque's monotonic loading behaviour. The function ψ_{IL} is fit to the loading envelope using a linear least squares procedure. The fitting of the load envelope is similar to the fitting process used in a previous study (Maher et al.,

2009) and aims to minimize the relative error between the nominal uniaxial stress predicted by ψ_{IL} using Eqn. 4.10 and that measured experimentally to obtain the constants a and b. The nominal stress of an incompressible material during initial uniaxial loading, P_{IL}, can be expressed as (Holzapfel, 2000):

$$P_{IL} = \frac{\partial \psi_{IL}}{\partial \lambda} = 2\left(\lambda - \lambda^{-2}\right)\frac{\partial \psi_{IL}}{\partial I_1} \qquad \text{(Eqn. 4.10)}$$

where λ is the uniaxial stretch the material has undergone in the direction of loading.

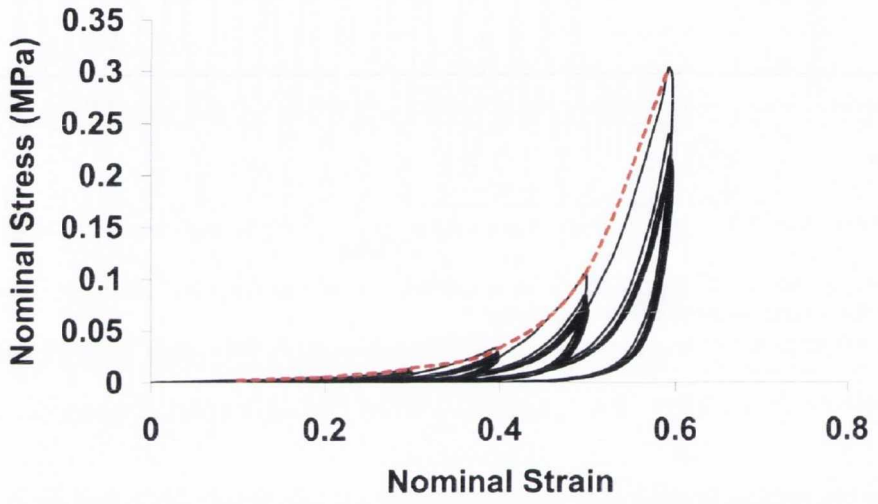

Figure 4.2: Typical response of atherosclerotic plaque to cyclic testing (sample 8(ii)). Dotted line represents the theoretical "load envelope" of the tissue.

The next step is to determine the material parameter c^* by fitting to the permanent deformations experienced at different levels of peak strain. A function, P_P, for nominal stress in an incompressible material with permanent deformations is defined as:

$$P_P = \lambda^{-1}\sigma = \lambda^{-1}\left[2(\lambda - \lambda^{-2})\left(\lambda\frac{\partial \psi_{IL}}{\partial I_1}\right) - 2\left(\lambda^* - \lambda^{*-2}\right)\left(\lambda\frac{\partial N}{\partial I_1^*}\right)\right] \qquad \text{(Eqn. 4.11)}$$

where λ^* is the maximum stretch that has occurred in the loading direction in the load history. The current stretch, λ, at which P_P is equal to zero gives the predicted inelastic deformation for a given value of λ^*. A linear least squares procedure is utilized to find the value of the parameter c^* that

results in the minimum combined relative error between inelastic deformation predicted using Eqn. 4.11 and that experimentally measured for all load levels.

The final step in the data-fitting procedure is to use the softening parameter D to improve the accuracy of the unloading and reloading behaviour predictions of the model. As the majority of the inelastic effect is seen to occur in the first load–unload cycle of each peak strain level while the subsequent reloading and unloading curves are nearly superimposed, see Fig. 4.2, the second loading curve in each cycle is assumed to represent the materials unload and reload behaviour. A least squares procedure is utilized to find the value of the parameters ζ_∞ and i, by minimizing the total relative error between experimental stress–strain response observed on reloading and that predicted by the model for all the peak loading levels. The nominal stress predicted by the model for a uniaxially loaded incompressible material, P (Eqn. 4.12), is utilized in this step using the values for a, b, and c^* calculated in previous steps.

$$P = (1 - D)P_P \qquad \text{(Eqn. 4.12)}$$

As an independent measure of the quality of the constitutive model fit the root mean square error χ was used (Balzani et al., 2011) (Eqn. 4.13).

$$\chi = \frac{\sqrt{\dfrac{\sum_i (data\ measured(i) - data\ calculated(i))^2}{n-q}}}{P_{ref}} \qquad \text{(Eqn. 4.13)}$$

where n is the number of data points and q is the number of constants to be fit. P_{ref} is the maximum experimental value measured for the data being fit. Each of the three fits described above (i.e., initial loading, magnitude of permanent deformation, and the unloading–reloading response) were analyzed separately. The averages of the two errors concerning the stress–strain response, χ_s, and the error for the permanent deformation fit, χ_{pd}, are reported in Table 4.2. The experimental data were analyzed to investigate any variation in the inelastic behaviour of atherosclerotic plaques due to their clinical classification (calcified, echolucent, and mixed). The constitutive model was

implemented as a user material in the finite element package ABAQUS. This user material was used to verify the curve-fitting resulted in a close match to the experimental data and that the constants obtained did not result in any instability in the material model.

Table 4.2: Constitutive model material constants fitted to experimental cyclic compression data.

Sample	Classification	a (kPa)	b	C* (kPa)	ζ_∞	i	χ_r	χ_{sat}
1(i)	Ca	70	0.5	11	0.9	0.03	0.0577	0.119
1(ii)	M	4.5	0.25	0.62	0.9	0.004	0.135	0.093
2(i)	M	23	0.7	4.5	0.95	0.03	0.129	0.092
2(ii)	M	1.9	0.0001	0.35	0	NA	0.115	0.008
3(i)	M	55	0.44	11.5	0.9	0.01	0.084	0.095
3(ii)	E	15.7	0.415	2.8	0.87	0.008	0.058	0.036
3(iii)	E	27	0.925	6.2	0.92	0.007	0.054	0.083
3(iv)	E	4.2	0.25	0.66	0.95	0.008	0.052	0.041
3(v)	E	11.5	1.165	2.1	0.91	0.014	0.064	0.031
4(i)	Ca	93	1.88	17.5	0.85	0.045	0.084	0.103
4(ii)	Ca	10	0.62	1.8	0.9	0.008	0.05	0.061
4(iii)	Ca	18	1.29	4.4	0.95	0.008	0.025	0.0424
5(i)	Ca	47	0.747	12	0.97	0.009	0.049	0.128
5(ii)	E	2.5	0.6	0.45	0.87	0.002	0.027	0.055
6(i)	Ca	40	5.3	5	0.65	0.01	0.092	0.085
6(ii)	Ca	120	4.35	26.9	0.85	0.011	0.116	0.0565
7(i)	M	100	0.5	14.5	0.92	0.018	0.053	0.101
7(ii)	M	80	0.6	11	0.9	0.017	0.0474	0.124
7(iii)	M	110	4.2	26	0.7	0.01	0.084	0.105
8(i)	Ca	150	1.22	28	0.84	0.015	0.027	0.131
8(ii)	M	9	1.72	2	0.9	0.01	0.0258	0.043
Overall	Mean ± SD	47.25±45.32	1.32±1.47	9.01±9.04	0.838±0.207	0.014±0.01	0.068±0.034	0.078±0.036
Calcified	Mean ± SD	68.5±49.49	1.99±1.82	13.33±10.04	0.864±0.099	0.017±0.013	0.063±0.032	0.091±0.035
Echolucent	Mean ± SD	12.18±9.87	0.67±0.37	2.44±2.32	0.904±0.034	0.008±0.004	0.051±0.049	0.049±0.021
Mixed	Mean ± SD	47.93±44.38	1.05±1.37	8.81±8.81	0.771±0.321	0.014±0.008	0.084±0.04	0.083±0.038

M—mixed, Ca—calcified, E—echolucent.

4.3 Results

4.3.1 Test data

The stress–strain response of a typical mixed classification plaque is shown in Fig. 4.2. This graph is representative of the behaviour seen in all of the plaque classifications in response to the applied cyclic loading; there is a large softening effect observed between the first loading cycle in each strain level and the subsequent cycles where the response is much more consistent. Unrecoverable deformation that increases with the peak applied load can also be observed. Differences in the loading and unloading response of the plaques indicate a hysteresis effect. The unloading response of the tissue is consistent for all cycles in each level of applied strain.

There is an approximately linear increase in the inelastic deformation occurring on unloading with increases in the peak applied strain in the plaques, see Fig. 4.3. This approximately linear relationship is observed for all three plaque types. The magnitude of inelastic strain on unloading from a given applied strain is relatively consistent for each plaque classification. For example, on unloading from 30% strain there is a residual inelastic strain of between 9 and 12.5% in echolucent plaques, illustrating the relatively low variability in inelastic strain. The magnitude of inelastic strain also does not appear to be significantly affected by the type of plaque, see Fig. 4.3d.

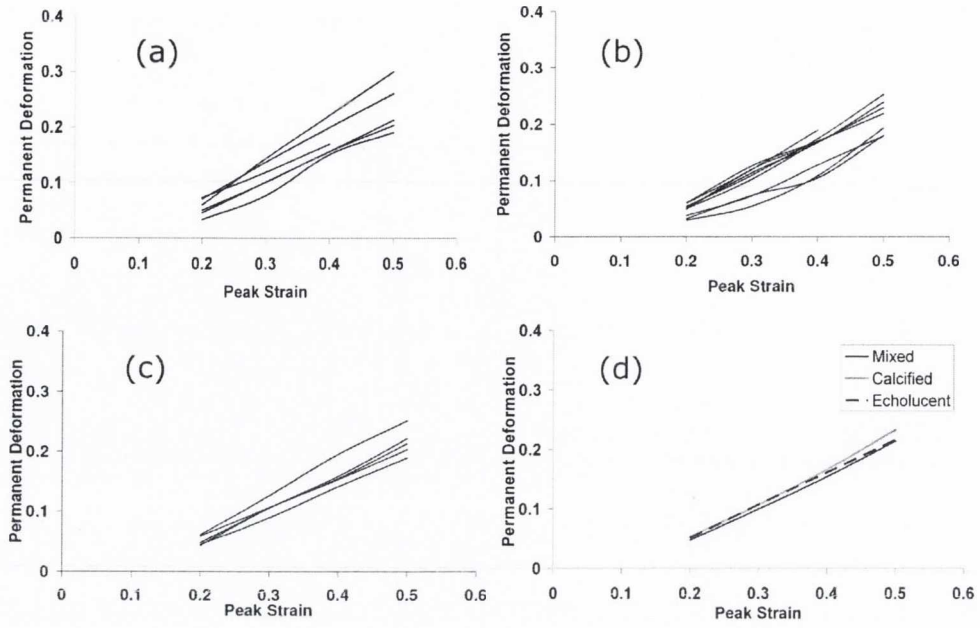

Figure 4.3: Unrecoverable strain at different applied peak strains for the plaque specimens grouped by clinical classification; (a) calcified; (b) mixed; (c) echolucent; (d) shows the mean inelastic strain for given applied strains for each classification.

4.3.2 Constitutive model data fitting

The fitted constitutive material constants for each of the plaque specimens are reported in Table 4.2. The mean constants for each plaque classification are similarly reported. The mean values of the constants a and b, which represent the initial loading behaviour and uniaxial loading response of the plaques, suggest that, similar to the trend observed previously (Maher et al., 2009) the calcified plaques are on average the stiffest plaque type, while the echolucent plaques are the least stiff. However, the large standard deviations illustrate that there is significant variation in the uniaxial loading behaviour of each plaque type. A relatively smaller magnitude of variability is observed in the inelastic constants, ζ_∞ and i of the softening parameter.

A good correlation with the experimental data was found quantitatively and qualitatively with the model; see the relatively small errors in Table 4.2. The ability of the constitutive model

used to describe the inelastic behaviour of the representative plaque behaviour for calcified, echolucent, and mixed plaque classifications is illustrated in Fig. 4.4. The initial loading behaviour of the plaque, the reloading curves, and the magnitude of inelastic strain predicted by the model for each strain level are seen to adequately approximate the behaviours observed in the mechanical tests.

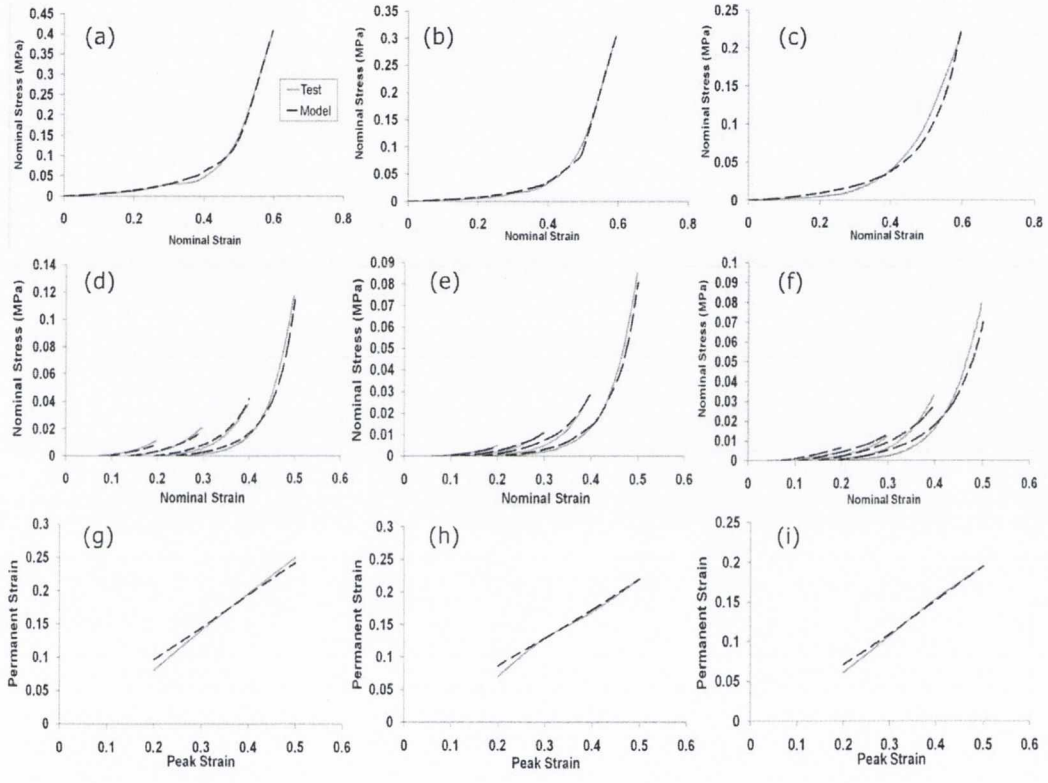

Figure 4.4: Constitutive model fit (dashed black line) to experimental data (gray line) for the load envelope of representative calcified (a), mixed (b), and echolucent (c) plaques; the second loading cycle of each strain level of each of the representative plaque plaques [(d), (e), and (f), respectively]; and the magnitude of residual strains on unloading for given applied strains [(g), (h), and (i), respectively]. The residual strain predicted by the model on unloading is equivalent to the zero-stress state.

4.4 Discussion

In this chapter, the inelastic behaviour of human carotid plaques in response to radial compression was investigated through mechanical testing. The inelastic effects observed in soft tissues include stress softening and inelastic deformations similar to what is observed in rubbers (Diani et al., 2006; Dorfmann and Ogden, 2004) and both phenomena were observed for carotid plaques here. Interestingly, it was observed that plaque composition had no significant effect on the magnitude of permanent deformations occurring on unloading of the plaque. It might be expected that plaques of different composition whose loading behaviour tends to be dependent on plaque type (Holzapfel et al., 2004; Maher et al., 2009) would experience different unloading responses. However, it is possible that different mechanisms of damage may be more prevalent in each plaque type, leading to similar end results. Clinical studies (Gil et al., 1996) have reported no significant difference in acute lumen gain for different plaque types with different mechanisms predominant for each classification.

The diameter of the samples used for mechanical testing was of a similar order of magnitude to the inhomogeneity observed in the tissue using both duplex ultrasound imaging and macroscopic visual observation. However, due to the resolution of the imaging used it is possible that smaller inhomogeneities such as micro-calcifications were not identified. Therefore, the test data provides global tissue mechanical properties specific to the local clinical classifications that can be made using duplex ultrasound.

There are a number of limitations to the testing protocol adopted in this study. The mechanical testing was performed at room temperature rather than a more biologically appropriate 37 °C. The data-fitting procedure assumes that homogeneous deformation occurs when the tissue is loaded uniaxially. Given that atherosclerotic plaque has been seen to exhibit anisotropic behaviour (Holzapfel et al., 2004) it is likely that the deformation would be inhomogeneous when loaded. Limitations of tissue availability and local variations in the mechanical properties of atherosclerotic plaques (Maher et al., 2009) prevented the use of the larger sample sizes needed for uniaxial or biaxial tensile testing, and as a result unconfined uniaxial compressive testing was performed on

plaque samples. As the major loading during the course of balloon angioplasty is circumferential tensile, this represents a notable limitation to the present study if using the data for modelling such clinical procedures. Understanding the relative contributions of radial and circumferential stresses in determining permanent deformation and stress softening during angioplasty is complicated by the fact that the plaque tissue itself is inhomogeneous, typically consisting of islands of stiffer tissue surrounded by more compliant tissue (Holzapfel et al., 2004). This results in a differing multi-axial stress state locally in regions near the interface between the tissue components particularly where there are large differences in the stiffness of the components, potentially increasing the importance of radial stresses locally in the tissue. The overall importance of this effect on the radial compressive stresses within the tissue will most likely increase with increasing plaque inhomogeneity. Regardless evaluating the radial compressive behaviour alone is not sufficient to develop a constitutive model to accurately describe plaque behaviour during angioplasty, although it could be argued that a constitutive model of inelasticity based on such data is an improvement on the use of purely elastic FE models which currently dominate the stent–artery interaction literature (Chua et al., 2004b; Early and Kelly, 2010; Early et al., 2009; Lally et al., 2005; Migliavacca et al., 2004; Pericevic et al., 2009; Zahedmanesh et al., 2010). This argument is partially motivated by the observation in our previous study (Maher et al., 2009) that human plaque tissue does not display dramatic tension–compression nonlinearity. Therefore, a constitutive model developed with this data would be capable of describing the initial loading behaviour of plaque with comparable accuracy to current isotropic hyperelastic models, and provides an initial, albeit limited, estimate of stress softening and permanent deformation on unloading. If future testing reveals significant tension–compression nonlinearity in the levels of stress softening and permanent deformation then clearly this data, by itself, will not be suitable for use in modelling clinical procedures such as angioplasty and stenting. Further studies are required to determine the inelastic properties of plaque following uniaxial and biaxial tensile testing. Coupling such data with FE modelling that considers the inhomogeneous nature of plaque tissue will allow the tissue to be more completely characterized.

It is possible that the compressive testing is capturing poro- or visco-elastic effects rather than a permanent inelastic strain effect. A preliminary study performed on porcine arterial tissue revealed little tissue recovery following dwell periods of up to 2 h. As the tissue was hydrated throughout the course of the test some recovery in mechanical properties would be expected if the reported ''permanent'' deformation was due in a large part to visco- or poro-elasticity of the material. Another challenge with testing biological tissue is ensuring uniform contact with the sample prior to the application of loading. Typically samples had a slightly uneven surface following removal. The magnitude of the preload in this study was chosen to ensure reasonably uniform contact with the specimen while minimizing the strain applied to the tissue.

There is currently little data available in the literature relating to the precise mechanisms of damage within atherosclerotic plaque on unloading. Mechanisms of lumen gain during angioplasty described clinically include plaque compression, fracture, and dissection among others (Honye et al., 1992; Waller, 1989). Plaque composition varies between the different classifications, so it is possible that dissimilar mechanisms are at work in each plaque type. Due to the likelihood of differing mechanisms of damage at work in each classification, and without sufficient evidence for the mechanisms involved, a more general phenomenological model was presented to describe the inelastic phenomena observed due to compressive loading in all plaque classifications as an initial step toward the characterization of the tissue inelasticity. This model is a simple method of representing the test data, and the strain energy constants provided by the model facilitate dissemination of the experimental findings.

The constitutive model proposed in this study results in a consistent quality fit, see Fig. 4.4 and Table 4.2. The load envelope was assumed to be equivalent to the uniaxial loading behaviour of the plaque. Ideally, the initial loading behaviour of the plaque should be determined from a separate uniaxial compression test. However, due to high inter-sample variations in plaque mechanical properties observed in a given classification, it was not possible to combine the results of separate tests for loading and unloading. High variability in the standard deviations in the constants a and b result from the highly variable stiffness of the loading response. As the levels of

permanent deformation are similar in plaques of varying stiffness it is necessary that there is high variability in the constant c^*. It should be noted that despite $\mathbf{C}^*$ only being updated on unloading inelastic effects develop in tissue during the loading phase. In this model, the effects of damage during the initial loading is incorporated into the constants of the load envelope a and b, while the inelastic constants c^*, ζ_∞, and i represent the differences between the loading and unloading–reloading behaviour of the tissue that occurs as a result of the inelasticity. The inelastic constants, ζ_∞, and i, were fit to the stress–strain response in the second loading cycle of each strain level. This decision was motivated by an interest in investigating repeated loading events of the lesion such as pre-stenting expansion by a balloon, stenting followed by post-stenting balloon expansion; as well as the effects of physiological loading of the lesion post-stenting due to movement (Robertson et al., 2008; Vos et al., 2003). The stress–strain response on unloading could have been used for the fit of ζ_∞, and i instead which would be of greater benefit to FE models in which only one loading–unloading cycle was present. Regardless the proposed model is more appropriate than the assumption of elasticity in determining the unloading behaviour of the plaque, particularly as stress softening phenomena observed during the first unloading cycle were more significant than hysteresis effects in subsequent loading and unloading cycles.

There are a number of limitations associated with the proposed constitutive model of plaque inelasticity. The constitutive model is phenomenological, and as such it is difficult to relate the material constants to a physical meaning. The main limitation of the model is the assumption of isotropy. The damage is isotropic and uses the maximum value of the strain-energy ψ_{IL} in its criteria for damage evolution. Therefore, only one type of loading regime can be adequately accounted for. If, for example, the tissue is loaded in compression in a given loading cycle and in tension in a subsequent loading cycle, damage will not progress unless the strain-energy ψ_{IL} reaches a greater value in tension than it obtained in the compression, which is not necessarily the case in reality. In the case of stenting procedures where pre- or post-expansion is used the loading mechanism on the tissue will be similar in each loading phase allowing models of inelasticity similar to that proposed here to be used. For models that include different loading regimes such as bending or torsion that occur in peripheral arteries (Vos et al., 2003) an anisotropic inelastic model

would need to be implemented (Gasser and Holzapfel, 2002). The loading behaviour defined by Eqn. 4.3 is also isotropic. Further potential limitations include the fact that residual stresses and strains were not considered as part of the constitutive formulation. This is in line with the observation of approximately zero opening angles for atherosclerotic plaques cut longitudinally (Auer et al., 2010). A rate-independent approach to inelasticity and damage has also been assumed, however, rate dependency cannot be ruled out without further testing.

In conclusion, this study investigated aspects of the inelastic response of carotid atherosclerotic plaques to radial compression in order to obtain a better understanding of plaque response to loading. This study also aimed to relate the inelastic mechanical properties to plaque classification, finding no significant difference between the magnitudes of residual strains between each classification. Further testing is still required in order to adequately describe atherosclerotic plaque response to other modes of loading that plaque will experience during angioplasty. Due to the limitations discussed earlier caution should be used when implementing the model, which is based solely on compressive testing data alone, to make predictions of lumen gain during clinical procedures. However, the data presented here can be combined with tensile data from future studies to more fully describe the tissue response. As such this study can be viewed as an initial step toward the complete characterization of the inelastic response of atherosclerotic plaque to mechanical loading.

Chapter 5 Site Specific Inelasticity of Arterial Tissue

Maher E.[1], Early, M.[1*], Creane A.[2], Lally C.[1, 2], Kelly D. J.[1]

*Biochemical analysis was performed by this author

[1] Trinity Centre for Bioengineering, School of Engineering, Trinity College Dublin, Dublin 2, Ireland.

[2]School of Mechanical and Manufacturing Engineering, Dublin City University, Glasnevin, Dublin 9, Ireland

For thesis purposes this chapter is modified from an article submitted to the Journal of Biomechanic

The large majority of the work discussed in this chapter was undertaken by the author of this thesis. The contributions of the other authors to this work are as follows: Dr. Kelly and Dr. Lally had a supervisory role on this study. Dr. Early performed the biochemical analysis of the tissue.

5.1 Introduction

Stenting and balloon angioplasty are common procedures to treat atherosclerotic arteries through mechanical loading of the lesion. In order to be able to predict the outcome of these procedures, and to properly analyse new cardiovascular medical device designs, a thorough understanding of both healthy and diseased arterial tissue mechanical behaviour is necessary. Arteries are multi-layered vessels with each layer containing different proportions of the main structural components of arteries, namely collagen, elastin fibrils and smooth muscle cells. Arteries can be divided into two broad categories: elastic and muscular arteries, with the diameter, layer thicknesses and layer compositions depending on the artery type (Martini, 2006). The mechanical properties of arteries are largely determined by the relative amounts of collagen, elastin and smooth muscle it contains, and the structural organization of these components. The elastin and collagen components are the main determinants of the elastic behaviour of arteries, with the lower stiffness elastin having prominence at low strains or pressures and the higher stiffness collagen fibres determining the large strain behaviour (Roach and Burton, 1957; Salvucci et al., 2009). The vascular smooth muscle content of the arteries is closely related to the viscoelastic properties of the tissue such as stress relaxation (Salvucci et al., 2009). As the proportional content of these components in arteries determines their mechanical behaviour it is clear that arterial mechanical properties will vary throughout the arterial tree.

A number of studies have investigated the elastic behaviour of arterial tissue (Garcia et al., 2011; Lally et al., 2004; Schulze-Bauer et al., 2003; Sommer et al., 2010) and its failure characteristics (Holzapfel et al., 2004; Stemper et al., 2007a; Teng et al., 2009; Walraevens et al., 2008). It has been reported that arterial tissue displays anisotropic characteristics (Garcia et al., 2011; Holzapfel et al., 2005; Holzapfel et al., 2004) which has been attributed to the orientation of the collagen fibres (Holzapfel, 2006) and to the anisotropy of the elastin network (Zou and Zhang, 2009). Viscoelastic behaviour such as stress relaxation (Silver et al., 2003; Yang et al., 2011) and strain rate dependency of the stress-strain response (Yang et al., 2011) has also been observed. While there are studies in the literature that compare the elastic (Patel and Janicki, 1970; Salvucci et al., 2009; Silver et al., 2003) or viscoelastic (Salvucci et al., 2009; Silver et al., 2003) behaviour

of different vessels, to the authors' knowledge no data exists characterising or comparing stress softening and the inelastic deformations that occur on unloading due to damage induced within the tissue and how this behaviour will vary throughout the arterial tree. As the ultimate goal of clinical procedures such as stenting and angioplasty is to maximise the post-procedure lumen gain, further work is required to characterise inelastic deformations due to the damage that results from over-stretching the tissue beyond the physiological domain.

Due to the difficulty in obtaining fresh human arterial specimens, porcine arteries are commonly used in studies to mechanically characterise arterial tissue (Dixon et al., 2003; Lally et al., 2004; Pandit et al., 2005; Silver et al., 2003). This approach has been justified due to the similarities between the human and porcine cardiovascular systems and the fact that porcine models are commonly used in the pre-clinical evaluation of medical devices. The objective of this study was to characterise the variation in the inelasticity of arterial tissue throughout the porcine arterial tree. In particular we sought to determine the magnitude of stress softening and residual inelastic deformations that result on unloading of arterial tissue from non-physiological strains. To further characterise this response, the anisotropic inelastic behaviour resulting from the structure of the vessels was also investigated. To this end, tissue from porcine thoracic aorta, proximal common carotid, femoral and right coronary arteries were subjected to radial compression, while aortic and carotid tissue was further tested in circumferential and longitudinal tension to characterise the anisotropy of the inelastic response.

5.2 Materials and methods

Arterial tissue was harvested from 3-4 month old female pigs using a scalpel within one hour of the pig being put down. Fat and connective tissue were trimmed from the arteries, which were then stored in 0.9% saline solution at 4°C. Four artery types were harvested; proximal common carotid arteries, femoral arteries, right coronary arteries and thoracic aorta. All testing was completed within 48 hrs of tissue harvesting. Mechanical testing was performed using a high precision testing

device adapted for testing biological specimens (Bose ElectroForce 3100, Bose Corporation, Gillingham, UK) with a load resolution of 6mN and a stroke resolution of 0.0015mm.

5.2.1 Site specific inelasticity of arterial tree

3.5 mm diameter cylindrical radial compressive samples removed from the aorta, femoral, carotid and coronary arteries of a single pig were loaded in uniaxial cyclic compression in order to determine the inelastic strains remaining in the tissue on unloading. Samples were placed on the lower platen and the upper platen was moved to apply a small compressive pre-load of 0.01 N to the sample at a crosshead speed of 0.001 mm/s. This ensured a consistent contact between the platen and the top of the sample. The sample thickness was then taken as the distance between the platens at this pre-load. The thickness of the samples tested was measured as 1.39±0.089 mm, 0.597±0.036 mm, 0.676±0.079 mm, 0.581±0.099 mm for aorta, carotid, femoral and coronary samples respectively. Samples were loaded cyclically at a strain-rate of 0.005 s-1 between 0 % strain and a peak compressive strain starting at 10% and increasing incrementally every 5 loading-unloading cycles by 10% up to a maximum of 60% similar to previous studies (Maher et al., 2011). Testing occurred inside a water bath filled with 0.9% saline solution in order to maintain sample hydration during testing. 6 samples from each artery were tested.

The hypothetical elastic response of the sample, i.e. the behaviour of the tissue if loaded in a monotonic uniaxial test, is estimated from the peak stress-strain points of each loading cycle which is termed the *load envelope* (Maher et al., 2011). The stresses in this study were expressed as the Cauchy stress σ,

$$\sigma = \frac{F}{A_0}\lambda \qquad \text{(Eqn. 5.1)}$$

where F is the magnitude of the compressive force, A_0 is the original cross-sectional area of the sample and λ is the stretch ratio. The residual inelastic strains were determined from the strain level

at which the 2nd loading cycle from each set of 5 exceeded 0 *MPa*. Therefore if at a stretch of 1 the stress is 0 *MPa* no inelastic deformation has occurred.

To analyse the stress softening that occurs in a sample due to cyclic loading to a specific applied strain, the % stress softening was defined as the percentage change in the area under the stress-stretch curve between the 1st and 2nd loading cycle for a given peak load, i.e.

$$\%\ Stress\ Softening = 100 * (A_1 - A_2)/A_1 \quad \text{(Eqn. 5.2)}$$

where A_1 is the area under the stress-stretch curve during the first loading cycle and A_2 is the area under the stress-strain curve during the second loading cycle. Two way analysis of variance (ANOVA) was used to determine statistical significance of the data, which was set at $P<0.05$. Minitab software version 15.1 (Minitab Inc, PA) was used for statistical analysis.

5.2.2 Anisotropic inelastic behaviour of arterial tissue

Due to their larger diameter, aorta and carotid arteries were tested in circumferential and longitudinal tension in addition to radial compression. These arteries were harvested from 2 pigs and 6 circumferential and longitudinal strips, approximately 2 mm wide and 10 mm long for the carotid and 3 mm wide and 17 mm long for the aorta, were excised. A similar loading profile as described for the compression testing was used for tensile testing. Strain was measured visually using a computer based video extensometer to measure changes in the distance between a grid of marks on a sample from the initial length determined after applying an initial pre-load of 0.01 N (Maher et al., 2009). The displacement rate used during testing was 0.065 mm/s (0.0038 – 0.0093 s^{-1}) and 0.035 mm/s (0.0042 – 0.0081 s^{-1}) for the aorta and carotid tensile specimens respectively. This rate was chosen so that the strain-rate was similar in magnitude to that of the compressive testing for comparative purposes. The loading and unloading behaviour of the arteries were compared in all three directions (circumferential tensile, longitudinal tensile and radial compressive) and a two way ANOVA was used to determine statistical differences.

5.2.3 Biochemical analysis

Biochemical analysis was used to determine the relative amounts of collagen and elastin in aorta, femoral and coronary arteries. Specimens were cut in two with a scalpel and the wet weight obtained. The samples were then immediately placed in a freezer at -84°C. One half was analysed for elastin content and the other for collagen content. This enabled the collagen to elastin ratio to be obtained for each specimen. A Fastin Elastin Assay (Biocolor, Newtownabbey, Northern Ireland) was used to measure the total elastin content in the arteries. As the collagen could not be suitably solubilised for use with a collagen assay; hydroxyproline was used as a measure of collagen content instead. Hydroxyproline is an amino acid, which is believed to occur exclusively with collagen, in a fixed ratio (Kafienah and Sims, 2004). Therefore, measurement of the hydroxyproline content allows calculation of the collagen content, based on a procedure described by Kafienah and Sims (2004). Previous experiments on the porcine aorta have assumed that the average collagen molecule contains 10% hydroxyproline residues (Davidson et al., 1985), and this ratio is assumed here. One way ANOVA was used to determine statistical significance between the collagen to elastic ratios of the different arteries ($P<0.05$).

5.3 Results

Stress softening and inelastic deformations were observed on unloading in tension and compression, see Fig. 5.1. The typical pre-conditioning effect whereby a consistent stress-strain response occurs after repeated loading cycles is observed. A consistent response is achieved after 3-4 cycles for all artery types; however the majority of the softening occurs during the initial loading-unloading cycle for a given applied strain. An overall significant difference in the inelastic deformations on unloading from different magnitudes of compressive strains was found between all artery types ($p < 0.05$), see Fig. 5.2. The largest inelastic strains were observed for the coronary artery while the aorta exhibited the lowest inelastic strains. A similar trend was also observed for the stress softening behaviour, where it tended to be greatest for the coronary artery while the aorta tended to exhibit the lowest % stress softening. However significant differences in the % stress

softening were found only for low values of applied strain ($P < 0.05$), see Fig. 5.2. The coronary artery had the highest collagen to elastin ratio of those tested while the aorta has the smallest ($P<0.05$), see Fig. 5.3.

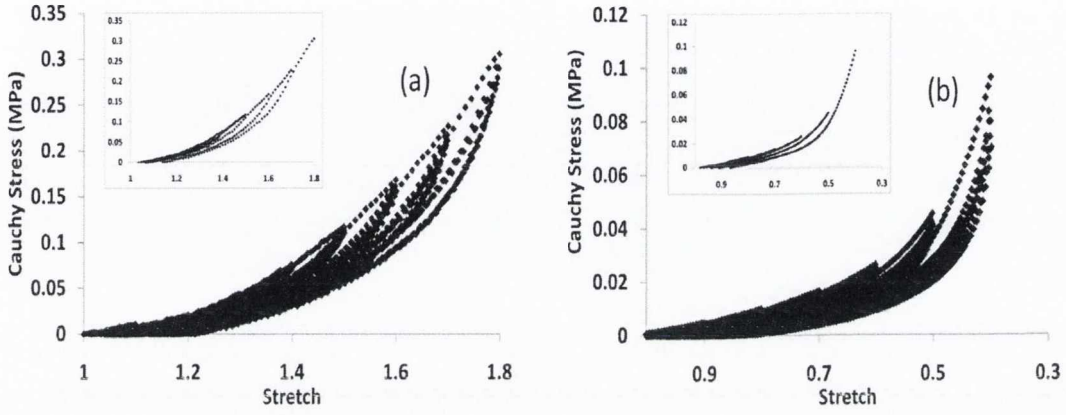

Figure 5.1: Typical stress stretch response of aortic tissue due to (a) tensile and (b) compressive loading. The magnitude of the compressive stress is used for ease of comparison. Inset shows first loading phase of each strain level only.

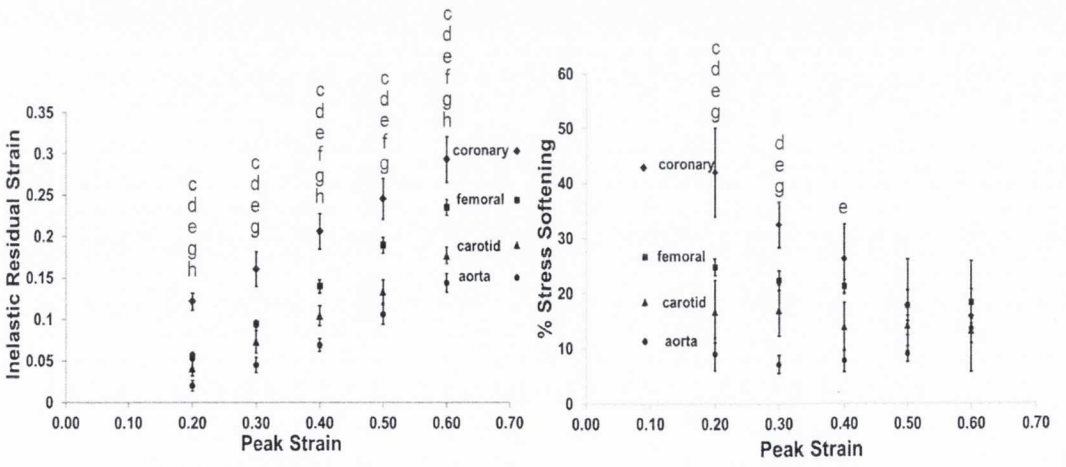

Figure 5.2: Magnitude of inelastic residual strains and % stress softening on unloading from various peak nominal strains in arterial samples due to compressive loading of samples from different locations in the arterial tree. c, d and e indicate statistical differences ($P<0.05$) between coronary samples and either femoral, carotid or aorta samples respectively; f and g statistical differences ($P<0.05$) between femoral and either carotid or aorta; and h statistical differences ($P<0.05$) between carotid and aorta on unloading from a given peak load.

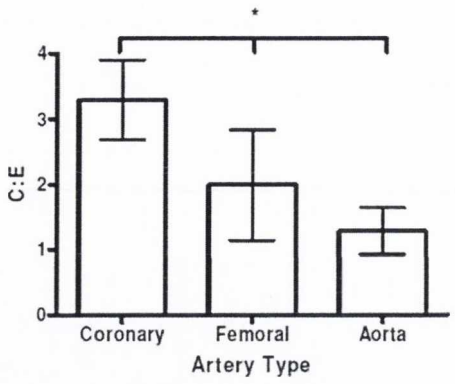

Figure 5.3: Collagen to elastin ratio (C:E) (mean ± standard deviation) of three different artery types. Statistical difference (P<0.05) is indicated with an asterisk (*).

Both the aorta and carotid artery were stiffest in the circumferential directions, see Fig. 5.4. A similar stress-strain response is observed for both longitudinal tension and radial compression in both arteries, with the radial compressive behaviour tending to be less stiff than the longitudinal tensile response. (The absolute magnitude of the radial compressive stresses is used in Fig. 5.4 to allow easier comparison with the tensile data.) A comparison between the *load envelopes* of the two arteries indicates that the carotid artery is stiffer in circumferential tension than the aorta.

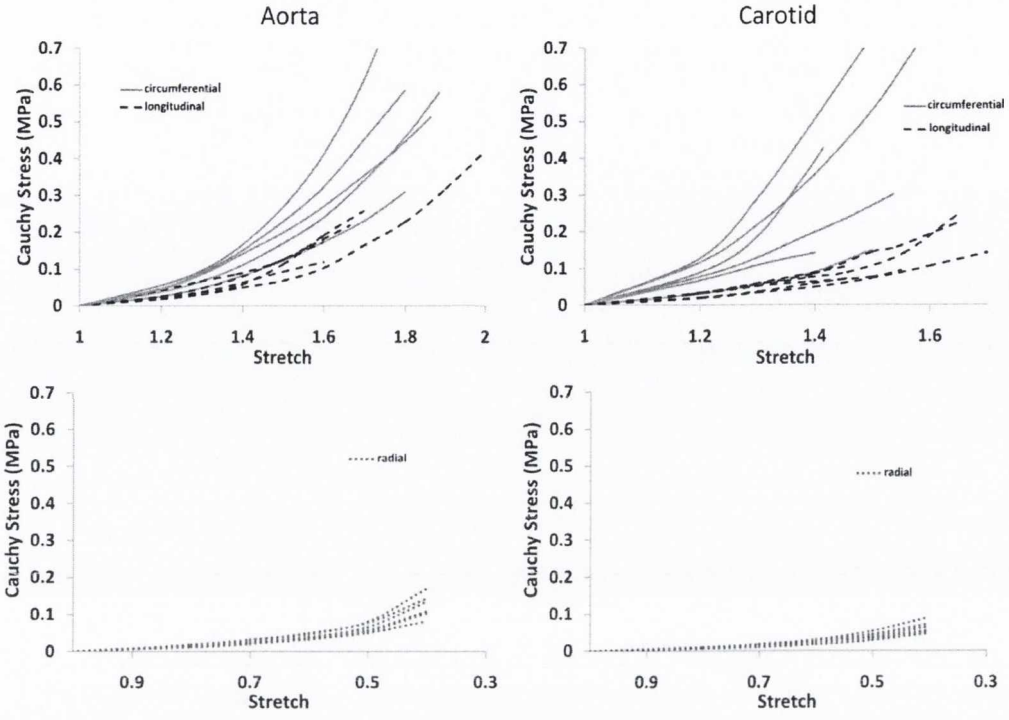

Figure 5.4: Magnitude of hypothetical circumferential and longitudinal tensile and radial compressive elastic loading response, estimated as the load envelope, for aortic and carotid samples.

The carotid also tends to be less stiff in radial compression than the aorta while no difference between the longitudinal tensile behaviour of either artery is apparent. The largest inelastic deformations are observed in radial compressive direction and the lowest in circumferential tensile direction (Fig. 5.5). A significant difference ($P < 0.05$) was found in the inelastic deformations between samples loaded in the three directions for both aorta and carotid arteries at large strains (Fig. 5.5). However for lower applied strain (around 20%) the residual strains in the tissue on unloading are not significantly different in the longitudinal or radial directions. This is particularly evident for the aorta where the inelastic strain magnitudes were almost identical for the radial compression and longitudinal tensile samples on unloading from 20% strain. For the carotid artery no significant difference in residual strain is observed between the circumferential and longitudinal directions on unloading from 20% strain, with higher residual

strains observed in the longitudinal direction on unloading from higher magnitudes of applied strain ($P < 0.05$). The ratios of the inelastic deformations (i.e. the ratios of inelastic deformation in the circumferential direction to those in either the longitudinal and radial directions) in each loading direction were found to be similar in both carotid and aortic tissue for large applied strains. On unloading from a 50 % applied strain the ratio of inelastic deformation in the radial direction to the circumferential direction is approximately 2 (1.9 and 2.1 for the carotid and aorta respectively), while the ratio of longitudinal deformation to circumferential is about 1.4 (1.378 and 1.371 for the carotid and aorta respectively). An approximately linear relationship between the inelastic strain measured and the peak strain applied is observed for all arteries in all directions, see Figs. 5.2 and 5.5.

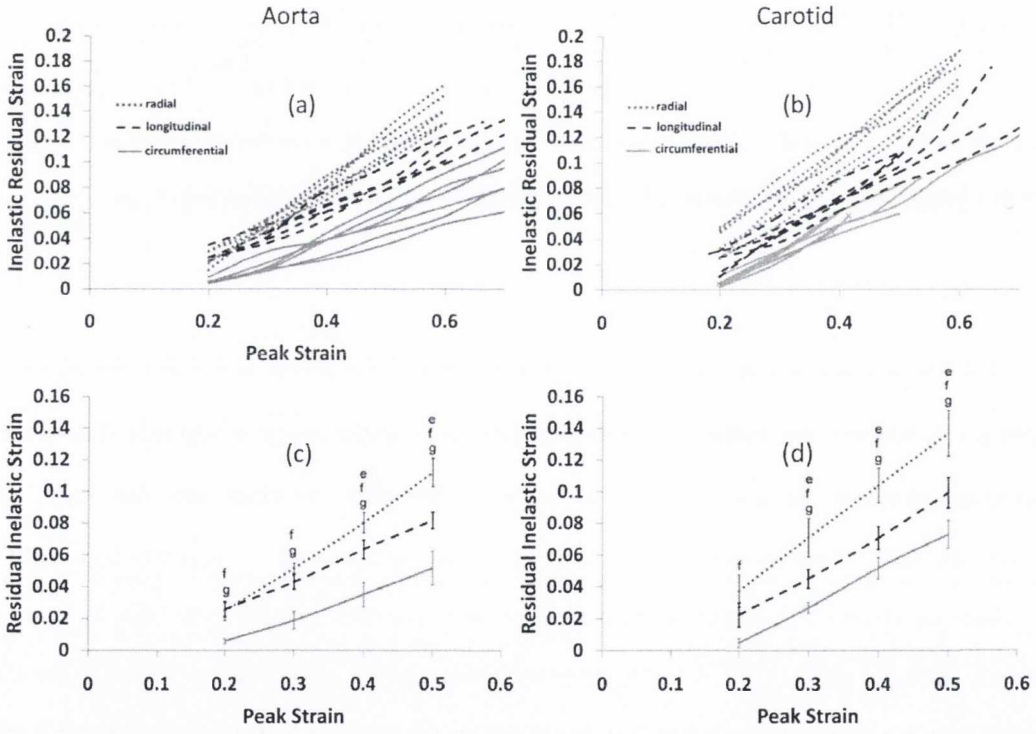

Figure 5.5: Magnitude of inelastic residual strains on unloading from various peak nominal strains applied uniaxially in three loading directions to (a) aortic and (b) carotid tissue samples and the respective mean value for both arteries (c), (d). e, f and g indicate statistical differences ($P<0.05$) between values in the radial and longitudinal, radial and circumferential and longitudinal and circumferential directions respectively.

No significant differences were found in the % stress softening observed due to loading in the three directions, see Fig. 6. However a large standard deviation was observed and stress softening tended to be greatest in the longitudinal direction.

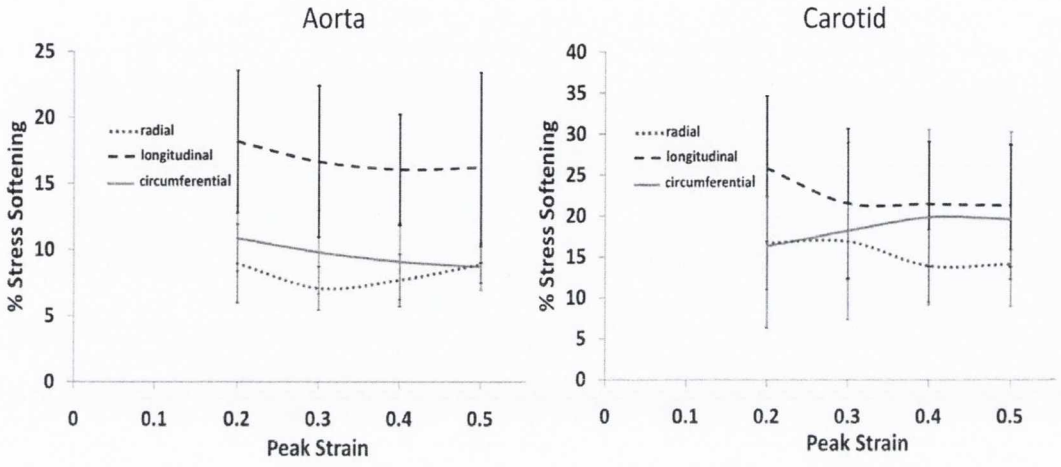

Figure 5.6: % stress softening on unloading from various peak nominal strains applied uniaxially in three loading directions to aortic and carotid tissue samples and the respective mean value for both arteries.

5.4 Discussion

The aim of this study was to characterise the magnitude of inelastic deformations due to loading throughout the arterial tree and to investigate the anisotropic inelastic behaviour of arterial tissue. The stress-strain behaviour of arterial tissue during cyclic testing was similar to other experiments applying cyclic pressure to blood vessels (Peña et al., 2010). In that study only one loading-unloading cycle was applied at each strain level, and the similarity in response can be attributed to the fact that the majority of stress softening occurs in the initial cycle of loading. This behaviour has been observed in other experiments often when referring to the pre-conditioning behaviour of arterial tissue (Holzapfel et al., 2005; Patel and Janicki, 1970). The greatest inelastic strains were observed in coronary tissue and the least in the aorta. The same trend was observed for the % stress softening in the samples. Both aortic and carotid tissue demonstrated anisotropic inelastic

behaviour where the highest inelastic strains were observed in the radial direction and the lowest in circumferential direction. The approximately linear relationship between inelastic deformations and applied stretches observed here has also been reported previously for atherosclerotic plaques (Maher et al., 2011).

Larger inelastic strains were observed in more muscular arteries where the ratio of collagen to elastin in the artery wall is highest. Furthermore, inelastic deformations were highest when the tissue is loaded in radial compression and lowest when loaded in the circumferential tensile direction. This suggests that the relative quantities and orientation of collagen, elastin and smooth muscle may all play a role in determining the magnitudes of inelastic deformations. The highest collagen to elastin ratio was observed in the coronary artery and the lowest in the aorta, in agreement with previous studies for aged canine arteries (Fischer and Llaurado, 1966). One can also assume that the collagen to elastin ratio of the unanalysed carotid artery falls between that of the aorta and coronary arteries as seen in canine arteries (Cox, 1978; Fischer and Llaurado, 1966). The higher inelastic deformations observed for muscular arteries, which possess a higher collagen to elastin ratio, suggest that the higher proportion of elastin in the media of elastic arteries is responsible for much of the elastic recovery in the tissue. It has been demonstrated that elastin behaves as a perfectly elastic material up to stretches of 1.6 (Fung and Sobin, 1981).

During tensile testing, the near circumferentially orientated collagen fibres and anisotropic elastin network most likely both contribute to the smaller inelastic strains observed in the circumferential direction in both aorta and carotid tissue. It is speculated that more of the damage occurs in the smooth muscle component of the arterial tissue than the collagen fibres. If this is the case, the anisotropy of the inelastic response in tension can potentially be explained as follows. During testing in the circumferential direction greater recoverable energy is stored in the collagen fibres compared to when loaded in other directions due to the preferred fibre orientation. These fibres are most likely crimped in their initial configuration so can experience larger levels of tissue strain without damage. Therefore the tissue recovers more in the circumferential direction on unloading. This phenomenon may also partially explain the observation of higher inelastic strains

in the radial direction than the longitudinal. Assuming incompressibility during unconfined radial compression, the circumferential fibre orientation in the tissue will result in large induced stretches in the longitudinal direction with much smaller stretches in the circumferential, resulting in greater smooth muscle damage in the matrix.

Preliminary testing was performed on aortic and coronary arterial tissue in an attempt to rule out possible viscoelastic or poroelastic effects contributing to the reported apparent inelasticity. A resting period of 2 h at 0% strain was added every five cycles before the peak strain value was increased. No significant difference was found between the levels of inelastic deformation on unloading between arterial samples tested with or without the relaxation period present, which suggests a damage driven process rather than recoverable behaviour. Relaxation time for strained arterial tissue to reach an equilibrium stress has been reported as varying between 10-150 min for porcine aorta and carotid (Silver et al., 2003). Others have seen that arterial tissue at low applied strains relaxes within a time of 900 s (Yang et al., 2011). This data suggests that if the inelastic deformations reported in this study were largely influenced by viscoelastic effects, at least partial recovery should be observed during the resting periods of the preliminary study.

There are a number of limitations associated with the current study. The tissue was tested at room temperature rather than at 37 °C, however there is data to suggest a dependence of temperature of the mechanical properties (Kang et al., 1995; Vilks et al., 1975), although others have observed an insensitivity of the mechanical response to temperature changes (Guinea et al., 2005). While the compressive samples were immersed in biological saline solution during testing the tensile samples were not. These samples were lightly sprayed regularly with biological saline solution in order to prevent drying out and reduce the possible effects of the sample not being immersed in fluid. In this study we assume that the peak stress-strain points of each strain level can be used to estimate the monotonic elastic loading behaviour of the tissue (the *load envelope*). Using the load envelopes as an estimate implies that the carotid artery will reach a stress of 0.2 MPa at a stretch of between 1.2 and 1.4 in the circumferential direction and 1.6 and 1.8 for the longitudinal direction. This correlates well with previous data reported for the proximal common carotid of

similarly aged pigs (Garcia et al., 2011) which may indicate that our assumption has some validity. The load envelopes demonstrate the typical anisotropic behaviour of arterial tissue and the data indicates that both the carotid and aorta are stiffer in the circumferential direction than the longitudinal which has been seen previously for both the carotid artery (Garcia et al., 2011) and the aorta (Yang et al., 2011). A similar stress-strain response is observed in longitudinal tension and radial compression if the magnitude of the Cauchy stress and nominal strain are considered. Only compression testing of coronary and femoral arteries was undertaken due to their small diameter which made circumferential tensile tests impractical. The length of the coronary artery limited the number of attainable longitudinal tensile samples. While the dominant loading experienced by arterial tissue during expansion of angioplasty balloons and stents is tensile, the data presented in this study demonstrates that the inelastic deformations that occur in both carotid and aortic tissue due to radial compressive loading is approximately twice that observed due to circumferential loading for large applied peak strains. The carotid artery also exhibited higher inelastic strains in tension and compression compared to aortic samples. Biaxial testing and the mechanical testing of arterial layers separately would also add to the data presented in this study. Large variations in the % stress softening observed made it difficult to draw any conclusions of how the structure-function relationship of the tissue affects the softening behaviour of the tissue.

In conclusion, this study characterised the inelastic response of common carotid, coronary, aorta and femoral arteries due to compressive loading and found that the largest inelastic strains occur in the more muscular arteries. This inelasticity would appear to correlate with the collagen to elastin ratio in the artery wall. It was observed that lower inelastic strains occur in the circumferential direction and we speculate that this is a result of the matrix in the media becoming more damaged due to loading than the collagen fibres, allowing greater recovery when stretched in the circumferential direction. A constitutive model that separates the response of the matrix and collagen fibres and the damage that occurs in each may provide further insight into the tissues inelastic response, and may prove useful in finite element simulations of stent artery interactions (Auricchio et al., 2011; Early and Kelly, 2011; Early and Kelly, 2010; Early et al., 2009; Mortier et al., 2010; Pericevic et al., 2009)

Chapter 6 An anisotropic inelastic constitutive model to describe stress softening and permanent deformation in arterial tissue

Maher E.[1], Lally C.[1, 2], Kelly D. J.[1]

[1] Trinity Centre for Bioengineering, School of Engineering, Trinity College Dublin, Dublin 2, Ireland.

[2]School of Mechanical and Manufacturing Engineering, Dublin City University, Glasnevin, Dublin 9, Ireland

For thesis purposes this chapter is modified from an article submitted to the Journal of Mechanical Behavior of Biomedical Materials

The large majority of the work discussed in this chapter was undertaken by the author of this thesis. The contributions of the other authors to this work are as follows: Dr. Kelly and Dr. Lally had a supervisory role on this study.

6.1 Introduction

Optimisation of vascular medical devices using the finite element method requires accurate constitutive models of arterial tissue. Developing such constitutive models is challenging due to the complex structure and composition of vascular tissue. At physiological levels of pressure, arteries exhibit highly nonlinear, anisotropic and viscoelastic responses to loading (Fung, 1981; Holzapfel et al., 2005). Furthermore, during procedures such as balloon angioplasty and stenting, arteries also experience non-physiological magnitudes of pressure and deformations. At these non-physiological loads arteries display inelastic behaviour as a result of damage to the tissue, which can be observed as a softening of the stress-strain response between loading cycles (Alastrué et al., 2008; Peña et al., 2010). Such structural changes due to tissue damage need be considered when modelling surgical interventions. The damage mechanisms responsible for softening of arterial tissue are not known, however it has been observed that in ligaments damage may occur as a result of tearing or plastic deformation of the fibrous component of the tissue or by a biomechanical degradation of extracellular matrix due to protease release associated with cell necrosis (Provenzano et al., 2002). The softening effect that occurs in fibrous soft tissue has been seen to largely depend on the previous maximum strain that the tissue has experienced. This behaviour is also observed in rubbers and is known as the Mullins effect (Mullins, 1948). Another phenomenon that occurs as a result of non-physiological loading is the presence of residual inelastic strains (or permanent set) on unloading. Both stress softening and permanent set have been observed for other soft tissues (Alastrué et al., 2008; Franceschini et al., 2006; Maher et al., 2011; Peña et al., 2011) and for healthy arterial tissue both in the literature (Calvo et al., 2007; Peña et al., 2010) and in chapter 5 of this thesis.

The mechanical behaviour of arterial tissue is commonly described using hyperelastic material models (Delfino et al., 1997; Holzapfel et al., 2000; Lally et al., 2004); however these models do not incorporate damage effects and as a result are limited when modelling the effects of non-physiological loading during surgical interventions. The Mullins effect theory does not account for inelastic strains and many damage models omit permanent set from the formulation (Calvo et al. 2007). A number of models have been proposed to describe stress softening in biological

tissues. These models are often based on continuum damage mechanics theory; where a reduction factor (Simo and Ju, 1987a; Simo and Ju, 1987b) related to the evolution of irreversible internal variables is applied to model either isotropic (Hokanson and Yazdani, 1997; Maher et al., 2011) or anisotropic damage (Alastrué et al., 2007; Balzani et al., 2006; Calvo et al., 2007; Peña and Doblare, 2009). In anisotropic models of soft tissue, damage can either be isolated to the anisotropic fibrous component (Balzani et al., 2006) or applied to both the isotropic matrix and fibrous components separately (Calvo et al., 2007). Other approaches to modelling stress softening include pseudoelastic constitutive models (Franceschini et al., 2006; Peña and Doblare, 2009) or multi-mechanism models that describe failure or deactivation of tissue components (Li and Robertson, 2009; Wulandana and Robertson, 2005). Relatively few constitutive models have been proposed to describe permanent set (Ehret and Itskov, 2009; Franceschini et al., 2006; Gasser and Holzapfel, 2002; Maher et al., 2011; Peña, 2011). Gasser and Holzapfel (2002) proposed a constitutive model for arterial tissue based on multisurface slip plasticity, where plastic deformations are due to slip in the collagen fibre component of the matrix. Peña (2011) used a formulation based on the evolution of internal variables to introduce inelastic softening to the anisotropic components of the model. Franceschini *et al* (2006) adapted a pseudoelastic formulation for particle filled rubbers (Dorfmann and Ogden, 2004; Ogden and Roxburgh, 1999) to model softening and permanent set for brain tissue. Other models have used a pseudo-elastic based approach to describe inelastic strains in carotid plaque (Maher et al., 2011).

Despite the significant progress that has been made in modelling the mechanical behaviour of arterial tissue, to the authors knowledge to date few models have been proposed to describe anisotropic stress softening and permanent set in arterial tissue. Without considering such phenomena it will not possible to develop constitutive models to accurately predict lumen gain during clinical procedures such as angioplasty and stenting. In this study an anisotropic inelastic constitutive model is formulated to describe stress softening and permanent set for arterial tissue. The formulation is split into an elastic softening, equivalent to the Mullins effect, based on a typical damage mechanics approach and an inelastic softening effect, which results in residual strains,

which is based on an additive split of the stress tensor and the irreversible evolution of internal variables.

6.2 Materials and methods

6.2.1 Anisotropic hyperelastic constitutive model

As arterial tissue is generally viewed as a nearly incompressible tissue, a multiplicative decomposition of the deformation gradient tensor, $\mathbf{F} = J^{1/3}\bar{\mathbf{F}}$, and the right Cauchy-Green strain tensor, $\mathbf{C} = J^{2/3}\bar{\mathbf{C}}$, into volumetric (dilatational) and isochoric (volume preserving) parts is performed (Flory, 1961); where J is the determinant of the deformation gradient tensor. This allows a decoupled representation of the strain energy density function ψ to be used.

$$\psi = \psi_{vol}(J) + \psi_{isch}(\bar{\mathbf{C}}, \mathbf{M}, \mathbf{N}) \qquad \text{(Eqn. 6.1)}$$

The volumetric term, ψ_{vol} is a function of the Jacobian determinant J and is defined here by the equation, $\psi_{vol} = (\kappa/2)\ln^2 J$ (Holzapfel, 2000). The isochoric part of the strain energy is a function of the modified right Cauchy-Green tensor $\bar{\mathbf{C}}$ and the structural tensors, $\mathbf{M} = \mathbf{m_0}\otimes\mathbf{m_0}$ and $\mathbf{N} = \mathbf{n_0}\otimes\mathbf{n_0}$ (Spencer, 1971). The structural tensors are functions of the unit vectors in the preferred fibre directions in the undeformed tissue $\mathbf{m_0}$ and $\mathbf{n_0}$, with the square of the stretch in the fibre directions given by the modified invariants $\bar{I}_4$ and $\bar{I}_6$, see Eqn. 6.2. Other invariants can also be associated with the structural tensors, but are commonly excluded from constitutive formulations due to the difficulty in quantifying them, and are not considered here.

$$\bar{I}_4 = \bar{\mathbf{C}}\colon\mathbf{M} \qquad \bar{I}_6 = \bar{\mathbf{C}}\colon\mathbf{N} \qquad \text{(Eqn. 6.2)}$$

We can now define the 2nd Piola-Kirchhoff stress $\mathbf{S}$ as:

$$\mathbf{S} = 2\frac{\partial\psi(\mathbf{C},\mathbf{M},\mathbf{N})}{\partial\mathbf{C}} = 2\frac{\partial\psi_{vol}(J)}{\partial J}\frac{\partial J}{\partial\mathbf{C}} + 2\frac{\partial\psi_{isch}(\bar{\mathbf{C}},\mathbf{M},\mathbf{N})}{\partial\bar{\mathbf{C}}}\frac{\partial\bar{\mathbf{C}}}{\partial\mathbf{C}} \qquad \text{(Eqn. 6.3)}$$

$$= \mathbf{S}_{vol} + \mathbf{S}_{isch}$$

where $\mathbf{S}_{vol}$ and $\mathbf{S}_{isch}$ are the volumetric and isochoric parts of the stress respectively. The isochoric part of the strain energy density can be split into isotropic and anisotropic components. In structural models this represents anisotropically orientated fibres in an isotropic matrix. Here the isotropic component is described using an exponential function of the modified strain invariant $\bar{I}_1 = tr\bar{\mathbf{C}}$, which has previously been used to model arterial tissues as isotropic (Delfino et al., 1997; Maher et al., 2011). The anisotropic components are exponential functions of the invariants $\bar{I}_4$ and $\bar{I}_6$ (Holzapfel et al., 2002):

$$\psi_{isch} = \psi_m + \psi_{4,6} = \frac{a}{b}\left(exp\left[\frac{b}{2}(\bar{I}_1 - 3)\right] - 1\right) + \sum_{j=4,6} \frac{k_1}{k_2}\left(exp\left[k_2(\bar{I}_j - 1)^2\right] - 1\right) \quad \text{(Eqn. 6.4)}$$

$$\mathbf{S}_{isch} = 2\sum_{i=m,4,6} \frac{\partial \psi_i(\bar{I}_i)}{\partial \bar{I}_i}\frac{\partial \bar{I}_i}{\partial \mathbf{C}} = \sum_{i=m,4,6} \bar{\mathbf{S}}_i \quad \text{(Eqn. 6.5)}$$

where a, b, k_1 and k_2 are material parameters evaluated through fitting the model to data from mechanical testing and $\bar{I}_m = \bar{I}_1$. The elasticity tensor in the material description$\mathbb{C}$ is similarly defined:

$$\mathbb{C}_{isch} = 4\sum_{i=m,4,6} \frac{\partial^2 \psi_i(\bar{I}_i)}{\partial \mathbf{C}^2} = \sum_{i=m,4,6} \bar{\mathbb{C}}_i \quad \text{(Eqn. 6.6)}$$

6.2.2 Elastic damage model

As is common in continuum damage mechanics theory when applied to soft tissues, damage is assumed to affect only the isochoric part of the constitutive model (Alastrué et al., 2007; Calvo et al., 2007; Simo, 1987). The isochoric elastically damaged strain energy density function ψ_{ED} is defined for such materials as:

$$\psi_{ED} = (1 - D_m)\psi_m(\bar{I}_1) + \sum_{j=4,6}(1 - D_j)\psi_j(\bar{I}_j) \qquad \text{(Eqn. 6.7)}$$

where ψ_m is the undamaged strain energy of the isotropic matrix and is a function of the modified first strain invariant. $\psi_j, j = 4, 6$ are the strain energy densities of the undamaged anisotropic family of fibres and $(1 - D_i)$, i = m, 4, 6 are scalar functions, known as the reduction factors, that act as internal variables with $D_i \in [0,1]$ defined as damage variables for the matrix (D_m) and the two fibre directions (D_4 and D_6 respectively).

Evaluating the Clausius-Duhem inequality for isothermal conditions, where the internal dissipation $D_{int} = -\dot{\psi} + {}^1/_2\,\mathbf{S}{:}\,\dot{\mathbf{C}} \geq 0$ and using standard arguments of continuum mechanics the following relationships can be established:

$$\mathbf{S}_{ED} = \sum_{i=m,4,6} 2(1 - D_i)\frac{\partial \psi_i(\bar{I}_i)}{\partial \mathbf{C}} = \sum_{i=m,4,6}(1 - D_i)\,\bar{\mathbf{S}}_i \qquad \text{(Eqn. 6.8)}$$

$$-\frac{\partial \psi}{\partial D_i}\dot{D}_i = \psi_i \dot{D}_i \geq 0 \quad \textit{where} \quad \psi_i \geq 0 \;\; \textit{and} \; i = m, 4, 6 \qquad \text{(Eqn. 6.9)}$$

where $\mathbf{S}_{ED}$ and $\bar{\mathbf{S}}_i$, i =*m, 4, 6* are the total isochoric, the isotropic part and the anisotropic parts of the second Piola-Kirchhoff stress respectively. Eqn. 6.9 shows that the evolution of the damage variables D_i is an irreversible process, where ψ_i are the thermodynamic forces which govern damage evolution.

We now define the strain space based criteria needed for damage evolution at any time during the loading process as (Simo, 1987):

$$\phi_i(\bar{\mathbf{C}}, \Xi_i^m) = \sqrt{2\psi_i(\bar{\mathbf{C}}(t))} - \Xi_i^m \leq 0 \qquad \text{(Eqn. 6.10)}$$

where $\Xi_i^m(t) = \max_{s=(0,t)} \sqrt{2\psi_i(\bar{\mathbf{C}}(s))}$ *and* $\Xi_i^t = \sqrt{2\psi_i(\bar{\mathbf{C}}(t))}$ (Eqn. 6.11)

with the damage criteria ϕ_i and the equivalent strain definition Ξ_i^t. $\phi_i = 0$ which characterises the damage surface whose normal is defined as $\mathbf{N}_i = \partial\phi_i/\partial\mathbf{C}$. The second criterion is based on the

double contraction $\mathbf{N}_i : \dot{\mathbf{C}}$, where $\mathbf{N}_i : \dot{\mathbf{C}} > 0$ describes loading when $\phi = 0$. Evolution of the damage variables D_i can be expressed by

$$\dot{D}_i = \begin{cases} D_i'(\Xi_i)\dot{\Xi}_i, & \text{if } \phi_i = 0 \text{ and } \mathbf{N}_i : \dot{\mathbf{C}} > 0 \\ 0 & \text{otherwise} \end{cases} \qquad \text{(Eqn. 6.12)}$$

where the functions $D_i'(\Xi_i) = \partial D_i / \partial \Xi_i$ characterise damage evolution in the tissue. Making use of the chain rule the isochoric part of the elasticity tensor in the material description $\mathbb{C}_{ED}$ can be derived from the second Piola-Kirchhoff stress tensor in Eqn. 6.8.

$$\mathbb{C}_{ED} = \mathbb{C}_m + \mathbb{C}_4 + \mathbb{C}_6 \qquad \text{(Eqn. 6.13)}$$

$$\text{where } \mathbb{C}_i = \begin{cases} (1 - D_i)\bar{\mathbb{C}}_i - \left[\frac{\partial D_i}{\partial \Xi_i}\right] \bar{\mathbf{S}}_i \otimes \bar{\mathbf{S}}_i, & \phi_i = 0 \; and \; \mathbf{N}_i : \dot{\mathbf{C}} > 0 \\ (1 - D_i)\bar{\mathbb{C}}_i, & otherwise \end{cases} \qquad \text{(Eqn. 6.14)}$$

with $\mathbb{C}_i$ as defined in equation 6.6. The reduction factors D_i are defined for all equations here as (Miehe, 1995):

$$D_i = d_\infty^i [1 - \exp(-\Xi_i^m / r_i)] \qquad \text{(Eqn. 6.15)}$$

with d_∞^i and r_i as material parameters determined through fitting to test data

.

6.2.3 Inelastic damage model

The inelastic damage formulation proposed here is characterised by an additive split of the isochoric part of the stress tensor into an elastic damage stress tensor and an inelastic damage stress tensor $\mathbf{S}_{IN}$. The elastic damage term, $\mathbf{S}_{ED}$ is defined as in the previous section.

$$\mathbf{S}_{isch} = \mathbf{S}_{ED} - \mathbf{S}_{IN} \qquad \text{(Eqn. 6.16)}$$

The general form of the isochoric strain energy density function can be written as:

$$\psi_{isch} = \psi_{ED} - \frac{1}{2}\sum_{i=m,4,6} \mathbf{S}_{IN}^{i} : \bar{\mathbf{C}} \qquad \text{(Eqn. 6.17)}$$

where ψ_{ED} is as defined in Eqn. 6.7.

To obtain the stress relation it is necessary to determine the time derivative of the strain energy and evaluate the Clausius-Duhem inequality as in the previous section. This results in the inequality

$$D_{int} = \left(\mathbf{S} - J\frac{\partial \psi_{vol}(J)}{\partial J}\mathbf{C}^{-1} - \sum_{i=m,4,6} J^{-2/3}\mathbb{P} : (1-D_i)2\frac{\partial \psi_i}{\partial \bar{\mathbf{C}}} + \sum_{i=m,4,6} J^{-2/3}\mathbb{P} : \mathbf{S}_{IN}^{i}\right)$$
$$: \frac{\dot{\mathbf{C}}}{2} + \sum_{i=m,4,6} \psi_i \dot{D}_i + \frac{1}{2}\sum_{i=m,4,6} \bar{\mathbf{C}} : \dot{\mathbf{S}}_{IN}^{i} \geq 0 \qquad \text{(Eqn. 6.18)}$$

from which one can derive the second Piola-Kirchhoff stress tensor $\mathbf{S}$ and the non-negative internal dissipation inequalities. $\mathbb{P} = \mathbb{I} - 1/3\,\mathbf{C}^{-1}\otimes\mathbf{C}$ is the deviatoric projection tensor in the material configuration, where $\mathbb{I}$ is the 4th order unit tensor. The dissipation inequalities for inelastic damage are defined in Eqn. 6.9.

$$\mathbf{S} = \mathbf{S}_{vol} + \sum_{i=m,4,6} (1-D_i)\bar{\mathbf{S}}_i - \sum_{i=m,4,6} \mathbf{S}_{IN}^{i} \qquad \text{(Eqn. 6.19)}$$

$$\frac{1}{2}\bar{\mathbf{C}} : \dot{\mathbf{S}}_{IN}^{i} \geq 0 \qquad \text{(Eqn. 6.20)}$$

Eqn. 6.20 shows that $\mathbf{S}_{IN}^{i}$ act as dissipative tensors such that if the strain applied to the tissue is tensile, i.e. $\bar{C}_{ij} > 0$ than the rate of change of the inelastic stress will be either positive or zero

$\dot{S}^i_{IN_{ij}} \geq 0$. The inelastic stresses $\mathbf{S}^i_{IN}$ are therefore dependent on the strain in the tissue and we propose criteria for evolution of the inelastic stresses based on the modified strain invariants:

$$\varphi_i(\bar{\mathbf{C}}, t) = \bar{I}_i(\bar{\mathbf{C}}) - I_i^* \leq 0 \qquad \text{(Eqn. 6.21)}$$

$$I_i^*(t) = \max_{s=(0,t)} \bar{I}_i(s) \qquad \text{(Eqn. 6.22)}$$

where $\bar{I}_i$, $i = 1, 4, 6$, are the modified strain invariants of the right Cauchy-Green strain tensor at any given strain and $I_i^*(t)$ are the maximum values of the strain invariants in the history of the material. As the strain energy density is a function of the strain invariants, when $\varphi_i = 0$ from Eqn. 6.21 we will get $\phi_i = 0$ from the elastic damage criterion from Eqn. 6.10. The normal to the inelastic yield surface, described by $\varphi_i = 0$, is defined as $\mathbf{N}^i_{IN} = \partial\varphi_i/\partial\mathbf{C}$. We define the evolution of the internal variables I_i^* and the inelastic stresses as follows:

$$\dot{I}_i^* = \begin{cases} 2\dfrac{\partial I_i^*}{\partial \mathbf{C}} : \dfrac{\dot{\mathbf{C}}}{2}, & if\ \varphi_i = 0\ and\ \mathbf{N}^i_{IN} : \dot{\mathbf{C}} \geq 0 \\ 0, & otherwise \end{cases} \qquad \text{(Eqn. 6.23)}$$

$$\mathbf{S}^i_{IN} = \begin{cases} 2\dfrac{\partial \psi^i_{IN}(I_i^*)}{\partial \mathbf{C}}, & if\ \varphi_i = 0\ and\ N^i_{IN} : \dot{\mathbf{C}} \geq 0 \\ constant, & otherwise \end{cases} \qquad \text{(Eqn. 6.24)}$$

where ψ^i_{IN} are the inelastic dissipated internal strain energies during the loading process for the matrix and family of fibres respectively. The above equations make use of the fact that when the inelastic yield criterion is met $\bar{I}_i = I_i^*$, and thus $\partial I_i^*/\partial\mathbf{C} = \partial\bar{I}_i/\partial\mathbf{C}$, in order to calculate the inelastic stresses. The inelastic dissipated internal strain energy ψ^i_{IN} has the same form as the elastic strain energy density functions,

$$\psi_{IN}^{m} = \frac{a^*}{b^*}\left(exp\left[\frac{b^*}{2}(I_1^* - 3)\right] - 1\right) \qquad \text{(Eqn. 6.25)}$$

$$\psi_{IN}^{j} = \frac{k_1^*}{k_2^*}\left(exp\left[k_2^*(I_j^* - 1)^2\right] - 1\right) \quad j = 4, 6 \qquad \text{(Eqn. 6.26)}$$

with a^*, b^*, k_1^* and k_2^* material constants to describe the inelastic damage effects fitted to mechanical test data. The material elasticity tensor can be defined using the chain rule as:

$$\mathbb{C} = \mathbb{C}_{ED} - \mathbb{C}_{INm} - \mathbb{C}_{IN4} - \mathbb{C}_{IN6} \qquad \text{(Eqn. 6.27)}$$

where

$$\mathbb{C}_{INi} = \begin{cases} 4\dfrac{\partial^2 \psi_{IN}^i}{\partial \mathbf{C}^2} = 4\dfrac{\partial^2 \psi_{IN}^i}{\partial I_i^* \partial I_i^*}\dfrac{\partial^2 I_i^*}{\partial \mathbf{C} \partial \mathbf{C}}, & \phi_i = 0 \; and \; \mathbf{N}_i : \dot{\mathbf{C}} > 0 \\ 0 \quad , & otherwise \end{cases} \qquad \text{(Eqn. 6.28)}$$

which again makes use of the fact that $\partial I_i^*/\partial \mathbf{C} = \partial \bar{I}_i/\partial \mathbf{C}$ when the inelastic yield conditions are met.

6.2.4 Characterisation of the inelastic response of arteries

The model as presented here is compared to the experimental stress-strain behaviour of aorta and carotid arterial tissue in response to cyclic uniaxial loading. Circumferential and longitudinal strips were tested in tension and cylindrical radial samples were tested in compression. Strain-controlled cyclic loading was applied to each specimen, periodically increasing the maximum strain level every 5 loading cycles. The experimental methodology and results are presented in full in Chapter 5. Inelastic strains were determined where the stress-strain curve crossed the strain axis on reloading.

The strain energy function defined in equation 6.17 with associated material constants was fit to the mechanical data of representative samples from samples in the longitudinal and

circumferential tensile directions. The fitting procedure used minimised the root mean square (*rms*) error for the stress-strain response and the inelastic strains as described in a previous study (Maher et al., 2011). The fitting to experimental data was performed numerically: the model presented in section 6.2.3 was implemented as a user material in the finite element code ABAQUS. Tensile boundary conditions were applied to a model to reproduce the experimental tensile loading and the resulting stress-strain curves in both the circumferential and longitudinal were compared to the experimental data. The fibre orientations were defined by the angle, β, between the fibres and the circumferential direction. In cylindrical polar coordinates the unit vectors $\mathbf{m_0}$ and $\mathbf{n_0}$ are defined as (Holzapfel et al., 2000):

$$[\mathbf{m_0}] = \begin{bmatrix} 0 \\ cos\beta \\ sin\beta \end{bmatrix} \qquad [\mathbf{n_0}] = \begin{bmatrix} 0 \\ cos\beta \\ -sin\beta \end{bmatrix} \qquad \text{(Eqn. 6.29)}$$

where β was included as a variable parameter in the model fitting procedure. The success of the model fits were analysed and model was also used to predict inelastic strains caused by radial compressive loading as a further test to determine how accurately the inelastic damage mechanisms were described by the model.

6.3 Results

The best fit material parameters for the aorta and carotid experimental data are presented in Table 6.1. The comparison between model predictions and experimental results is illustrated in Figs. 6.1-6.4. Good agreement between the experimental data and the model were found when comparing the stress-strain response on loading and reloading, see Fig. 6.1. The quality of fit was worst in the transition region between low and high stiffness regions. However the fit in these regions was still of reasonably good quality, see Fig. 6.1. The total *rms* error for the 2nd loading cycles in both directions, χ_s is presented in Table 6.1 as a measure of the quality of the fit.

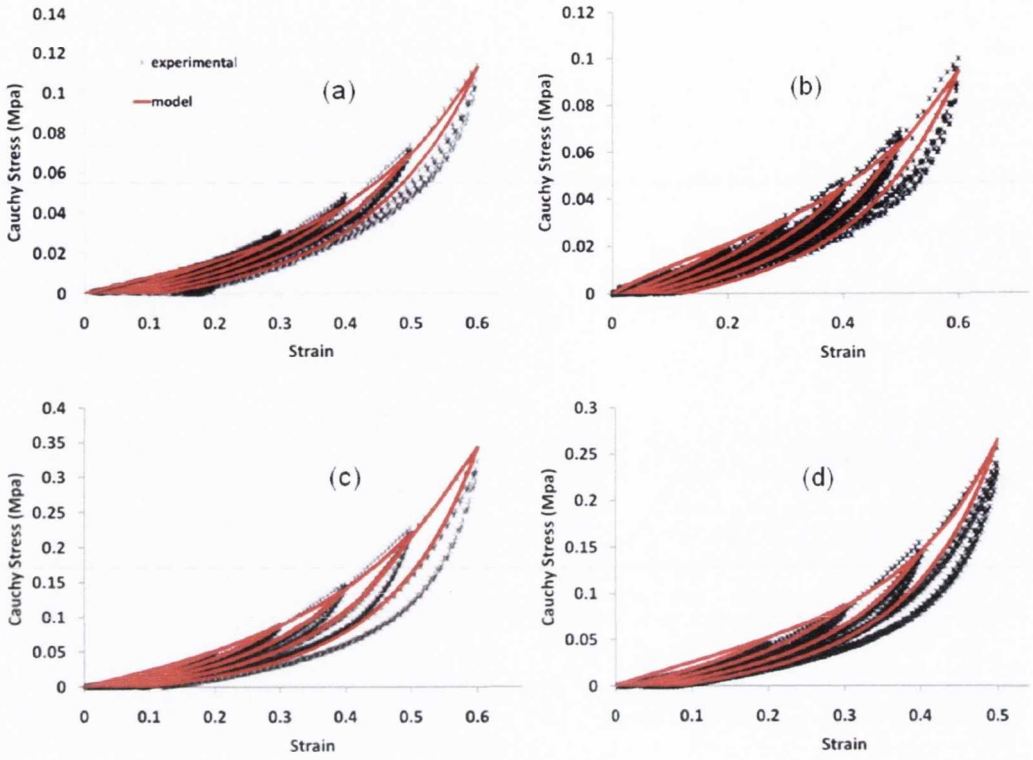

Figure 6.1: Comparison between constitutive model fit and experimental results for the stress-strain response in the longitudinal ((a) and (b)) and circumferential ((c) and (d)) for aorta and carotid tissue samples respectively

Table 6.1: Optimised material parameters for aortic and carotid specimens

Aorta						
$a(MPa)$	b	$k_1(MPa)$	k_2	d_∞^m	r_m	d_∞^f
0.035	3.5	0.0125	0.7	0.7	0.16	0.9
r_f	$a^*(MPa)$	b^*	$k_1^*(MPa)$	k_2^*	$\beta(°)$	χ_s
0.15	0.0034	0.001	0.0001	0.0001	20	0.082
Carotid						
$a(MPa)$	b	$k_1(MPa)$	k_2	d_∞^m	r_m	d_∞^f
0.05	3.2	0.011	0.95	0.8	0.13	0.75
r_f	$a^*(MPa)$	b^*	$k_1^*(MPa)$	k_2^*	$\beta(°)$	χ_s
0.08	0.0035	0.001	0.0002	0.0001	15	0.037

To aid clarity of the fit, comparisons for the elastic loading response, or load envelope, are shown in Fig. 6.2. In addition, the 2nd loading curves for each strain level are illustrated in Fig. 6.3. There is a good quality of fit with the elastic loading in both longitudinal and circumferential directions, see Fig. 6.2.

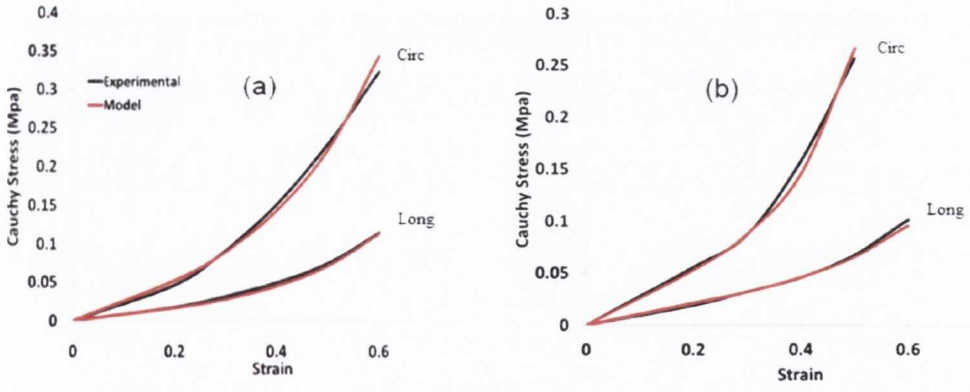

Figure 6.2: Comparison of stress-strain response predicted by the model with experimental data of the load envelope for (a) aorta and (b) carotid arteries in the circumferential and longitudinal directions

The model was able to accurately predict the softening behaviour in both the longitudinal and tensile directions, see Fig. 6.3. The worst quality fits were found at low strains in the circumferential direction for both arteries with the model predicting less softening than observed experimentally. (Only the 2nd loading curve is shown to aid clarity in the figure.) The inelastic strain fits again show good quality fits for loading in the circumferential and longitudinal directions, see Fig. 6.4. The inelastic strains in the circumferential direction are generally overestimated at small strains. This is due to damage initiation occurring when the tissue stretch is beginning in the model. It is likely, as is seen in ligaments, that damage initiation will not occur immediately, particularly in the collagen fibres (Provenzano et al., 2002). Good agreement in the magnitude of inelastic strains observed in the radial direction is found up to approximately 40% compressive strain after which the model tends to over-estimate the inelastic deformations. Overall, a good agreement with the experimental data is found.

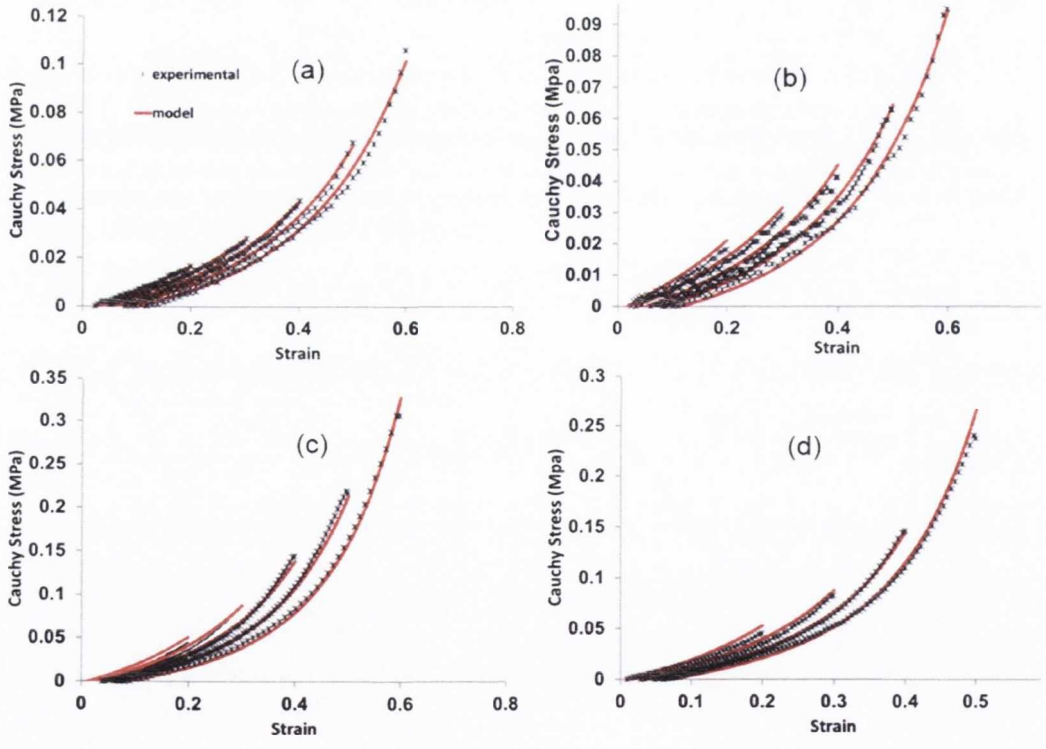

Figure 6.3: Experimental and model comparison of stress-strain curve for the 2nd loading cycle at each strain level in longitudinal (a) aorta and (b) carotid samples; and circumferential (c) aorta and (d) carotid samples.

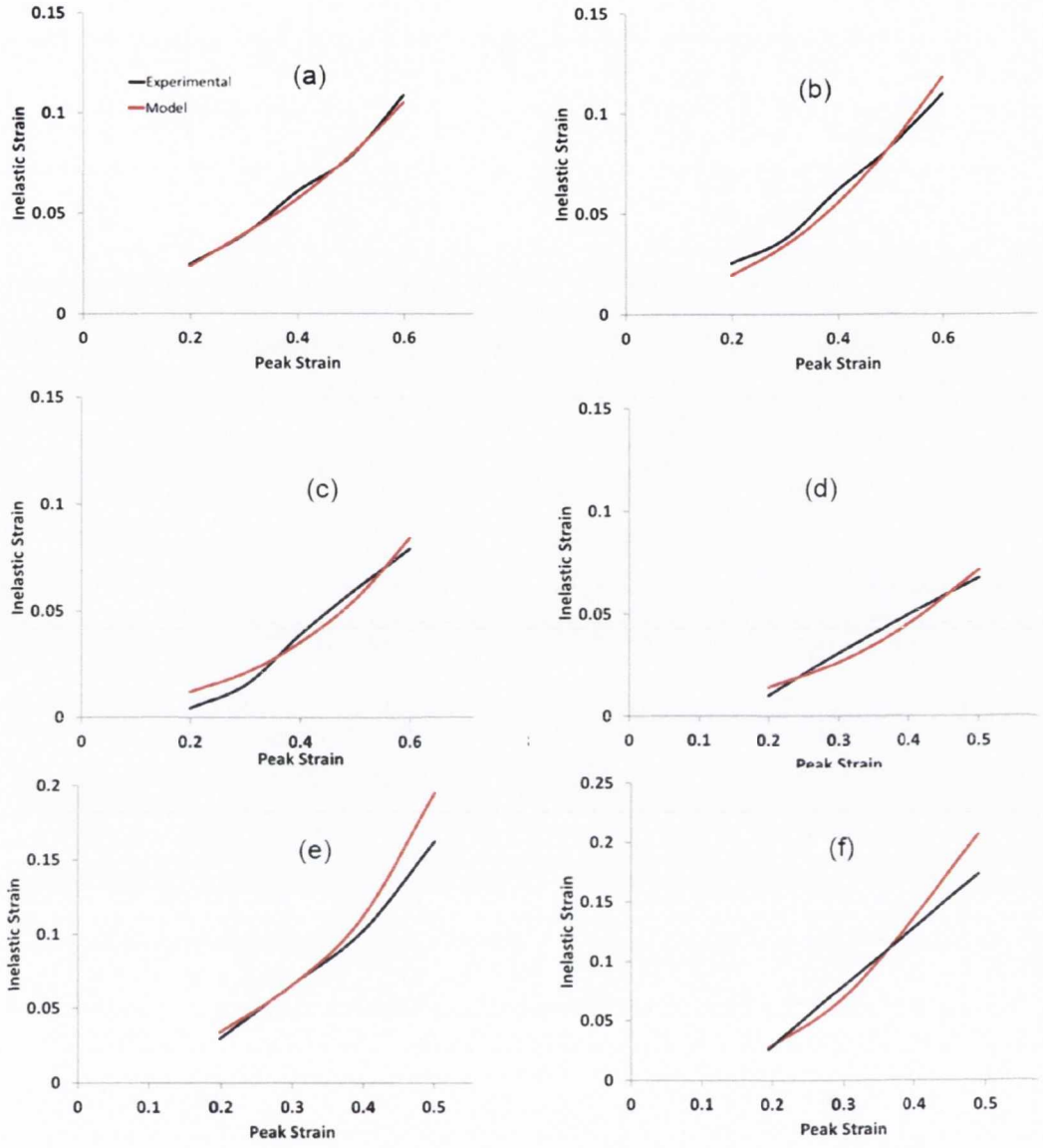

Figure 6.4: Inelastic strain on unloading from various peak strains in the longitudinal ((a) and (b)), circumferential ((c) and (d)) and radial ((e) and (f)) directions for aorta and carotid artery respectively.

6.4 Discussion

In this study, a constitutive model was presented to describe damage and inelastic deformations in vascular tissue. The model was presented in terms of elastic damage, which followed the typical

continuum damage mechanics structure of modelling the Mullins effect, and inelastic damage, which is characterised by an additive split of the stress tensor and the evolution of internal variables based on the maximum value of the modified strain invariants in the load history. The model was shown to successfully describe the typical soft tissue damage phenomena of stress softening, with good quality fits for the experimental data obtained. The assumption of independent damage mechanisms existing for the fibres and base matrix allows the model to predict the significant softening with small inelastic strains which is observed in the circumferential direction. The values obtained from the inelastic constants, d_{∞}^{i} and r_i, suggest that significant elastic damage occurs in both matrix and fibres which results in a significant softening effect in both longitudinal and circumferential directions. The inelastic constants corresponding to the fibres are however smaller than the corresponding constants for the matrix. This results in lower magnitudes of inelastic strains in the circumferential direction where the stiff, presumably less inelastic fibres have more of an influence. This may indicate that collagen fibres in arterial tissue act to constrain the inelastic deformations that occur more prominently in the other constituents, e.g. elastin, smooth muscle or ground matrix. It should be noted however that as a phenomenological model the fibre directions here do not represent true collagen fibre families and are a representation of the overall anisotropic behaviour of the arteries which limits the insight into individual arterial component behaviour the model may provide.

The exact mechanisms through which damage occurs in arterial tissue is unknown, but for example failure of crosslinks between fibres might result in an elastic softening effect while failure or slip of the fibres in the matrix might result in inelastic damage. Such damage mechanisms have been hypothesised by Parry et al (1978) where non-recoverable creep is prevented through non-covalent crosslinks between fibres and matrix and small diameter fibres result in more of these links as they provide a greater surface area per unit mass. Parry et al further hypothesise that large diameter fibres maximise covalent intrafibrillar crosslinks thereby increasing the stiffness of the tissue. The breaking of non-covalent crosslinks resulting in slip of collagen fibres in the matrix has been used to describe inelastic deformations in arterial tissue (Gasser and Holzapfel, 2002). The mechanisms of damage in the matrix are made more complex due to the number of components

that it consists of. The elastin network contains intrafibrillar crosslinks that also contribute to the stiffness in the artery (Greenwald, 2007). Damage of these links may induce softening, while slip or damage of other components may result in inelastic damage. The constitutive model developed as part of this study describes the damage effects as energy dissipation which occurs discontinuously during loading as damage progresses.

There are few models in the literature that account for both softening and permanent set. The ability to account for both these behaviours gives the proposed model an advantage over models that describe the Mullins effect based on traditional continuum damage mechanics. Considering permanent deformation is particularly important in the case of vascular tissue where the end goal of many surgical interventions is to increase the final lumen size through mechanical loading. Models that have been fit to experimental data for other soft tissues that include softening and permanent set (Ehret and Itskov, 2009; Franceschini et al., 2006; Peña, 2011) also have the potential to be used for arterial tissue. Gasser and Holzapfel (2002) proposed a constitutive model based on multi-surface slip of collagen fibres; however the model was not fit to experimental data.

There are several limitations to the constitutive model presented in this study. The damage processes are described using a phenomenological model and as such it is difficult to relate the inelastic constants to a physical meaning. Viscoelasticity is not considered and would likely play a role in the softening effect. Viscoelastic effects can be observed in the difference between the reloading and unloading curves (i.e. a hysteresis effect). Failure is also not considered here. Failure behaviour was omitted as tissue failure was generally absent from the experimental model used in this study. Failure could be included with relative ease into the elastic damage variables D_i by introducing a maximum value of the equivalent strain measure Ξ_i^m above which $D_i = 1$ (Calvo et al., 2007; Pena et al., 2009). Preconditioning effects could be added to the model through the introduction of a continuous damage mechanism (Pena et al., 2009).

Using the tensile data the model can predict inelastic strains due to radial compression with good accuracy at low to medium strains. At high strains however the inelastic strains are overestimated. This may be as a result of fluid extrusion that might occur at high compressive

strains. It has been seen that arteries behave as nearly incompressible materials during arterial expansion (Carew et al., 1968). However the compressive stresses will be comparatively small during the expansion of a healthy artery and it may be possible that at higher magnitudes of radial compression the assumption of near-imcompressibility is no longer valid. This may explain the increase in damage and overestimation of compressive stresses that occurs at high strains. However as circumferential tension is the dominant loading mechanism during arterial expansion during procedures such as angioplasty and stenting these high compressive strains shouldn't be reached.

Despite these limitations the model could predict the experimental behaviour of healthy arterial tissue with good accuracy. The constitutive model is one of the few inelastic models that have been fit to arterial tissue experimental data that considers both softening and inelastic strains. The modelling of these inelastic effects allows for more accurate finite element analyses of interventions such as balloon angioplasty or stenting by accounting for tissue damage during loading and hence the resulting lumen gain.

Chapter 7 Finite element modelling of an idealised balloon angioplasty considering the inelastic behaviour of the overstretched artery wall and atherosclerotic plaque

Maher E.[1], Lally C.[1, 2], Kelly D. J.[1]

[1] Trinity Centre for Bioengineering, School of Engineering, Trinity College Dublin, Dublin 2, Ireland.

[2]School of Mechanical and Manufacturing Engineering, Dublin City University, Glasnevin, Dublin 9, Ireland

The large majority of the work discussed in this chapter was undertaken by the author of this thesis. The contributions of the other authors to this work are as follows: Dr. Kelly and Dr. Lally had a supervisory role on this study.

7.1 Introduction

Common treatments for atherosclerotic arteries include balloon angioplasty, stenting or a combination of the two. The objective of balloon angioplasty is to reduce the severity of a stenosis by increasing lumen size through mechanical loading. Finite element analysis is often used in the evaluation of these procedures and in stent design. The mechanisms of expansion of the lesion during balloon angioplasty include disruption or dissection of the plaque, compression of the plaque and overstretch resulting in distension of the remnant non-diseased vessel wall and compliant plaque components (Kovach et al., 1993; Waller, 1989). It is common practice in the finite element analysis to approximate the behaviour of both healthy and diseased arterial tissue using hyperelastic material models (Early and Kelly, 2010). Arterial tissue under physiological loading conditions can be considered an anisotropic nonlinear elastic tissue for which a hyperelastic material model would be suited. However, it has been observed experimentally that under supra-physiological loading conditions that neither arterial nor plaque tissue behave as elastic materials (Calvo et al., 2007; Maher et al., 2011). As seen in Chapters 4 and 5 both non-recoverable deformations and stress softening are observed for both atherosclerotic plaques and healthy arterial tissue when loaded in compression or tension beyond physiological levels. The omission of inelastic tissue behaviour in finite element analyses results in an inability to accurately quantify lumen gain post angioplasty or stenting. As a result the finite element analysis of balloon angioplasty has focussed on the inflation stage of balloon angioplasty, for example correlating the peak arterial stresses with rupture sites (Lee et al., 1993; Li et al., 2006).

In order to adequately model balloon angioplasty the inelastic nature of arterial tissue needs to be considered. Few models have been described in the literature that incorporates inelastic arterial behaviour into a simulation of balloon angioplasty. Calvo et al (2007) modelled the expansion of a monolayer artery without consideration of the plaque. The model included softening effects but no inelastic strains. Gasser et al (2007a) modelled plastic deformation in the media during balloon angioplasty. The plaque was modelled as a rigid body and the inelastic properties of the media were assumed. It was suggested that for the expansion of an eccentric plaque, with stiffer plaque properties than the neighbouring arterial tissue, that the mode of expansion would be

predominantly through overstretch of the non-diseased medial wall. Holzapfel *et al* also modelled the expansion of a layer specific lesion where the individual plaque component elastic properties were determined through mechanical testing (Holzapfel et al., 2002). This model also confined inelastic effects to the non-diseased arterial wall; in this case to the media and intima. MRI imaging was used to determine the vessel geometry in this model. The predictions of such models agree with clinical findings post-angioplasty which demonstrate that the presence of a stiff collageneous plaque cap results in minimal changes to the plaque structure but with circumferential stretching of the wall opposite the plaque (Toussaint et al., 1998).

While such models have greatly improved our understanding of the mechanics of clinical procedures such as angioplasty, they assume that the plaque is stiffer than the healthy arterial tissue and that no inelastic behaviour is observed in the plaque itself. It has been observed experimentally that average plaque mechanical properties depends on the plaque classification, with softer echolucent classification plaques possibly being of a lower stiffness than healthy arterial tissue in some cases (Maher et al., 2009). It has also been observed that atherosclerotic plaques of each classification behave inelastically when loaded. The objective of this study is to predict the effects of plaque type and inelasticity on the outcome of balloon angioplasty of a concentric lesion. The atherosclerotic plaque (Maher et al., 2011) and non-diseased arterial tissue (see, Chapters 5 and 6) mechanical properties were determined from data available from previous studies. To the author's knowledge this is the first finite element study of a balloon angioplasty procedure to include both artery and plaque inelasticity. It is hoped that such analyses can increase our understanding of the mechanisms through which vessel damage and hence lumen gain occur during angioplasty.

7.2 Materials and Methods

The finite element package ABAQUS was used to simulate an idealised balloon angioplasty of a diseased carotid artery. A simplified diseased arterial geometry, shown in Fig. 7.1, where the dimensions of the healthy artery portion were based on the approximate range for the carotid artery dimensions in humans (Denarié et al., 2000) and the size of the stenosis was chosen to correspond

to the higher values of % area stenosis determined through imaging of carotid lesions (Creane et al., 2010). The artery was modelled as a 40 mm long straight cylindrical vessel with 6 mm internal diameter and 0.5 mm wall thickness in the healthy segment. A 20 mm long concentric atherosclerotic plaque geometry was modelled which was designed to become gradually thicker towards the centre of the lesion to a maximum thickness of 1 mm. Balloon expansion was approximated by the expansion under displacement control of an arbitrarily stiff 15 mm length cylinder (the balloon) inside the vessel. Due to symmetry a one eight model with appropriate boundary condition along the axis of symmetry was used. Contact between the balloon and vessel was applied using a slave master approach where the slave nodes are constrained from penetrating the master surface by means of a penalty method. 8 node brick linear hybrid elements were used to mesh the artery, plaque and balloon. A mesh convergence study was performed, with the mesh shown in Fig. 7.1 resulting in convergence. The balloon was expanded by 1.1 mm radially using displacement constraints on the inner surface of the balloon, which resulted in the balloon expanding until the outer balloon surface reached the healthy arterial section diameter before an unloading phase.

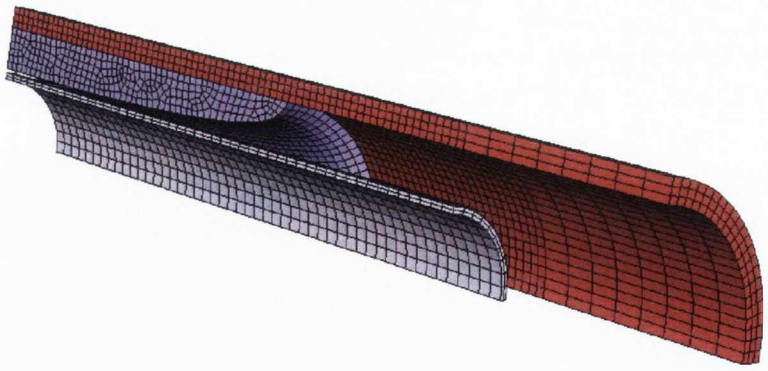

Figure 7.1: Model geometry showing the non-diseased healthy artery wall (red), the atherosclerotic plaque (purple) and the balloon (grey)

The mechanical properties of the healthy geometry are taken from previous curve fits of porcine carotid arterial tissue, see Section 6. Four different models were considered, where the atherosclerotic plaque material properties were different for each of the simulations. These

mechanical properties corresponded to the properties of a stiff calcified or a softer echolucent classifications of plaque (Maher et al., 2009, 2011). Each plaque classification was modelled as either an anisotropic hyperelastic or anisotropic inelastic material. The material model used for all plaque and artery properties is described in detail in Section 6.2 and the fitted constant are given in Table 7.1. The anisotropic plaque mechanical were estimated from previous experimental data (Maher et al., 2011), making use of the observation that carotid atherosclerotic plaques demonstrate a similar nominal stress-strain relationship in circumferential tension and radial compression (Maher et al., 2009) and assuming that the ratio of the magnitudes of inelastic deformation due to loading in the circumferential direction and radial direction are the same as in the healthy carotid artery. The fibre angle is assumed to be 15 degrees from the circumferential direction for all materials.

Table 7.1: Material parameters for carotid artery and atherosclerotic plaques. The dashed values represent an arbitrary non-zero value that has no effect on the mechanical behaviour of the tissue

Carotid						
$a(MPa)$	b	$k_1(MPa)$	k_2	d_∞^m	r_m	d_∞^f
0.05	3.2	0.011	0.95	0.8	0.13	0.75
r_f	$a^*(MPa)$	b^*	$k_1^*(MPa)$	k_2^*		
0.08	0.0035	0.001	0.0002	0.0001		
Echolucent	**Elastic**					
$a(MPa)$	b	$k_1(MPa)$	k_2	d_∞^m	r_m	d_∞^f
0.0122	0.55	0.0011	0.1	0	-	0
r_f	$a^*(MPa)$	b^*	$k_1^*(MPa)$	k_2^*		
-	0	-	0	-		
Echolucent	**Inelastic**					
$a(MPa)$	b	$k_1(MPa)$	k_2	d_∞^m	r_m	d_∞^f
0.014	0.87	0.0015	1.4	0.8	0.13	0.75
r_f	$a^*(MPa)$	b^*	$k_1^*(MPa)$	k_2^*		
0.08	0.002	0.001	0.00003	0.0001		
Calcified	**Elastic**					
$a(MPa)$	b	$k_1(MPa)$	k_2	d_∞^m	r_m	d_∞^f
0.055	0.02	0.0065	0.7	0	-	0
r_f	$a^*(MPa)$	b^*	$k_1^*(MPa)$	k_2^*		
-	0	-	0	-		
Calcified	**Inelastic**					
$a(MPa)$	b	$k_1(MPa)$	k_2	d_∞^m	r_m	d_∞^f
0.08	1.2	0.012	1.1	0.79	0.15	0.74
r_f	$a^*(MPa)$	b^*	$k_1^*(MPa)$	k_2^*		
0.092	0.007	0.0001	0.0003	0.0002		

7.3 Results

Before deflation of the angioplasty balloon, a lumen gain of 33.3% is achieved. The post-angioplasty lumen gain is predicted to be very small if hyperelastic plaque properties (i.e where inelasticity is only implemented in the non-diseased arterial tissue) are assumed. This is particularly true for the hyperelastic calcified plaque model where the increase in minimum lumen diameter was less than 1% post-angioplasty. The increase in minimal lumen diameter for the hyperelastic echolucent plaque model was approximately 3 times the magnitude of that observed for the calcified plaque (~ 2.5 % increase). The inclusion of inelastic material properties to the plaque models significantly increased the predicted magnitudes of lumen gain for both plaque classifications. Interestingly the lumen gain predicted for both plaque types were nearly identical when inelastic models for both artery and plaque were implemented (~7.47% for the calcified plaque and ~ 7.5% for the echolucent plaque).

Residual stresses were induced in both the plaque and artery on unloading due to the differing inelasticity of the healthy artery tissue and the plaque, see Figs. 7.2 and 7.3. The magnitudes of these residual stresses are significantly affected by the plaque material model implemented. When the plaque was modelled as calcified hyperelastic, the maximum predicted residual circumferential tensile stress in the plaque was approximately 1.8 kPa, while in the artery compressive circumferential tensile stresses were predicted whose peak value was over 50% greater in magnitude than the stresses observed in the plaque (~ 2.8 kPa). For the hyperelastic echolucent plaque the residual tensile stresses in the plaque and compressive stresses in the artery had peak magnitudes of approximately 1.4 kPa and 1.6 kPa respectively. These values differed significantly when inelastic plaque properties were considered, inducing residual compressive stresses in the plaque and tensile in the artery for both models. For the inelastic echolucent plaque models the peak magnitudes of these values were 1.24 kPa in the plaque and 2.9 kPa in the artery, while the largest magnitude induced residual stresses were predicted in the inelastic calcified plaque (7.25 kPa) with the magnitude in the artery similar to those observed in the inelastic echolucent model (2.8 kPa). The tensile and compressive residual stresses result from a

combination of the compliance difference in the plaque and artery as well as the inelasticity of the plaque and artery. For example, when a hyperelastic model is used for the plaque, the plaque will want to return to its original geometry on unloading, while the inelastic arteries zero stress-state will be changed. The result is that the final geometry will be between the two zero-stress states, thus inducing these residual stresses.

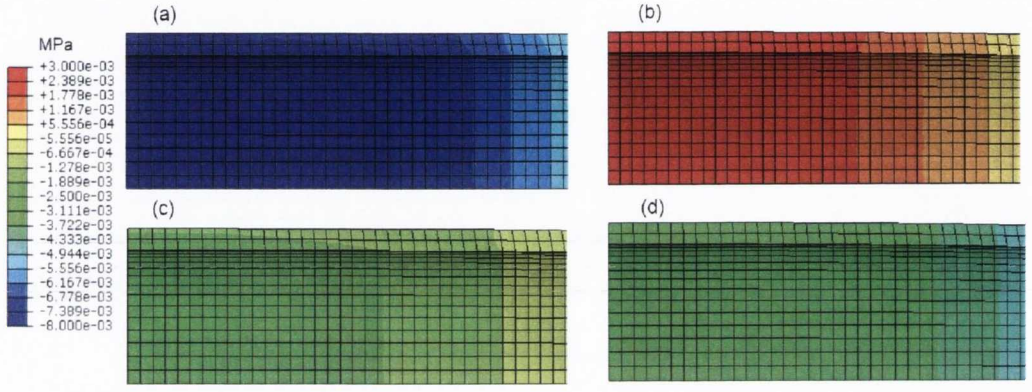

Figure 7.2: Circumferential residual stresses (MPa) predicted in the artery on unloading for (a) elastic calcified plaque model, (b) inelastic calcified plaque model, (c) elastic echolucent plaque model and (d) inelastic echolucent plaque model

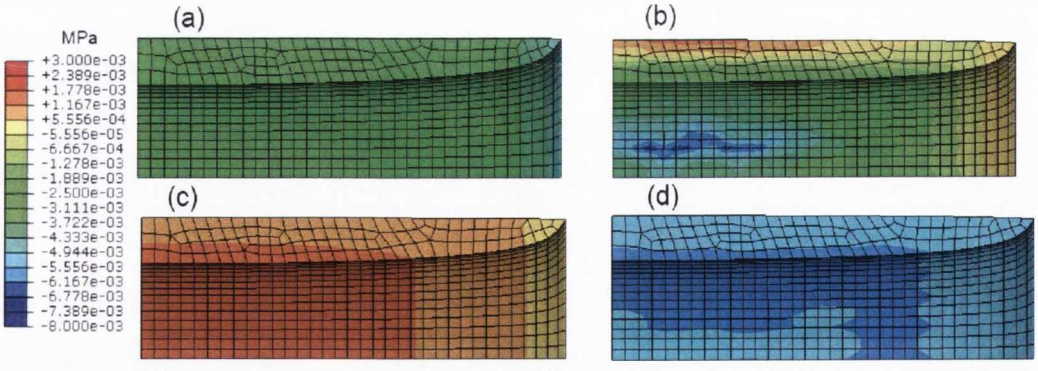

Figure 7.3: Circumferential residual stresses (MPa) predicted in the plaque on unloading for (a) elastic calcified plaque model, (b) inelastic calcified plaque model, (c) elastic echolucent plaque model and (d) inelastic echolucent plaque model

Both inelastic damage and elastic damage are dependent on the peak strains in the tissues load history. As such the areas of maximum elastic and inelastic damage will be the same. The maximum values of the damage terms within the arterial tissue are predicted to occur at the inner surface of the artery wall towards the centre of the lesion where the plaque is thickest, see Fig. 7.4. The values of arterial damage in both the matrix and fibre components were largely independent of the plaque material properties, with slightly lower levels of damage predicted in the artery wall of the echolucent plaque models. The fibre damage is confined to areas undergoing circumferential tension but matrix damage also occurs in the artery wall adjacent to the plaque as it experiences a slight narrowing due to deformation of the arterial wall during the balloon expansion process. The plaque damage is also greatest at the inner surface near the where the thickness is greatest (Fig. 7.5). The damage that occurs in the plaque is greater than that seen in the healthy arterial tissue with greatest damage predicted for the calcified plaque. As expected, the areas of greatest damage coincide with the areas of peak stresses during inflation. The magnitude of stress was predicted to be highest in the circumferential direction in all models. For the arterial tissue and echolucent plaque the maximum peak stresses were predicted to be less than 100 kPa during inflation. The highest stresses predicted in the calcified plaque were approximately 260 kPa. While the internal strain energy densities and hence the stresses are different in the fibre and matrix components, the damage is similar in both components, see Fig. 7.6.

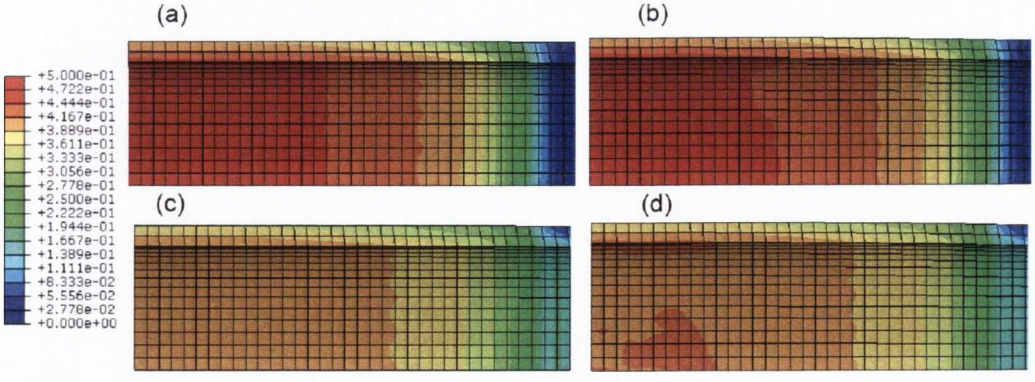

Figure 7.4: Elastic damage in the fibre of the healthy artery for (a) the elastic calcified plaque model and (b) the inelastic calcified plaque model. Elastic damage of the matrix component is shown in (c) and (d) for the elastic and inelastic calcified plaque models respectively.

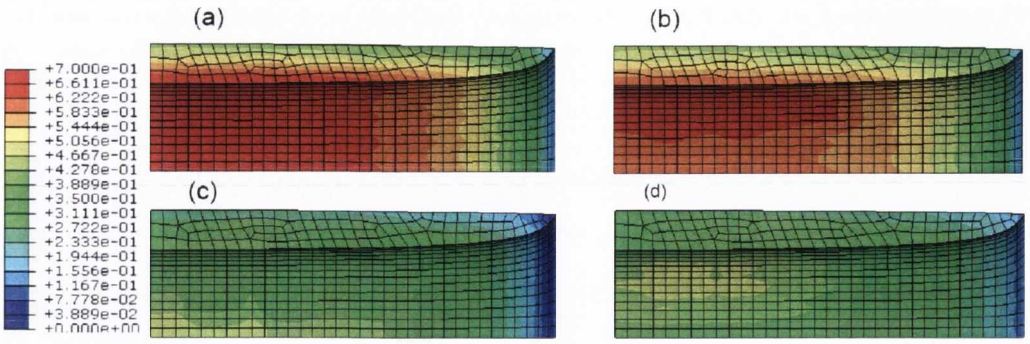

Figure 7.5: Elastic damage of the (a) fibre and (b) matrix components of the inelastic calcified plaques. Elastic damage of the (c) fibre and (d) matrix components of the inelastic echolucent plaque.

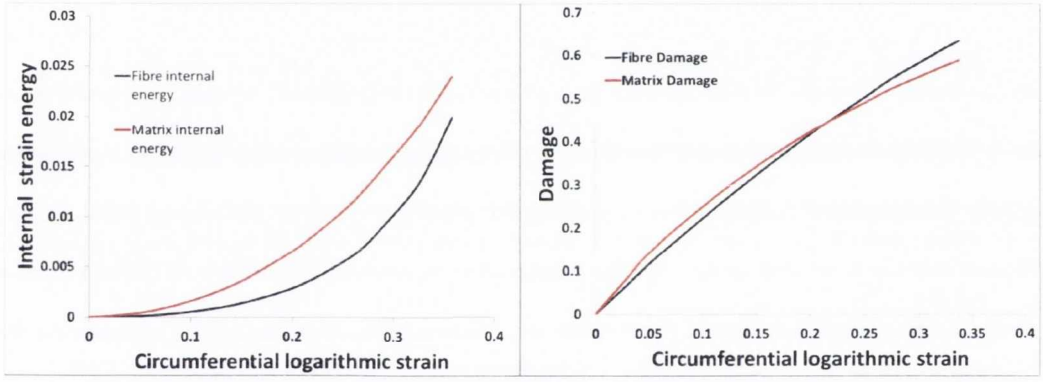

Figure 7.6: Internal strain energy density (left) and damage in the matrix and fibres at a node on the lumen surface of the plaque

7.4 Discussion

The incorporation of inelastic damage into models of atherosclerotic plaque has a large effect on predicted vessels mechanics compared to the models that assume hyperelastic material behaviour. A significantly greater lumen gain was predicted for both echolucent and calcified plaques when these inelastic effects were considered. The inelastic plaque models predicted nearly identical lumen gains for the calcified and echolucent lesions. This has been observed clinically, where plaque type had no significant effect on lumen gain post-angioplasty (Gil et al., 1996). During loading the highest plaque stresses occurred where the plaque was thickest and this also

corresponded to the area of greatest damage. The coincidence of peak inflation strains and the maximum inelasticity has been observed in other studies (Gasser and Holzapfel, 2007a). The choice of material model for the plaque had a significant effect on the residual stresses in the artery and plaque on unloading. This would have implications for remodelling algorithms of arterial tissue and highlights the importance of model choice for certain applications. The highest stresses were predicted during inflation of the calcified plaques. Average failure stresses for carotid atherosclerotic plaques have been reported as 366.6 ± 220.5 kPa by Lawlor et al (2011). Failure stresses of 254.8 ± 79.8 kPa and 179 ± 56 kPa have also been reported for fibrous plaque and calcified iliac plaque respectively (Holzapfel et al., 2004). However the classification methodology was different for the iliac plaque study than it was here. Comparing to these values our model indicates that failure of the calcified plaque near the surface is a possibility during expansion and as such the addition of failure into the material model would be advantageous.

To the author's knowledge no other study has performed a finite element analysis of a cardiovascular intervention incorporating inelastic models for both artery and plaque. Analyses that have focussed on overstretch of the arterial wall have been performed modelling the plaque as rigid or hyperelastic (Gasser and Holzapfel, 2007a; Holzapfel et al., 2002). These models generally focussed on stiff eccentric plaques which resulted in a prediction of minimal damage to the artery wall behind the plaque and significant overstretch of the arterial wall opposite the plaque which results in lumen gain. However it is seen here that this assumption does not hold for concentric plaques. In the models presented here the most significant damage occurred in the plaque, particularly for the calcified plaque.

There are a number of limitations to this study. The vessel geometry is idealised as a straight cylindrical vessel while in reality carotid plaques are more likely to form at the much more complex geometry of the carotid bifurcation. Another significant limitation is that the plaque is modelled as a homogeneous material which has been shown experimentally not to be the case (Maher et al., 2009). Also while plaque thickness was determined by using values of % area stenosis (Creane et al., 2010), the model significantly underestimates the plaque burden by ignoring

expansive remodelling. The tensile plaque properties are estimated and combined with inelastic compressive data for carotid atherosclerotic plaques and more mechanical testing is needed to validate the assumptions made. Balloon inflation during angioplasty is a pressure controlled process and not displacement controlled as modelled here. This was done to simplify the model as the main interest of this study was the vessel response to peak loading conditions during angioplasty, i.e. when the balloon is fully inflated. It should be noted that these models assume that the balloon expands fully to its nominal diameter. The possibility of under-expansion of the stiff calcified plaque or overexpansion of the vessel beyond the healthy lumen diameter as commonly occurs during angioplasty is not considered.

Despite these limitations this study demonstrates the importance of using of an anisotropic inelastic material model for computational modelling of clinical procedures such as balloon angioplasty and stenting. Material constants for the atherosclerotic plaques were estimated from test data of previous studies. The results suggest that the inelastic damage properties of atherosclerotic plaque play a significant role in the mechanical environment and lumen gain post-angioplasty and should be included in finite element models when predictions of lumen gain are of importance.

Chapter 8 Discussion

8.1 Overview

The objective of this thesis was to increase our understanding of the biomechanics of healthy and diseased arterial tissue. In the future such knowledge could potentially be used to improve both the treatment and potentially the prevention of atherosclerosis. A number of studies were undertaken to achieve this aim. Comprehensive investigations into the elastic and inelastic mechanical properties of atherosclerotic plaques were carried out. A further study was undertaken investigating the site-dependent inelastic behaviour of healthy arterial tissue. In order to adequately describe the observed mechanical behaviour appropriate constitutive models needed to be developed. An isotropic inelastic model was used to describe the inelastic behaviour of the atherosclerotic plaque while an anisotropic inelastic model was proposed for the modelling of arterial tissue. The data from these previous studies were then used as the basis for a finite element analysis of balloon angioplasty in order to investigate the influence of both plaque type and the assumption of tissue inelastic behaviour for the plaque the artery wall.

8.2 Mechanical properties of cardiovascular tissue

8.2.1 Atherosclerotic plaque

At the onset of this study no data was available in the literature on the mechanical properties of carotid atherosclerotic plaques, with the main focus of research being on aortic plaques (Lee et al., 1991; Lee et al., 1992; Topoleski et al., 1997). More recent studies have also characterised the mechanical response of these lesions (Barrett et al., 2009; Ebenstein et al., 2009; Lawlor et al., 2011). Atherosclerotic plaques were found to have a highly nonlinear behaviour in both

compression and tension for all plaque types. Such behaviour has been observed previously (Loree et al., 1994; Salunke et al., 2001), and in only one study was a more linear behaviour observed for calcified plaque (Holzapfel et al., 2004). It is important to note that the mechanical testing of atherosclerotic plaques presented here was performed on fresh tissue immediately after carotid endarterectomy. This may result in differences between this study and others performed on cadaveric tissue due to the changes of stored tissue mechanical properties (Stemper et al., 2007b). Lawlor et al (2011) recently reported similar behaviour to that observed in this study when comparing the ultimate tensile strength and strain of fresh carotid atherosclerotic plaques

Duplex ultrasound with grey scale median imaging was used to determine plaque type and plaques were classified as echolucent, mixed or calcified. It was found that on average calcified plaques were stiffest while echolucent plaque samples had the lowest stiffness, see Fig. 3.3. However there was a large amount of variability within each classification which resulted in this difference between plaque classifications being statistically insignificant. Others have found calcified plaques to be the stiffest plaque type (Ebenstein et al., 2009; Holzapfel et al., 2004). The high variability within clinical classification determined by ultrasound has been observed recently in other studies (Lawlor et al., 2011). A possible effect of plaque location on the mechanical properties was also observed with plaques taken from the common carotid having the stiffest response and plaque samples from the external carotid having the least stiff behaviour, see Fig. 3.4. This may be an indication of the importance of using site specific mechanical properties for atherosclerotic plaques as is done when modelling the response of healthy vessels from different locations in the arterial tree.

Inelastic behaviour was observed for atherosclerotic plaques of all types when loaded cyclically. The behaviour is similar to that seen in many soft tissues with significant stress softening occurring between the first and second loading cycles and unrecoverable inelastic residual strains on unloading. An approximately linear relationship was observed between peak load experienced by the sample and the inelastic strains on unloading for all plaque types (Fig. 4.3).

Interestingly, plaque composition was found to have no effect on the mean inelastic deformations. This may in part explain the clinical observation that no significant differences in lumen gain following balloon angioplasty were observed clinically between different types of plaque (Gil et al., 1996).

8.2.2 Healthy artery

As with atherosclerotic plaques, stress softening and inelastic strains were observed for arterial tissue at supra-physiological loads as is typical for overstretched arterial tissue (Holzapfel et al., 2000). The inelastic response of the tissue was observed to be both anisotropic and site dependant. Inelastic deformations were highest in arterial radial compressive samples and lowest in circumferential tensile samples with higher magnitudes of unrecoverable strain in more muscular arteries that have a high collagen to elastin ratio. Significant variation was observed in the % stress softening in each loading direction and while no significant differences could be determined, stress softening tended to be greater in the longitudinal direction. While stress softening and inelastic deformation has been observed previously (Holzapfel et al., 2000) and in some instances incorporated into a constitutive model (Peña, 2011), to the author's knowledge this is the first study to show in depth experimental results for these phenomena throughout the arterial tree. This data could be used as a basis for future modelling of arterial tissue and could be incorporated into a number of constitutive frameworks for modelling inelastic phenomena in arterial tissue (Gasser and Holzapfel, 2002; Peña, 2011), including that presented in this thesis.

A hypothesis of the damage mechanisms that occur in arterial tissue was proposed to explain the observed behaviour. It is suggested that the damage phenomena (stress softening and unrecoverable strains) that are observed in arteries loaded in any give direction occur in both the collagen fibres and matrix (composed of elastin fiber network, smooth muscle cells and ground matrix). Furthermore, the mechanisms that induce softening of the artery (termed softening damage) may be largely independent of those resulting in inelastic strains on unloading (inelastic damage). From our test data it appears that inelastic damage is largely isolated to the matrix, and as

elastin should behave relatively elastically at the loads applied it is suggested that damage due to overstretch of smooth muscle is a dominant mechanism for inelastic damage of arterial tissue. This would further explain the larger magnitudes of inelastic deformation observed for muscular arteries, where the media contains a higher smooth muscle and a lower elastin content than in elastic arteries whose media contains more elastin. The lower inelastic strains as a result of circumferential loading are thought to be a result of relatively little inelastic damage occurring in the near circumferentially orientated collagen fibres, while the similar levels of stress softening observed in each direction implies stress-softening damage occurs in both the collagen fibres and matrix.

This hypothesis can be related to a number of previous proposals for inelastic mechanisms in the literature. Castaneda-Zuniga *et al* (1980) hypothesised that the permanent widening (inelastic damage) of arteries during angioplasty was due to overstretching of the muscle fibres which were observed experimentally as the deformation of muscle cell nuclei. The mechanisms of elastic and inelastic damage in the collageneous fiber component could be explained by the damage mechanisms proposed by Parry et al (1978) where damage to intra-fibrillar crosslinks result in softening and damage to crosslinks between the fibres and matrix result in fibre slip (inelastic damage). No definite mechanism of inelastic damage was proposed; however as the elastin network includes similar intra-fibrillar crosslinks that tend to increase artery stiffness, damage to these links may result in stress-softening.

8.2.3 Limitations

There are a number of limitations that apply to each of the testing methodologies used to determine mechanical properties. All testing is performed at room temperature and the tissue response to loading may be different at *in vivo* temperatures. There are conflicting reports in the literature regarding the temperature dependence of arterial mechanical properties (Guinea et al., 2005; Kang et al., 1995). As a result any error associated with this limitation is unknown. For the tensile experiments the tested samples were not immersed in saline solution and it is possible that the loss

of water content in the samples may affect mechanical properties. In order to reduce this effect tensile samples were regularly lightly sprayed with saline. For the determination of inelastic strains of both healthy and diseased tissue it is difficult to completely rule out viscoelastic and poroelastic phenomena as playing important roles. Preliminary tests of arterial tissue showed no significant recovery of inelastic deformations when the testing methodology included rest periods between cycles.

The resolution of the ultrasound imaging may also provide a further limitation in the classification of plaque samples tested. Higher resolution imaging such as high resolution MRI (Holzapfel et al., 2004) may lead better characterisation of the inhomogeneous nature of plaques and allow the presence of smaller particles such as micro-calcifications to be identified. As Duplex ultrasound is commonly used clinically to characterise plaques *in vivo,* it was decided to use it as a basis for classification in order to provide a more clinical relevance to the test data presented. For the mechanical testing of arterial tissue the artery was tested as a single layer to determine the overall properties of the vessel wall. Layer specific testing may provide further insight into the mechanical behaviour of arteries. It should be noted that more testing is required to characterise the behaviour of both healthy artery and atherosclerotic plaques. This is particularly true for the tensile plaque behaviour due to the scarcity of test data.

8.3 Constitutive modelling

8.3.1 Isotropic hyperelastic model

The elastic loading behaviour of atherosclerotic plaques were characterised using a 2^{nd} order polynomial strain energy function. This study is one of the few investigations into the mechanical properties of atherosclerotic plaques that characterised the constitutive stress-strain response of the tissue. This is particularly the case for carotid plaques where only one other study has used an istropic hyperelastic material model to describe the behaviour of plaque specimens (Lawlor et al.,

2011). While an isotropic hyperelastic characterisation has its limitations, most notably the response of atherosclerotic plaques is not isotropic (Holzapfel et al., 2004), these models are commonly used to describe plaque tissue in finite element models and the data presented can be readily incorporated into such models as the polynomial form constitutive model used is readily available in most commercial finite element packages.

8.3.2 Isotropic inelastic model

In Chapter 4 an isotropic inelastic model is presented in order to describe the inelastic behaviour of atherosclerotic plaques due to compressive loading. The constitutive model is formulated in such a way as to ease the dissemination of experimental data from the material constants in Table 4.2. A number of assumptions are made in this model; damage is only applied on unloading and the peak stress-strain points of each loading cycle describe the monotonic uniaxial behaviour of the tissue. The monotonic loading behaviour is termed the load envelope. The constants relating to the load envelope a and b can be used directly in a hyperelastic material model as in the study by Delfino et al (1997). As stated previously the lack of mechanical test data for atherosclerotic plaques means the ease at which the uniaxial stress-strain response can be extracted is of importance. The assumption that the load envelope is equivalent to the monotonic loading behaviour of the tissue has been partially validated for healthy carotid tissue in Chapter 5.

There are a number of limitations specific to this model. As with the hyperelastic model the isotropic loading does not fully describe the tissue behaviour. The applied damage is also isotropic which limits the model to use with a single loading regime. For finite element models that wish to include complex loading such as torsion and bending, this model may be inappropriate as a result. The fact that inelasticity is only applied on unloading would also not be consistent with the known mechanisms of damage which build up during loading. The choice of model was made largely due to the ease of extracting mechanical test data from it. This will allow the data here to be combined with tensile data with greater ease in the future. As this is the first study to model the inelastic

behaviour of atherosclerotic plaques, the data fits provided with it may be of some use in finite element modelling despite its limitations.

8.3.3 Anisotropic inelastic model

An anisotropic inelastic damage based model was formulated to describe arterial tissue damage as described in Section 8.2.2. This model provided accurate fits for the circumferential and longitudinal inelastic tensile response of healthy carotid and aortic tissue. The model also allowed accurate predictions of the inelastic deformations resulting from radial compression. The stress-softening damage effect is relatively large in both the matrix and fiber components while the inelastic damage is greater in the matrix. This is in agreement with our hypothesis of damage. In this model damage can only evolve during loading which is a more accurate interpretation of the development of tissue damage than in the isotropic damage model. The precise mechanisms of damage are not included directly into the model but both softening and inelastic damage are described by the evolution of phenomenological internal variables. The model is unique in that in considers the application of two damage mechanisms to both the matrix and fibrous components. Gasser et al (2002) modelled inelastic damage (fibre slip) of the collagen fibres through a multisurface slip plasticity based model while Peña et al (2011) modelled elastic and inelastic damage of fibrous components and stress-softening damage of the matrix component. In order to model the behaviour of vena cava samples the fibres directions were set perpendicular to each other to describe the loading behaviour in the axial and circumferential directions. This study is one of the few studies to account for inelastic deformations and stress softening for soft tissues and to the author's knowledge the only model that has been applied to model these anisotropic phenomena for arterial tissue.

This constitutive model can be implemented in a finite element model of balloon angioplasty or stenting to describe arterial tissue response. This should allow for a large improvement on the accuracy of the finite element models over the commonly used isotropic hyperelastic description of the tissue. It could also be used in the modelling of other fibrous soft

tissues. In section 7 the model was also applied to atherosclerotic plaque using the compressive data presented in Chapter 4 and estimating the circumferential tensile properties.

8.3.4 Limitations

In addition to the model specific limitations discussed above there are those common to all three models. Viscoelastic behaviour such as creep and stress relaxation are excluded from these models. It is commonly accepted that healthy arterial tissue behaves viscoelastically and creep and relaxation has also been observed experimentally for atherosclerotic plaques (Salunke et al., 2001). Rate dependency of the tissue response is also ignored. Despite the inclusion of damage into two of the models failure was not incorporated due to lack of experimental data. This could be incorporated with relative ease into the reduction factor of the anisotropic inelastic model as describe in section 6.4. Each of the models are phenomenological based models and as such it is difficult to relate the material constants to physical effects. While the introduction of families of fibres is a move towards a more mechanistic approach the model and damage applied are phenomenological based in order to describe the effects on the tissue mechanical properties of the proposed damage mechanisms rather than the mechanisms themselves.

8.4 Finite element model of balloon angioplasty

A finite element model of a simplified balloon angioplasty was analysed with the intention of illustrating the use of the anisotropic inelastic model and of investigating the importance of considering such effects in models of angioplasty. What we found is that for concentric plaques minimal post angioplasty lumen gain is achieved due to balloon expansion particularly for the calcified plaque model. However by including inelastic properties lumen gain was much more significant with the % diameter increase approximately 10 times greater for the calcified and 3 times greater for the echolucent plaque models. Balloon angioplasty models in the literature commonly use elastic or rigid plaque material models (Gasser and Holzapfel, 2007a; Holzapfel et

al., 2002). Eccentric plaque geometries and stiff plaque properties are commonly used in these models which result in much of the overstretch in the arterial wall opposite the lesion. From our results however we can conclude that for concentric plaques, and possibly for eccentric plaques in which plaque deposits form around the inner circumference of the artery, it is necessary to incorporate damage into the plaque model. It was also seen that including the inelastic plaque models resulted in a large change in the residual stresses of the plaque and artery on unloading, which may have implications for remodelling algorithms. Limitations of this model include the use of simplified geometry, homogeneous mechanical properties for artery and plaque and the use of a displacement controlled expansion. The fact that residual stresses were neglected is also a significant limitation of this finite element study. The plaque mechanical properties were estimated from available experimental data; however more data is needed to improve this characterisation.

8.5 Conclusions

The aim of this thesis was to increase our fundamental understanding of the mechanical behaviour of healthy and diseased arterial tissue. The following conclusions can be made:

- Mean plaque stress-strain behaviour is stiffer for calcified plaques and least stiff for echolucent plaques.
- Large variations of plaques properties exist within between plaques, within plaques and within each plaque classification, supporting the use of patient specific finite element modelling.
- The magnitude of inelastic strains is independent of plaque classification.
- The magnitude of inelastic strains of healthy arterial tissue is site dependent and has an approximately linear relationship with the peak applied loads.
- It is hypothesised that inelastic damage of healthy arterial tissue is largely a result of overstretch of the smooth muscle component while the inelastic anisotropy is a result of the mechanical behaviour of the near circumferentially orientated collagen fibres in the media.

- An anisotropic inelastic damage model was developed to account for the damage phenomena observed in healthy arterial tissue due to overstretch and was fit to experimental data from aortic and carotid arterial tissue.
- It is important to include the inelastic properties of both vessel and plaque in order to estimate lumen gain in finite element modelling, particularly for concentric lesions.

8.6 Future work

- More mechanical testing of atherosclerotic plaques is needed to characterisation of the tissue in both hyperelastic and inelastic material models. This is particularly needed for tensile data. Specifically anisotropic cyclic testing of plaques similar to what was performed on healthy arteries here would be greatly beneficial.
- A more complete investigation of healthy arterial inelastic properties is needed. This may include layer specific testing and testing of human tissue both of which would provide further insight into the mechanical response of tissue to supra-physiological loading. More testing following the methodology in this paper would also be beneficiary.
- Future testing of arterial tissue could include the selective digestion of elastin and collagen individually, investigating the effects that a lack of one of the structural components has on the tissue inelasticity and how it differs throughout the arterial tree.
- The anisotropic inelastic model may be improved through the addition of failure modes and viscoelasticity.
- Improvements on the simplified finite element model of balloon angioplasty can be made by incorporating more realistic geometries, inhomogeneity of the plaque, residual stresses prior to loading and the use of pressure controlled expansion.
- Incorporating the anisotropic inelastic model into stent expansion simulations may see beneficial results in the optimisation of stent design to minimise the stresses induced during loading while maximising lumen gain.

References

Alastrué, V., E. Peña, *et al.*, 2008. Experimental study and constitutive modelling of the passive mechanical properties of the ovine infrarenal vena cava tissue. Journal of Biomechanics 41, 3038-3045.

Alastrué, V., J.F. Rodríguez, *et al.*, 2007. Structural damage models for fibrous biological soft tissues. International Journal of Solids and Structures 44, 5894-5911.

Auer, M., R. Stollberger, *et al.*, 2010. In vitro angioplasty of atherosclerotic human femoral arteries: analysis of the geometrical changes in the individual tissues using MRI and image processing. Annals of Biomedical Engineering 38, 1276-1287.

Auricchio, F., M. Conti, *et al.*, 2011. Carotid artery stenting simulation: From patient-specific images to finite element analysis. Medical Engineering & Physics 33, 281-289.

Auricchio, F., M. Di Loreto, *et al.*, 2001. Finite-element Analysis of a Stenotic Artery Revascularization Through a Stent Insertion. Computer Methods in Biomechanics and Biomedical Engineering 4, 249-263.

Balzani, D., S. Brinkhues, *et al.*, 2011. Constitutive Framework for the Modeling of Damage in Collagenous Soft Tissues with Application to Arterial Walls. Comp. Methods Appl. Mech. Engrg.

Balzani, D., J. Schröder, *et al.*, 2006. Simulation of discontinuous damage incorporating residual stresses in circumferentially overstretched atherosclerotic arteries. Acta Biomaterialia 2, 609-618.

Baroncini, L.A., A. Pazin Filho, *et al.*, 2006. Ultrasonic tissue characterization of vulnerable carotid plaque: correlation between videodensitometric method and histological examination. Cardiovascular Ultrasound 4, 32.

Barrett, S.R., M.P. Sutcliffe, *et al.*, 2009. Experimental measurement of the mechanical properties of carotid atherothrombotic plaque fibrous cap. Journal of Biomechanics.

Bashore, T.M., 2008. Heart Disease, In: McPhee, S.J., Papadakis, M.A., Tierney, L.M. (Eds.) Current Medical Diagnosis and Treatment 2008. McGraw-Hill.

Bedoya, J., C. Meyer, *et al.*, 2006. Effects of Stent Design Parameters on Normal Artery Wall Mechanics. Journal of Biomechanical Engineering 128, 757-765.

Berenson, G.S., S.R. Srinivasan, *et al.*, 1998. Association between multiple cardiovascular risk factors and atherosclerosis in children and young adults. The Bogalusa Heart Study. New England Journal of Medicine 338, 1650-1656.

Berne, R.M., S.R. Geiger, *et al.*, 1979. Handbook of physiology: a critical, comprehensive presentation of physiological knowledge and concepts. The cardiovascular system. Formerly Section 2: Circulation. The heart. American Physiological Society.

Bund, S.J., A.A. Oldham, *et al.*, 1996. Mechanical properties of porcine small coronary arteries in one-kidney, one-clip hypertension. Journal of vascular research 33, 175-180.

Burton, A.C., 1954. Relation of Structure to Function of the Tissues of the Wall of Blood Vessels. Physiological Reviews 34, 619-642.

Calvo, B., E. Peña, *et al.*, 2007. An uncoupled directional damage model for fibred biological soft tissues. Formulation and computational aspects. International Journal for Numerical Methods in Engineering 69, 2037-2057.

Carew, T.E., R.N. Vaishnav, *et al.*, 1968. Compressibility of the arterial wall. Circulation research 23, 61-68.

Carmines, D.V., J.H. McElhaney, *et al.*, 1991. A piece-wise non-linear elastic stress expression of human and pig coronary arteries tested in vitro. Journal of Biomechanics 24, 899-906.

Castaneda-Zuniga, W.R., A. Formanek, *et al.*, 1980. The mechanism of balloon angioplasty. Radiology 135, 565-571.

Cheng, C.P., N.M. Wilson, *et al.*, 2006. In vivo MR angiographic quantification of axial and twisting deformations of the superficial femoral artery resulting from maximum hip and knee flexion. Journal of Vascular and Interventional Radiology 17, 979-987.

Cheng, G.C., H.M. Loree, *et al.*, 1993. Distribution of circumferential stress in ruptured and stable atherosclerotic lesions: A structural analysis with histopathological correlation. Circulation 87, 1179-1187.

Chua, S.N.D., B.J. Mac Donald, *et al.*, 2003. Finite element simulation of stent and balloon interaction. Journal of Materials Prcessing Technology 143-144.

Chua, S.N.D., B.J. Mac Donald, *et al.*, 2004a. Effects of varying slotted tube (stent) geometry on its expansion behaviour using finite element method. Journal of Materials Prcessing Technology 155-156, 1764-1771.

Chua, S.N.D., B.J. MacDonald, *et al.*, 2004b. Finite element simulation of slotted tube (stent) with the presence of plaque and artery by balloon expansion. Journal of Materials Processing Technology 155-156, 1772-1779.

Chuong, C.J., Y.C. Fung, 1984. Compressibility and constitutive equation of arterial wall in radial compression experiments. Journal of Biomechanics 17, 35-40.

Collins, J.A., H.R. Busby, *et al.*, 2009. Mechanical Design of Machine Elements and Machines. Wiley and Sons.

Cox, R.H., 1975. Anisotropic properties of the canine carotid artery in vitro. Journal of Biomechanics 8, 293-300.

Cox, R.H., 1977. Effects of age on the mechanical properties of rat carotid artery. The American Journal of Physiology 233, H256-263.

Cox, R.H., 1978. Passive mechanics and connective tissue composition of canine arteries. The American Journal of Pysiology 234, H533-541.

Creane, A., E. Maher, *et al.*, 2010. Finite element modelling of diseased carotid bifurcations generated from in vivo computerised tomographic angiography. Computers in Biology and Medicine 40, 419-429.

Davidson, J.M., K.E. Hill, *et al.*, 1985. Longitudinal gradients of collagen and elastin gene expression in the porcine aorta. The Journal of Biological Chemistry 260, 1901-1908.

Davies, M.J., 2000. The pathophysiology of acute coronary syndromes. Heart 83, 361-366.

Delfino, A., N. Stergiopulos, *et al.*, 1997. Residual strain effects on the stress field in a thick wall finite element model of the human carotid bifurcation. Journal of Biomechanics 30, 777-786.

Denarié, N., J. Gariepy, *et al.*, 2000. Distribution of ultrasonographically-assessed dimensions of common carotid arteries in healthy adults of both sexes. Atherosclerosis 148, 297-302.

Diani, J., M. Brieu, *et al.*, 2006. A damage directional constitutive model for Mullins effect with permanent set and induced anisotropy. European Journal of Mechanics A/Solids 25, 483-496.

Dixon, S.A., R.G. Heikes, *et al.*, 2003. Constitutive modeling of porcine coronary arteries using designed experiments. Journal of Biomechanical Engineering 125, 274-279.

Dorfmann, A., R.W. Ogden, 2004. A constitutive model for the Mullins effect with permanent set in particle-reinforced rubber. International Journal of Solids and Structures 41, 1855-1878.

Driessen, N.J., G.W. Peters, *et al.*, 2003. Remodelling of continuously distributed collagen fibres in soft connective tissues. Journal of Biomechanics 36, 1151-1158.

Dumoulin, C., B. Cochelin, 2000. Mechanical Behaviour modelling of balloon-expandable stents. Journal of Biomechanics 33, 1461-1470.

Early, M., D. Kelly, 2011. The consequences of the mechanical environment of peripheral arteries for nitinol stenting. Medical and Biological Engineering and Computing, 1-10.

Early, M., D.J. Kelly, 2010. The role of vessel geometry and material properties on the mechanics of stenting in the coronary and peripheral arteries. Proceedings of the Institution of Mechanical Engineers. Part H 224, 465-476.

Early, M., C. Lally, *et al.*, 2009. Stresses in peripheral arteries following stent placement: a finite element analysis Computer Methods in Biomechanics and Biomedical Engineering 12, 25-33.

Ebenstein, D.M., D. Coughlin, *et al.*, 2009. Nanomechanical properties of calcification, fibrous tissue, and hematoma from atherosclerotic plaques. Journal of Biomedical Materials Research. Part A 91, 1028-1037.

Ehret, A.E., M. Itskov, 2009. Modeling of anisotropic softening phenomena: Application to soft biological tissues. International Journal of Plasticity 25, 901-919.

Emery, J.L., J.H. Omens, *et al.*, 1997. Strain softening in rat left ventricular myocardium. Journal of Biomechanical Engineering 119, 6-12.

Erbel, R., M. Haude, *et al.*, 1998. Coronary-artery stenting compared with balloon angioplasty for restenosis after initial balloon angioplasty. Restenosis Stent Study Group. New England Journal of Medicine 339, 1672-1678.

Etave, F., G. Finet, *et al.*, 2001. Mechanical properties of coronary stents determined by using finite element analysis. Journal of Biomechanics 34, 1065-1075.

Fayad, P., 2007. Endarterectomy and stenting for asymptomatic carotid stenosis: a race at breakneck speed. Stroke 38, 707-714.

Fischer, G.M., J.G. Llaurado, 1966. Collagen and elastin content in canine arteries selected from functionally different vascular beds. Circulation Research 19, 394-399.

Flory, P.J., 1961. Thermodynamic relations for high elastic materials. Transactions of the Faraday Society 57, 829-838.

Franceschini, G., D. Bigoni, *et al.*, 2006. Brain tissue deforms similarly to filled elastomers and follows consolidation theory. Journal of the Mechanics and Physics of Solids 54, 2592-2620.

Fung, Y.C., 1981. Biomechanics : mechanical properties of living tissues / Y.C. Fung. Springer-Verlag, New York :.

Fung, Y.C., K. Fronek, *et al.*, 1979. Pseudoelasticity of arteries and the choice of its mathematical expression. American Journal of Pysiology 237, H620-631.

Fung, Y.C., S.Q. Liu, 1995. Determination of the mechanical properties of the different layers of blood vessels in vivo. Proc Natl Acad Sci U S A 92, 2169-2173.

Fung, Y.C., S.Q. Liu, *et al.*, 1993. Remodeling of the constitutive equation while a blood vessel remodels itself under stress. Journal of Biomechanical Engineering 115, 453-459.

Fung, Y.C., S.S. Sobin, 1981. The Retained Elasticity of Elastin Under Fixation Agents. Journal of Biomechanical Engineering 103, 121-122.

Furie, K.L., S.E. Kasner, *et al.*, 2011. Guidelines for the prevention of stroke in patients with stroke or transient ischemic attack: a guideline for healthcare professionals from the american heart association/american stroke association. Stroke 42, 227-276.

Garcia, A., E. Pena, *et al.*, 2011. Experimental study and constitutive modelling of the passive mechanical properties of the porcine carotid artery and its relation to histological analysis: Implications in animal cardiovascular device trials. Medical Engineering & Physics 33, 665-676.

Gasser, T.C., G.A. Holzapfel, 2002. A rate-independent elastoplastic model for biological fiber-reinforced composites at finite strains:continuum basis,algorithmic formulation and finite element implementation. Computational Mechanics 29, 340-360.

Gasser, T.C., G.A. Holzapfel, 2007a. Finite element modeling of balloon angioplasty by considering overstretch of remnant non-diseased tissues in lesions. Computational Mechanics 40, 47-60.

Gasser, T.C., G.A. Holzapfel, 2007b. Modeling Plaque Fissuring and Dissection during Balloon Angioplasty Intervention. Annals of Biomedical Engineering 35, 711-723.

Gasser, T.C., R.W. Ogden, *et al.*, 2006. Hyperelastic modelling of arterial layers with distributed collagen fibre orientations. Journal of the Royal Society Interface 3, 15-35.

Gasser, T.C., C.A.J. Schulze-Bauer, *et al.*, 2002. A Three-dimensional Finite Element Model for Arterial Clamping. Journal of Biomechanics 124, 355-363.

Geng, Y.J., L.E. Henderson, *et al.*, 1997. Fas is expressed in human atherosclerotic intima and promotes apoptosis of cytokine-primed human vascular smooth muscle cells. Arteriosclerosis, thrombosis, and vascular biology 17, 2200-2208.

Gil, R., C. Di Mario, *et al.*, 1996. Influence of plaque composition on mechanisms of percutaneous transluminal coronary balloon angioplasty assessed by ultrasound imaging. American Heart Journal 131, 591-597.

Girerd, X.J., C. Acar, *et al.*, 1992. Incompressibility of the human arterial wall: an in vitro ultrasound study. Journal of Hypertension 10, S111-S114.

Glagov, S., H.S. Bassiouny, *et al.*, 1997. Mechanical determinants of plaque modeling, remodeling and disruption. Atherosclerosis 131, S13-S14.

Glagov, S., C. Zarins, *et al.*, 1988. Hemodynamics and atherosclerosis. Insights and perspectives gained from studies of human arteries. Archives of Pathology & Laboratory Medicine 112, 1018-1031.

Gow, B.S., D. Schonfeld, *et al.*, 1974. The dynamic elastic properties of the canine left circumflex coronary artery. Journal of Biomechanics 7, 389-395.

Greenwald, S.E., 2007. Ageing of the conduit arteries. The Journal of Pathology 211, 157-172.

Gruntzig, A.R., A. Senning, *et al.*, 1979. Nonoperative dilatation of coronary-artery stenosis: percutaneous transluminal coronary angioplasty. New England Journal of Medicine 301, 61-68.

Guinea, G.V., J.M. Atienza, *et al.*, 2005. Thermomechanical behavior of human carotid arteries in the passive state. American Journal of Physiology, Heart and Circulatory Physiology 288, H2940-2945.

Guo, X., X. Lu, *et al.*, 2005. Transmural strain distribution in the blood vessel wall. Am J Physiol Heart Circ Physiol 288, H881-H886.

Gurm, H.S., J.S. Yadav, *et al.*, 2008. Long-term results of carotid stenting versus endarterectomy in high-risk patients. New England Journal of Medicine 358, 1572-1579.

Hariton, I., G. deBotton, *et al.*, 2007. Stress-modulated collagen fiber remodeling in a human carotid bifurcation. Journal of Theoretical Biology 248, 460-470.

Hayashi, K., Y. Imai, 1997. Tensile property of atheromatous plaque and an analysis of stress in atherosclerotic wall. Journal of Biomechanics 30, 573-579.

Hokanson, J., S. Yazdani, 1997. A constitutive model of the artery with damage Mechanics Research Communications 24, 151-159.

Holzapfel, G.A., 2000. Nonlinear Solid Mechanics. John Wiley & Sons.

Holzapfel, G.A., 2006. Determination of material models for arterial walls from uniaxial extension tests and histological structure. Journal of Theoretical Biology 238, 290-302.

Holzapfel, G.A., C.T. Gasser, *et al.*, 2000. A New Constitutive Framework for Arterial Wall Mechanics and a Comparative Study of Material Models. Journal of Elasticity 61, 1-48.

Holzapfel, G.A., T.C. Gasser, 2001. A viscoelastic model for fiber-reinforced composites at finite strains: Continuum basis, computational aspects and applications. Computer Methods in Applied Mechanics and Engineering 190, 4379-4403.

Holzapfel, G.A., G. Sommer, *et al.*, 2005. Determination of layer-specific mechanical properties of human coronary arteries with nonatherosclerotic intimal thickening and related constitutive modeling. American Journal of Physiology, Heart and Circulatory Physiology 289, H2048-2058.

Holzapfel, G.A., G. Sommer, *et al.*, 2004. Anisotropic Mechanical Properties of Tissue Components in Human Atherosclerotic Plaques. Journal of Biomechanical Engineering 126, 657-665.

Holzapfel, G.A., M. Stadler, *et al.*, 2002. A Layer-Specific Three-Dimensional Model for the Simulation of Balloon Angioplasty using Magnetic Resonance Imaging and Mechanical Testing. Annals of Biomedical Engineering 30, 753-767.

Honye, J., D.J. Mahon, *et al.*, 1992. Morphological effects of coronary balloon angioplasty in vivo assessed by intravascular ultrasound imaging. Circulation 85, 1012-1025.

Humphrey, J.D., 2002. Cardiovascular Solid Mechanics: Cells, Tissues, and Organs. Springer.

Humphrey, J.D., S.L. Delange, 2004. An Introduction to Biomechanics: Solids and Fluids, Analysis and Design. Springer.

Insull, W., Jr., 2009. The pathology of atherosclerosis: plaque development and plaque responses to medical treatment. American Journal of Medicine 122, S3-S14.

Kafienah, W., T.J. Sims, 2004. Biochemical methods for the analysis of tissue-engineered cartilage. Methods in Molecular Biology 238, 217-230.

Kang, T., J. Resar, *et al.*, 1995. Heat-induced changes in the mechanical behavior of passive coronary arteries. Journal of Biomechanical Engineering 117, 86-93.

Kiousis, D.E., T.C. Gasser, *et al.*, 2007. A Numerical Model to Study the Interaction of Vascular Stents with Human Atherosclerotic Lesions. Annals of Biomedical Engineering 35, 1857-1869.

Kovach, J.A., G.S. Mintz, *et al.*, 1993. Sequential intravascular ultrasound of the mechanisms of rotational atherectomy and adjunct balloon angioplasty. Journal of the American College of Cardiology 22, 1024-1032.

Ku, D.N., B.N. McCord, 1993. Cyclic stress causes rupture of the atherosclerotic plaque cap. Circulation 88, 1362.

Lally, C., F. Dolan, *et al.*, 2005. Cardiovascular stent design and vessel stresses:a finite element analysis. Journal of Biomechanics 38, 1574-1581.

Lally, C., A.J. Reid, *et al.*, 2004. Elastic behavior of porcine coronary artery tissue under uniaxial and equibiaxial tension. Annals of Biomedical Engineering 32, 1355-1364.

Lawlor, M.G., M.R. O'Donnell, *et al.*, 2011. Experimental determination of circumferential properties of fresh carotid artery plaques. Journal of Biomechanics 44, 1709-1715.

Lee, R.T., A.J. Grodinsky, *et al.*, 1991. Structure-Dependent Dynamic Mechanical Behavior of Fibrous Caps From Human Atherosclerotic Plaques. Circulation 83, 1764-1770.

Lee, R.T., H.M. Loree, *et al.*, 1993. Computational structural analysis based on intravascular ultrasound imaging before in vitro angioplasty: Prediction of plaque fracture locations. Journal of the American College of Cardiology 21, 777-782.

Lee, R.T., S.G. Richardson, *et al.*, 1992. Prediction of mechanical properties of human atherosclerotic tissue by high-frequency intravascular ultrasound imaging. An in vitro study. Arteriosclerosis, thrombosis, and vascular biology 12, 1-5.

Li, D., A.M. Robertson, 2009. A structural multi-mechanism damage model for cerebral arterial tissue. Journal of Biomechanical Engineering 131, 101013.

Li, J., D. Mayau, *et al.*, 2008. A constitutive model dealing with damage due to cavity growth and the Mullins effect in rubber-like materials under triaxial loading. Journal of the Mechanics and Physics of Solids 56, 933-973.

Li, Z.Y., S. Howarth, *et al.*, 2006. Stress analysis of carotid plaque rupture based on in vivo high resolution MRI. Journal of Biomechanics 39, 2611-2622.

Liang, D.K., D.Z. Yang, *et al.*, 2005. Finite element analysis of the implantation of a balloon-expandable stent in a stenosed artery. International Journal of Cardiology 104, 314-318.

Libby, P., 1995. Molecular bases of the acute coronary syndromes. Circulation 91, 2844-2850.

Liu, Z., Z. Shi, *et al.*, 2009. Carotid artery stenting versus carotid endarterectomy: systematic review and meta-analysis. World J Surg 33, 586-596.

Lloyd-Jones, D., R. Adams, *et al.*, 2009. Heart Disease and Stroke Statistics—2009 Update A Report From the American Heart Association Statistics Committee and Stroke Statistics Subcommittee. Circulation 119, e21-e181.

Loree, H.M., A.J. Grodinsky, *et al.*, 1994. Static circumferential tangential modulus of human atherosclerotic tissue. Journal of Biomechanics 27, 195-204.

Loree, H.M., R.D. Kamm, *et al.*, 1992. Effects of fibrous cap thickness on peak circumferential stress in model atherosclerotic vessels. Circulation research 71, 850-858.

Maher, E., A. Creane, *et al.*, 2009. Tensile and compressive properties of fresh human carotid atherosclerotic plaques. Journal of Biomechanics 42, 2760-2767.

Maher, E., A. Creane, *et al.*, 2011. Inelasticity of Human Carotid Atherosclerotic Plaque. Annals of Biomedical Engineering.

Malek, A.M., S.L. Alper, *et al.*, 1999. Hemodynamic shear stress and its role in atherosclerosis. JAMA 282, 2035-2042.

Martini, F.H., 2006. Fundamentals of Anatomy and Physiology, 7th Edition. Benjamin-Cummings.

Miehe, C., 1995. Discontinuous and continuous damage evolution in Ogden-type large-strain elastic materials. European Journal of Mechanics, A/Solids 14, 697-720.

Migliavacca, F., L. Petrini, *et al.*, 2002. Mechanical behavior of coronary stents investigated through the finite element method. Journal of Biomechanics 35, 803-811.

Migliavacca, F., L. Petrini, *et al.*, 2004. Stainless and shape memory alloy coronary stents: a computational study on the interaction with the vascular wall. Biomechanics and Modeling in Mechanobiology 2, 205-217.

Milnor, W.R., 1982. Hemodynamics. Williams & Wilkins.

Mooney, M., 1940. A theory of Large Elastic Deformation. Journal of Applied Physics 11, 582-592.

Mortier, P., G.A. Holzapfel, *et al.*, 2010. A novel simulation strategy for stent insertion and deployment in curved coronary bifurcations: comparison of three drug-eluting stents. Annals of Biomedical Engineering 38, 88-99.

Mullins, L., 1948. Effect of Stretching on the Properties of Rubber, Vol 21. RUBDIV, 281-300 pp.

Naghavi, M., P. Libby, *et al.*, 2003. From vulnerable plaque to vulnerable patient: a call for new definitions and risk assessment strategies: Part I. Circulation 108, 1664-1672.

Naghdi, P.M., J.A. Tarpp, 1975. The Significance of Formulating Plasticity Theory with Reference to Loading Surfaces in Strain Space. International Journal of Engineering Science 13, 785-797.

Natali, A.N., P.G. Pavan, *et al.*, 2005. Anisotropic elasto-damage constitutive model for the biomechanical analysis of tendons. Medical Engineering & Physics 27, 209-214.

Newby, A.C., 2005. Dual role of matrix metalloproteinases (matrixins) in intimal thickening and atherosclerotic plaque rupture. Physiological Reviews 85, 1-31.

Nicolaides, A.N., S.K. Kakkos, *et al.*, 2002. Ultrasound plaque characterisation, genetic markers and risks. Pathophysiology of haemostasis and thrombosis 32, 371-377.

Ogden, R.W., 1984. Nonlinear Elastic Deformations. John Wiley & Sons, New York.

Ogden, R.W., D.G. Roxburgh, 1999. A pseudo-elastic model for the Mullins effect in filled rubber. Proc Roy Soc London A 455.

Ozolanta, I., G. Tetere, *et al.*, 1998. Changes in the mechanical properties, biochemical contents and wall structure of the human coronary arteries with age and sex. Medical Engineering & Physics 20, 523-533.

Pandit, A., X. Lu, *et al.*, 2005. Biaxial elastic material properties of porcine coronary media and adventitia. American journal of physiology. Heart and circulatory physiology 288, H2581-2587.

Parry, D.A.D., G.R.G. Barnes, *et al.*, 1978. A Comparison of the Size Distribution of Collagen Fibrils in Connective Tissues as a Function of Age and a Possible Relation between Fibril Size Distribution and Mechanical Properties. Proceedings of the Royal Society of London. Series B. Biological Sciences 203, 305-321.

Patel, D.J., D.L. Fry, 1969. The elastic symmetry of arterial segments in dogs. Circulation research 24, 1-8.

Patel, D.J., J.S. Janicki, 1970. Static elastic properties of the left coronary circumflex artery and the common carotid artery in dogs. Circulation Research 27, 149-158.

Peña, E., 2011. Prediction of the softening and damage effects with permanent set in fibrous biological materials. Journal of the Mechanics and Physics of Solids 59, 1808-1822.

Peña, E., V. Alastrue, *et al.*, 2010. A constitutive formulation of vascular tissue mechanics including viscoelasticity and softening behaviour. Journal of Biomechanics 43, 984-989.

Peña, E., B. Calvo, *et al.*, 2008. On finite-strain damage of viscoelastic-fibred materials. Applications to soft biological tissues. International Journal for Numerical Methods in Engineering 74, 1198-1218.

Peña, E., M. Doblare, 2009. An anisotropic pseudo-elastic approach for modelling Mullins effect in fibrous biological materials. Mechanics Research Communications 36, 784-790.

Peña, E., P. Martins, *et al.*, 2011. Mechanical characterization of the softening behavior of human vaginal tissue. Journal of the mechanical behavior of biomedical materials 4, 275-283.

Pena, E., J.A. Pena, *et al.*, 2009. On the Mullins effect and hysteresis of fibered biological materials: A comparison between continuous and discontinuous damage models. International Journal of Solids and Structures 46, 1727-1735.

Pericevic, I., C. Lally, *et al.*, 2009. The influence of plaque composition on underlying arterial wall stress during stent expansion: The case for lesion-specific stents. Medical Engineering & Physics 31, 428-433.

Petrini, L., F. Migliavacca, *et al.*, 2004. Numerical investigation of the intravascular coronary stent flexibility. Journal of Biomechanics 37, 495-501.

Prendergast, P.J., C. Lally, *et al.*, 2003. Analysis of Prolapse in Cardiovascular Stents: A Constitutive Equation for Vascular Tissue and Finite-Element Modelling. Journal of Biomechanical Engineering 125, 692-699.

Prot, V., B. Skallerud, 2009. Nonlinear solid finite element analysis of mitral valves with heterogeneous leaflet layers. Computational Mechanics 43, 353-368.

Provenzano, P.P., D. Heisey, *et al.*, 2002. Subfailure damage in ligament: a structural and cellular evaluation. Journal of Applied Physiology 92, 362-371.

Richardson, P.D., M.J. Davies, *et al.*, 1989. Influence of Plaque Configuration and Stress Distribution on Fissuring of Coronary Atherosclerotic Plaques. Lancet 2 (8669), 941-944.

Roach, M.R., A.C. Burton, 1957. The reason for the shape of the distensibility curves of arteries. Canadian Journal of Biochemistry and Physiology 35, 681-690.

Robertson, S.W., C.P. Cheng, *et al.*, 2008. Biomechanical response of stented carotid arteries to swallowing and neck motion. Journal of Endovascular Therapy 15, 663-671.

Rogers, C., Y.D. Tseng, *et al.*, 1999. Balloon-Artery Interactions During Stent Placement : A Finite Element Analysis Approach to Pressure, Compliance, and Stent Design as Contributors to Vascular Injury. Circulation research 84, 378-383.

Salunke, N.V., L.D.T. Topelski, *et al.*, 2001. Compressive stress-relaxation of human atherosclerotic plaque. Journal of Biomedical Materials Research 35, 17-127.

Salvucci, F.P., D. Bia, *et al.*, 2009. Association between mechanics and structure in arteries and veins: theoretical approach to vascular graft confection. Conf Proc IEEE Eng Med Biol Soc 2009, 4258-4261.

Schaar, J.A., C.L. De Korte, *et al.*, 2003. Characterizing Vulnerable Plaque Features with Intravascular Elastography. Circulation 108, 2636-2641.

Schulze-Bauer, C.A., C. Morth, *et al.*, 2003. Passive biaxial mechanical response of aged human iliac arteries. Journal of Biomechanical Engineering 125, 395-406.

Schulze-Bauer, C.A., P. Regitnig, *et al.*, 2002. Mechanics of the human femoral adventitia including the high-pressure response. Am J Physiol Heart Circ Physiol 282, H2427-2440.

Schwamm, L.H., A. Pancioli, *et al.*, 2005. Recommendations for the establishment of stroke systems of care: recommendations from the American Stroke Association's Task Force on the Development of Stroke Systems. Circulation 111, 1078-1091.

Schwartz, R.S., D.R. Holmes, 1994. Pigs, Dogs, Baboons, and Man: Lessons for Stenting from Animal Studies. Journal of Interventional Cardiology 7, 355-368.

Seshiah, P.N., D.J. Kereiakes, *et al.*, 2002. Activated monocytes induce smooth muscle cell death role of macrophage colony-stimulating factor and cell contact. Circulation 105, 174-180.

Sigwart, U., J. Puel, *et al.*, 1987. Intravascular stents to prevent occlusion and restenosis after transluminal angioplasty. New England Journal of Medicine 316, 701-706.

Silver, F.H., P.B. Snowhill, *et al.*, 2003. Mechanical behavior of vessel wall: a comparative study of aorta, vena cava, and carotid artery. Annals of Biomedical Engineering 31, 793-803.

Simo, J.C., 1987. On a fully three-dimensional finite-strain viscoelastic damage model: Formulation and computational aspects. Computer Methods in Applied Mechanics and Engineering 60, 153-173.

Simo, J.C., J.W. Ju, 1987a. Strain- and stress-based continuum damage models--I. Formulation. International Journal of Solids and Structures 23, 821-840.

Simo, J.C., J.W. Ju, 1987b. Strain- and stress-based continuum damage models - II. Computational aspects. International Journal of Solids and Structures 7, 841-869.

Sokolis, D.P., E.M. Kefaloyannis, *et al.*, 2006. A structural basis for the aortic stress-strain relation in uniaxial tension. Journal of Biomechanics 39, 1651-1662.

Sommer, G., P. Regitnig, *et al.*, 2010. Biaxial mechanical properties of intact and layer-dissected human carotid arteries at physiological and supraphysiological loadings. Am J Physiol Heart Circ Physiol 298, H898-912.

Sotoudeh, M., Y.S. Li, *et al.*, 2002. Induction of apoptosis in vascular smooth muscle cells by mechanical stretch. American Journal of Physiology - Heart and Circulatory Physiology 282.

Spencer, A.J.M., 1971. Theory of Invariants, In: Eringen, A.C. (Ed.) Continuum Physics. Academic Press, pp. 240-253.

Stary, H.C., 2000. Natural history and histological classification of atherosclerotic lesions: an update. Arteriosclerosis, thrombosis, and vascular biology 20, 1177-1178.

Stary, H.C., A.B. Chandler, *et al.*, 1995. A definition of advanced types of atherosclerotic lesions and a histological classification of atherosclerosis. A report from the Committee on Vascular Lesions of the Council on Arteriosclerosis, American Heart Association. Circulation 92, 1355-1374.

Stary, H.C., A.B. Chandler, *et al.*, 1994. A definition of initial, fatty streak, and intermediate lesions of atherosclerosis. A report from the Committee on Vascular Lesions of the Council on Arteriosclerosis, American Heart Association. Circulation 89, 2462-2478.

Stemper, B.D., N. Yoganandan, *et al.*, 2007a. Mechanics of arterial subfailure with increasing loading rate. Journal of Biomechanics 40, 1806-1812.

Stemper, B.D., N. Yoganandan, *et al.*, 2007b. Mechanics of Fresh, Refrigerated, and Frozen Arterial Tissue. Journal of Surgical Research 139, 236-242.

Swindle, M.M., D.C. Moody, 1992. Swine as Models in Biomedical Research. Oowa State University Press.

Tan, L.B., D.C. Webb, *et al.*, 2001. A method for investigating the mechanical properties of intracoronary stents using finite element numerical simulation. International Journal of Cardiology 78, 51-67.

Tanaka, E., H. Yamada, 1990. Inelastic constitutive modeling for blood vessels based on viscoplasticity. Front Med Biol Eng 2, 177-180.

Tang, G.L., J.S. Matsumura, *et al.*, 2008. Carotid angioplasty and stenting vs carotid endarterectomy for treatment of asymptomatic disease: single-center experience. Archives of surgery 143, 653-658.

Tegos, T.J., K.J. Alomiris, *et al.*, 2001. Significance of Sonographic Tissue and Surface Characteristics of Carotid Plaques. American Journal of Neuroradiology 22, 1605-1612.

Teng, Z., D. Tang, *et al.*, 2009. An experimental study on the ultimate strength of the adventitia and media of human atherosclerotic carotid arteries in circumferential and axial directions. Journal of Biomechanics 42, 2535-2539.

Topoleski, L.D., N.V. Salunke, 2000. Mechanical behavior of calcified plaques: a summary of compression and stress-relaxation experiments. Z Kardiol 89 Suppl 2, 85-91.

Topoleski, L.D.T., N.V. Salunke, *et al.*, 1997. Composition- and history-dependent radial compressive behavior of human atherosclerotic plaque. Journal of Biomedical Materials Research 35, 117-127.

Toussaint, J.-F., J.F. Southern, *et al.*, 1998. Behavior of Atherosclerotic Plaque Components After in Vitro Angioplasty and Atherectomy Studied by High Field MR Imaging. Magnetic Resonance Imaging 16, 175-183.

Treolar, L.R.G., 1943. The Elasticity of Long-Chain Molecules. Transactions of the Faraday Society 39, 241-246.

Vaishnav, R.N., J.T. Young, *et al.*, 1972. Nonlinear anisotropic elastic properties of the canine aorta. Biophysical Journal 12, 1008-1027.

van Andel, C.J., P.V. Pistecky, *et al.*, 2003. Mechanical properties of porcine and human arteries: implications for coronary anastomotic connectors. Annals of Thoracic Surgery 76, 58-64; discussion 64-55.

Velican, C., D. Velican, 1985. Study of coronary intimal thickening. Atherosclerosis 56, 331-344.

Vengrenyuk, Y., S. Carlier, *et al.*, 2006. A hypothesis for vulnerable plaque rupture due to stress-induced debonding around cellular microcalcifications in thin fibrous caps. Proc Natl Acad Sci U S A 103, 14678-14683.

Vilks, Y.K., Y.Z. Saulgozis, *et al.*, 1975. Effect of temperature on changes of tensile stress at constant elongation in certain human soft tissues. Mechanics of Composite Materials 11, 780-784.

Vito, R.P., H. Demiray, 1982. A two-layered model for arterial wall mechanics. In: Proc 35th Annual Conf Eng Med Biol.

Volokh, K.Y., D.A. Vorp, 2008. A model of growth and rupture of abdominal aortic aneurysm. Journal of Biomechanics 41, 1015-1021.

Vos, A.W., M.A. Linsen, *et al.*, 2003. Carotid artery dynamics during head movements: a reason for concern with regard to carotid stenting? Journal of Endovascular Therapy 10, 862-869.

Waller, B.F., 1989. The eccentric coronary atherosclerotic plaque: morphologic observations and clinical relevance. Clinical Cardiology 12, 14-20.

Walraevens, J., B. Willaert, *et al.*, 2008. Correlation between compression, tensile and tearing tests on healthy and calcified aortic tissues. Medical Engineering & Physics 30, 1098-1104.

Whitcher, F.D., 1997. Simulation of in vivo loading conditions of nitonol vascular stent structures. Computers and Structures 64, 1005-1011.

Wolinsky, H., S. Glagov, 1964. Structural Basis for the Static Mechanical Properties of the Aortic Media. Circulation research 14, 400-413.

Woo, C., W. Kinm, *et al.*, 2008. A study on the material properties and fatigue life prediction of natural rubber component. Materials Science and Engineering A, 376-381.

Wu, W., M. Qi, *et al.*, 2007. Delivery and release of nitinol stent in carotid artery and their interactions: a finite element analysis. Journal of Biomechanics 40, 3034-3040.

Wulandana, R., A.M. Robertson, 2005. An inelastic multi-mechanism constitutive equation for cerebral arterial tissue. Biomech Model Mechanobiol 4, 235-248.

Yang, T., C.K. Chui, *et al.*, 2011. Quasi-linear viscoelastic modeling of arterial wall for surgical simulation. Int J Comput Assist Radiol Surg.

Zahedmanesh, H., D. John Kelly, *et al.*, 2010. Simulation of a balloon expandable stent in a realistic coronary artery-Determination of the optimum modelling strategy. Journal of Biomechanics 43, 2126-2132.

Zanchi, A., N. Stergiopulos, *et al.*, 1998. Differences in the mechanical properties of the rat carotid artery in vivo, in situ, and in vitro. Hypertension 32, 180-185.

Zhou, J., Y.C. Fung, 1997. The degree of nonlinearity and anisotropy of blood vessel elasticity. Proc Natl Acad Sci U S A 94, 14255-14260.

Zou, Y., Y. Zhang, 2009. An experimental and theoretical study on the anisotropy of elastin network. Annals of Biomedical Engineering 37, 1572-1583.

Appendix A Effect of unloaded time on inelastic residual strains in porcine arteries

A.1 Introduction

The testing methodology used in chapters 4 and 5 and fit to in chapter 6 is similar to that performed to characterise stress-softening in soft tissues in the literature (Peña, 2011). While this is a relatively well established method for characterising the softening in tissue, it is unknown if the inelastic residual strains that are observed in the tissue on unloading are a permanent effect due to damage or if it is largely due to visco-elastic or poro-elastic effects. A similar method has been used to characterise softening and permanent set (residual strains resulting from damage or alterations in the tissue due to loading) in soft tissues (Peña, 2011). In this study, the test methodology that is used in the main chapters of this thesis has been altered to include an unloaded rest or 'dwell' period in the loading regime to allow for possible material recovery.

Relaxation time for strained arterial tissue to reach an equilibrium stress has been reported as varying between 10-150 min for porcine aorta and carotid (Silver et al., 2003). Others have seen that arterial tissue at low applied strains relaxes within a time of 900 s (Yang et al., 2011). This data suggests that if the inelastic deformations reported in this study were largely influenced by viscoelastic effects, that an unloaded rest period of 2 hrs should be sufficient for the majority of recovery in the tissue to occur. Smooth muscle is considered to be the main artery component involved in visco-elastic behaviour. The greatest residual strains are observed in the coronary artery in compression, which is a muscular artery; as a result the coronary artery is tested in this study as it is most likely to exhibit significant relaxation. The effect of adding the dwell is analysed and used to determine whether the residual strains observed are largely a result of damage or if the tissue recovers due to visco-elastic or poro-elastic behaviour.

A.2 Materials and Methods

Right coronary arteries were harvested from 3-4 month old female pigs using a scalpel within one hour of the pig being put down. Fat and connective tissue were trimmed from the arteries, which were then stored in 0.9% saline solution at 4°C. All testing was completed within 48hrs of tissue harvesting. Mechanical testing was performed using a high precision testing device adapted for testing biological specimens (Bose ElectroForce 3100, Bose Corporation, Gillingham, UK) with a load resolution of 6mN and a stroke resolution of 0.0015mm.

3.5 mm diameter cylindrical radial compressive samples removed from coronary arteries were loaded in uniaxial cyclic compression in order to determine the inelastic strains remaining in the tissue on unloading. Samples were placed on the lower platen and the upper platen was moved to apply a small compressive pre-load of 0.01 N to the sample at a crosshead speed of 0.001 mm/s. This ensured a consistent contact between the platen and the top of the sample. The sample thickness was then taken as the distance between the platens at this pre-load. Samples were loaded cyclically at a strain-rate of 0.005 s-1 between 0 % strain and a peak compressive strain starting at 10% and every 5 loading-unloading cycles, following a rest period at 0 % strain of 2 hrs, the peak strain is increased incrementally by 10% up to a maximum of 60%. Testing occurred inside a water bath filled with 0.9% saline solution in order to maintain sample hydration during testing. 6 coronary samples in total were tested using this methodology. A further 6 samples were tested using the methodology described in chapter 5 (i.e. no rest period between increases in cyclic peak strain)

In order to investigate the effects of the dwell on the residual strains, the residual strain in the samples was measured during the 2nd loading cycle (as in chapters 4 and 5) and also during the first loading cycle of the subsequent peak strain level, after the rest period. The difference in the residual strain measured before and after the rest period is the measure of how much the tissue has recovered. The results residual strain measured in samples tested using the methodology where no

rest was measured were also compared to the results of those tested with a rest period included. Residual strain is defined here as the strain, relative to the original thickness of the specimen, at which the stress in the sample begins to increase from zero.

A.3 Results

It was found that the recovery in the tissue in all cases was < 10 % and in many cases < 5 % of the residual strain was recovered, see Fig A.1. The maximum recovery of the residual strain was 8.7 % after 2 hrs resting, this also corresponded to the highest magnitude difference in residual strain measured before and after of 0.02. This resulted in the residual strain in the sample reducing from 0.231 before the rest period to 0.211 after. For four of the six specimens tested the magnitude of the strain recovery was ≤ 0.01 for peak applied strains up to 0.4.

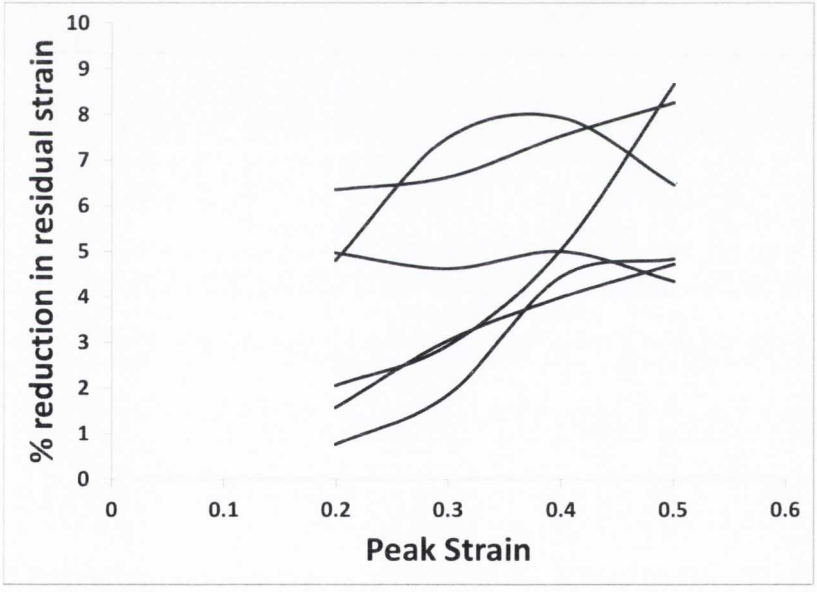

Figure A. 1: % recovery/reduction of residual strain in a sample after 2 hr rest period.

No significant difference was found in the residual strains determined using the two testing test methodologies. The mean residual strains measured when a dwell is included are only slightly below that of when no dwell is included, ~ 0.01 at high strains, see Fig A.2.

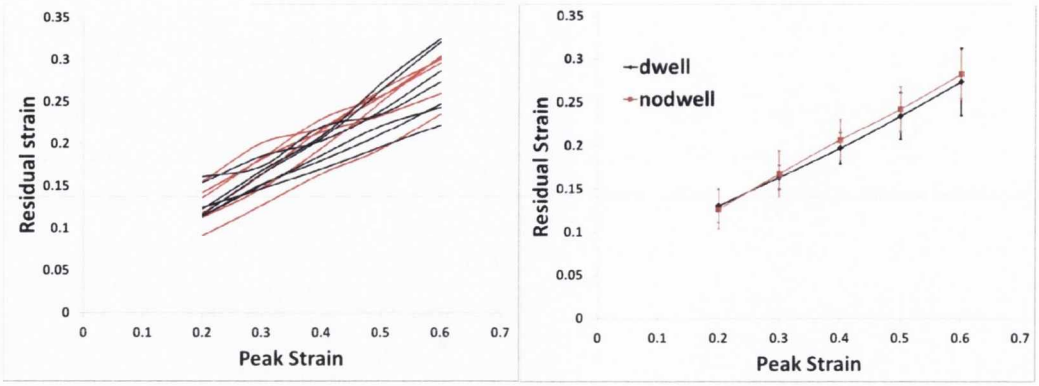

Figure A. 2: Residual strains measured for samples tested, where a dwell either was or was not included

A.4 Discussion

In all cases over 90 % of the magnitudes of the residual strains that are measured prior to the rest period remain in the tissue after 2 hrs. As studies indicate that the recovery time of arterial tissue varies between 10 – 150 min (Silver et al, 2003) it is reasonable to assume that the majority of the recovery in the samples occurs during the 2 hour resting period. As the recovery is generally small, it appears that the inelastic residual strains observed are largely a result of damage in the tissue. Testing that incorporates longer dwell times may result in further recovery in the tissue, however this may be impractical in a study measuring deformations at multiple strain levels due to possible concerns of tissue degradation with time during testing. As no significant difference was observed in the residual strain measured between samples tested with or without the dwell and the tissue recovery is generally small, it is concluded that the use of the test methodology in chapters 4 and 5 lead to satisfactory estimates of the residual strains that occur due to damage.